International Journal of Antennas and Propagation

Mutual Coupling in Antenna Arrays 2013

Guest Editors: Hoi-Shun Lui, Yantao Yu, Hon Tat Hui, Jian Yang, and Hao Ling

Mutual Coupling in Antenna Arrays 2013

International Journal of Antennas and Propagation

Mutual Coupling in Antenna Arrays 2013

Guest Editors: Hoi-Shun Lui, Yantao Yu, Hon Tat Hui, Jian Yang, and Hao Ling

Editorial Board

Contents

Hindawi Publishing Corporation
International Journal of Antennas and Propagation
Volume 2014, Article ID 295832, 2 pages
http://dx.doi.org/10.1155/2014/295832

Editorial
Mutual Coupling in Antenna Arrays 2013

Hoi-Shun Lui,[1] Yantao Yu,[2] Hon Tat Hui,[3] Jian Yang,[4] and Hao Ling[5]

[1] *School of Information Technology and Electrical Engineering, The University of Queensland, St. Lucia, QLD 4072, Australia*
[2] *College of Communication Engineering, Chongqing University, Chongqing 400044, China*
[3] *Department of Electrical and Computer Engineering, National University of Singapore, Singapore 117576*
[4] *Department of Signals and Systems, Chalmers University of Technology, 41296 Gothenburg, Sweden*
[5] *Department of Electrical and Computer Engineering, The University of Texas at Austin, TX 78712, USA*

Correspondence should be addressed to Hoi-Shun Lui; h.lui@uq.edu.au

Received 14 January 2014; Accepted 14 January 2014; Published 9 March 2014

The invention of antenna arrays opened up the door for microwave sensing and communications. Most applications of antenna arrays are in the defense and wireless communications areas. The introduction of multiple-input-multiple-output (MIMO) concept in recent years has opened up further opportunities in that the system performance can be maintained with a smaller number of antennas. The existence of mutual coupling effect, that is, the electromagnetic interaction between antenna elements, appears as an undesirable effect in most of these cases. The transmitted and received signals can be significantly distorted such that the signals no longer depend solely on the antenna elements, but also on the array structure and the surrounding environment. Such distortions result in the reduction of channel capacities in communications applications, as well as poor accuracies in ranging and direction finding. In most applications, the mutual coupling effect is unknown. A major challenge is then to characterize this undesirable effect and to accurately estimate the unknown parameters (range, direction) without *a priori* knowledge of the signal environment.

This special issue, which is the third one in its series, provides an international forum for researchers to disseminate their results and ideas to tackle some of these challenging research problems. Five dedicated papers have contributed to this special issue. These papers concern the mutual coupling and its impacts on MIMO communications, direction finding, and MIMO radar. To help interested readers with a quick reference to the main themes of these papers, we briefly introduce them as follows.

The first paper entitled "*Self-interference cancellation-based mutual-coupling model for full-duplex single-channel MIMO systems*," concerns the mutual coupling problem in MIMO communications. The paper addresses the self-interference and mutual-interference of a full-duplex single-channel MIMO communications system.

In the presence of mutual coupling, the array manifold is perturbed, which results in poor accuracies in direction finding. The paper "*Accurate DOA estimations using microstrip adaptive arrays in the presence of mutual coupling effect*" proposes a method to calibrate the undesirable mutual coupling effect for arrays with non-omni-directional radiating elements. The third paper, entitled "*2-D direction of arrival estimation for cross array in the presence of mutual coupling*," introduces a noniterative algorithm based on the Propagation Method for accurate two-dimensional direction finding problems using a cross array in the presence of mutual coupling. The paper "*AR model-based direction-of-arrival estimation of coherent signals in the presence of unknown mutual coupling*" provides a novel signal processing solution based on a spatial autoregression (AR) model for coherent direction finding of uniform linear arrays.

The fifth paper of this special issue, entitled "*Root-MUSIC based angle estimation for MIMO radar with unknown mutual coupling*," explores the direction finding solutions in MIMO radar. A Root-MUSIC based solution is proposed to estimate the incoming signal direction with unknown mutual coupling.

All papers appearing in this special issue have been subject to a strict peer-reviewing process. They are of high

quality and address the mutual coupling problem from different perspectives. Through this special issue, we have provided a medium of dissemination for valuable ideas and conclusions on mutual coupling research. At the same time, we hope that more research innovations can be stimulated for future advances on this subject.

Hoi-Shun Lui
Yantao Yu
Hon Tat Hui
Jian Yang
Hao Ling

Hindawi Publishing Corporation
International Journal of Antennas and Propagation
Volume 2014, Article ID 547540, 6 pages
http://dx.doi.org/10.1155/2014/547540

Research Article

2D Direction of Arrival Estimation for Cross Array in the Presence of Mutual Coupling

Weiwei Hu, Aijun Zhang, and Changming Wang

The School of Mechanical Engineering, Nanjing University of Science and Technology, Jiangsu 210094, China

Correspondence should be addressed to Changming Wang; hww1986116@163.com

Received 6 August 2013; Accepted 12 November 2013; Published 4 March 2014

Academic Editor: Yantao Yu

This paper proposes a new method for cross array to estimate two-dimensional direction of arrival (2-D DOA) in the presence of mutual coupling. In this method, the array elements which are affected by the same mutual coupling are chosen on x-axis and z-axis, respectively. Then a new matrix is constructed with the proper entries of cross covariance matrix of the chosen elements outputs on x-axis and z-axis. Propagation method (PM) and rotational invariance techniques for uniform linear array (ULA) are utilized in the constructed matrix to obtain two parameters correlated with elevations and azimuths. While calculating and pairing the two parameters, only once eigendecomposing and several division operations are required with the relationship among the matrix, its eigenvalues, and corresponding eigenvectors. Simulations are presented to validate the performance of the proposed method.

1. Introduction

Mutual coupling between elements has a serious effect on precision and resolution of the direction of arrival estimation algorithms [1, 2]. Therefore, there are lots of works addressing this issue of how to restrain the effects of mutual coupling. Many calibration algorithms have been proposed in the past decades. Friedlander and Weiss presented an iterative procedure to compensate the mutual coupling and perturbation of gain and phase [3]. In [4], Sellone and Serra constructed an objective function based on covariance matrix matching, dealt with mutual coupling matrix and its conjugate transpose as unrelated ones, and searched the optimal solution with iterative procedure. However, the multidimensional search needed for the associated nonlinear optimal search is computationally complicated in [3, 4]. Wang et al. made use of banded complex symmetric Toeplitz characteristic of the mutual coupling matrix of ULA and rank reduction (RARE) algorithm to obtain azimuths and mutual coupling coefficients [5], while Lin and Yang utilized banded complex symmetric circular Toeplitz characteristic of the mutual coupling matrix of uniform circle array (UCA) [6]. These two methods are only suitable for ULA and UCA, respectively. The idea from [5] was applied to cross array, but the transformed matrix related to the ideal steering vector has no universal form for reasons of the array configuration and the variable mutual coupling degree of freedom [7]. The literature [8] presented a decoupling algorithm for ULA. It chooses the proper elements whose ideal steering vector can be separated from the mutual coupling coefficients and then employs the outputs of the chosen elements to construct MUSIC spatial spectral estimator. Nevertheless this method can only estimate one-dimensional direction and needs the spectral peak search. In [9, 10], this method [8] was applied to uniform rectangular array (URA) and uniform hexagon array (UHA), respectively, to estimate two-dimensional directions, but the configurations of planar arrays are complicated and lots of auxiliary elements are needed.

In order to estimate 2-D DOA in the presence of mutual coupling, a method for cross array which has a simpler configuration than those for planar arrays is presented in this paper. The method is based on PM algorithm utilizing signal subspace eigenvectors algorithm for the array consisting of the chosen elements which are affected by the same mutual

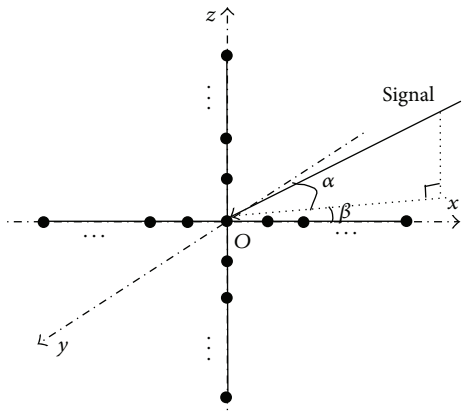

Figure 1: The cross array configuration.

coupling. It is not an iterative algorithm, and the spectral peak search is not required. It can estimate the 2-D DOA accurately without estimating the mutual coupling coefficients.

2. Problem Formulation

Consider a cross array consisting of two ULAs located on x-axis and z-axis, respectively. The ULAs share the middle element as reference at origin of coordinates. Each ULA has $2M + 1$ sensors with element spacing of d, which means that there exist $4M + 1$ ones in the whole array because of the sharing element. Assume that K narrowband, far-field, noncoherent signals with the same wave length λ ($\lambda = 2d$) impinge on this array, and the kth source's elevation and azimuth are α_k and β_k, respectively. The array configuration is shown in Figure 1.

Let $\mathbf{C}$ and t denote the mutual coupling matrix (MCM) and the time index, respectively. The output of the array can be expressed as

$$\mathbf{Y}(t) = \mathbf{CAS}(t) + \mathbf{N}(t), \tag{1}$$

where $\mathbf{Y}$, $\mathbf{A}$, $\mathbf{S}$, and $\mathbf{N}$ represent the received signal vector, the ideal steering matrix, the source signal vector, and the stochastic noise (additive white Gauss noise whose mean is zero and variance is σ^2) vector, respectively. They can be described as (the time index t is omitted for brevity)

$$\begin{aligned}
\mathbf{Y} &= \left[x_1, \ldots, x_M, \ldots, x_{2M+1}, z_1, \ldots, z_M, \ldots, z_{2M+1}\right]^T,\\
\mathbf{A} &= \left[\mathbf{a}(\alpha_1, \beta_1), \ldots, \mathbf{a}(\alpha_k, \beta_k), \ldots, \mathbf{a}(\alpha_K, \beta_K)\right],\\
\mathbf{a}(\alpha_k, \beta_k) &= \left[e^{j2\pi dM \cos\alpha_k \cos\beta_k/\lambda}, \ldots, 1, \ldots,\right.\\
&\qquad e^{-j2\pi dM \cos\alpha_k \cos\beta_k/\lambda},\\
&\qquad \left. e^{j2\pi dM \sin\alpha_k/\lambda}, \ldots, 1, \ldots, e^{-j2\pi dM \sin\alpha_k/\lambda}\right]^T,\\
\mathbf{S} &= \left[s_1, \ldots, s_k, \ldots, s_K\right]^T,\\
\mathbf{N} &= \left[n_{x_1}, \ldots, n_{x_M}, \ldots, n_{x_{2M+1}}, n_{z_1}, \ldots, n_{z_M}, \ldots, n_{z_{2M+1}}\right]^T,
\end{aligned} \tag{2}$$

where superscript T denotes transpose.

As shown in [3], the MCM of ULA can be expressed as a banded complex symmetric Toeplitz matrix $\mathbf{B}$

$$\mathbf{B} = \text{Toeplitz}\left\{1, b_1, \ldots, b_p\right\}, \tag{3}$$

where integer p denotes the mutual coupling degree of freedom, which means the coefficient of mutual coupling is assumed to be zero if the distance between the two sensors exceeds pd.

Based on the MCM model of ULA by (3), the MCM of cross array has the following form:

$$\mathbf{C} = \begin{bmatrix} \mathbf{B} & \mathbf{D} \\ \mathbf{D} & \mathbf{B} \end{bmatrix}, \tag{4}$$

where $\mathbf{B}$ is the MCM of ULA on x- or z-axis, and $\mathbf{D}$ describes the mutual coupling between the two ULAs. The matrix $\mathbf{D}$ can be presented by

$$\mathbf{D} = \begin{bmatrix} \mathbf{JD}_1\mathbf{J} & \mathbf{h}_1^T & \mathbf{JD}_1 \\ \mathbf{h}_1 & 1 & \mathbf{h}_1\mathbf{J} \\ \mathbf{D}_1\mathbf{J} & (\mathbf{h}_1\mathbf{J})^T & \mathbf{D}_1 \end{bmatrix}, \tag{5}$$

where

$$\begin{aligned}
\mathbf{h}_1 &= \left[\mathbf{0}_{(M-p)\times 1}\ b_p\ \cdots\ b_1\right],\\
\mathbf{J} &= \begin{bmatrix} 0 & 0 & \cdots & 1 \\ 0 & 0 & \iddots & \vdots \\ \vdots & 1 & \ddots & 0 \\ 1 & \cdots & 0 & 0 \end{bmatrix}_{M\times M}.
\end{aligned} \tag{6}$$

$\mathbf{D}_1 = (d_{ij})_{M\times M}$, d_{ij} denotes the coefficient of mutual coupling between the two elements spacing $\sqrt{i^2 + j^2}d$, and d_{ij} satisfies

$$\begin{aligned}
d_{ij} &= d_{ji},\\
d_{ij} &= \begin{cases} \neq 0 & \sqrt{i^2 + j^2} < p \\ = 0 & \sqrt{i^2 + j^2} > p. \end{cases}
\end{aligned} \tag{7}$$

3. Proposed Method

The ideal steering vector of ULA elements affected by the same mutual coupling can be separated from the mutual coupling coefficients, which means they can be decoupled easily. Let $\widetilde{\mathbf{Y}}'$ and $\widetilde{\mathbf{Y}}''$ be the outputs of elements affected by the same mutual coupling on x-axis and z-axis, respectively.

$\widetilde{\mathbf{Y}}'$ can be written as

$$\begin{aligned}\widetilde{\mathbf{Y}}' &= \mathbf{HY} \\ &= \sum_{k=1}^{K} \begin{bmatrix} b_p {u_k}^M + \cdots + {u_k}^{M-p} + \cdots b_p {u_k}^{M-2p} \\ \vdots \\ b_p {u_k}^{2p} + \cdots + {u_k}^p + \cdots b_p \\ b_p + \cdots + {u_k}^{-p} + \cdots b_p {u_k}^{-2p} \\ \vdots \\ b_p {u_k}^{2p-M} + \cdots + {u_k}^{p-M} + \cdots b_p {u_k}^{-M} \end{bmatrix} s_k + \widetilde{\mathbf{N}}_1 \\ &= \sum_{k=1}^{K} f_k s_k \widetilde{\mathbf{a}}_k + \widetilde{\mathbf{N}}_1 = \widetilde{\mathbf{A}}_1 \mathbf{T}_1 \mathbf{S} + \widetilde{\mathbf{N}}_1,\end{aligned} \tag{8}$$

where $f_k = b_p {u_k}^M + \cdots + {u_k}^{M-p} + \cdots b_p {u_k}^{M-2p}$,

$$\mathbf{H} = \begin{bmatrix} \mathbf{H}_1 & \underbrace{\mathbf{0}}_{2(M-2p+1)\times(2M+1)} \end{bmatrix},$$

$$\mathbf{H}_1 = \begin{bmatrix} \underbrace{\mathbf{0}}_{(M-2p+1)\times p} & \mathbf{I} & \underbrace{\mathbf{0}}_{(M-2p+1)\times(2p-1)} & \mathbf{0} & \underbrace{\mathbf{0}}_{(M-2p+1)\times p} \\ \mathbf{0} & \mathbf{0} & \mathbf{0} & \mathbf{I} & \mathbf{0} \end{bmatrix},$$

$$\widetilde{\mathbf{a}}_k = \left[1, \ldots, {u_k}^{-(M-2p)}, {u_k}^{-M}, \ldots, {u_k}^{-2M+2p}\right]^T, \tag{9}$$

$$u_k = \exp\left(\frac{j2\pi d \cos\alpha_k \cos\beta_k}{\lambda}\right),$$

$$\widetilde{\mathbf{A}}_1 = \left[\widetilde{\mathbf{a}}_1, \ldots, \widetilde{\mathbf{a}}_k, \ldots, \widetilde{\mathbf{a}}_K\right],$$

$$\mathbf{T}_1 = \mathrm{diag}\left\{f_1, \ldots, f_k, \ldots, f_K\right\}.$$

There are no entries of $\mathbf{D}$ in (8) as the chosen elements on x-axis are not affected by the sensors on z-axis, because the distances between them are out of pd.

Similarly, $\widetilde{\mathbf{Y}}''$ can be expressed as

$$\widetilde{\mathbf{Y}}'' = \widetilde{\mathbf{A}}_2 \mathbf{T}_2 \mathbf{S} + \widetilde{\mathbf{N}}_2, \tag{10}$$

where $\widetilde{\mathbf{A}}_2 = [\widetilde{\mathbf{b}}_1, \ldots, \widetilde{\mathbf{b}}_k, \ldots, \widetilde{\mathbf{b}}_K]$,

$$\mathbf{T}_2 = \mathrm{diag}\left\{g_1, \ldots, g_k, \ldots, g_K\right\}, \tag{11}$$

$$\widetilde{\mathbf{b}}_k = \left[1, \ldots, {v_k}^{-(M-2p)}, {v_k}^{-M}, \ldots, {v_k}^{-2M+2p}\right]^T, \tag{12}$$

$$g_k = b_p {v_k}^M + \cdots + {v_k}^{M-p} + \cdots b_p {v_k}^{M-2p}, \tag{13}$$

$$v_k = \exp\left(\frac{j2\pi d \sin\alpha_k}{\lambda}\right). \tag{14}$$

In order to introduce rotational invariance techniques for ULA to this array, $\widetilde{\mathbf{Y}}'$ is partitioned into two parts, so is $\widetilde{\mathbf{Y}}''$. They are denoted by $\widetilde{\mathbf{Y}}_{11}$, $\widetilde{\mathbf{Y}}_{12}$, $\widetilde{\mathbf{Y}}_{21}$, and $\widetilde{\mathbf{Y}}_{22}$, respectively:

$$\begin{aligned}\widetilde{\mathbf{Y}}_{11} &= \begin{bmatrix} \widetilde{\mathbf{Y}}'_{(1:M-2p)} \\ \widetilde{\mathbf{Y}}'_{(M-2p+2:2M-4p+1)} \end{bmatrix}, \\ \widetilde{\mathbf{Y}}_{12} &= \begin{bmatrix} \widetilde{\mathbf{Y}}'_{(2:M-2p+1)} \\ \widetilde{\mathbf{Y}}'_{(M-2p+3:2M-4p+2)} \end{bmatrix}, \\ \widetilde{\mathbf{Y}}_{21} &= \begin{bmatrix} \widetilde{\mathbf{Y}}''_{(1:M-2p)} \\ \widetilde{\mathbf{Y}}''_{(M-2p+2:2M-4p+1)} \end{bmatrix}, \\ \widetilde{\mathbf{Y}}_{22} &= \begin{bmatrix} \widetilde{\mathbf{Y}}''_{(2:M-2p+1)} \\ \widetilde{\mathbf{Y}}''_{(M-2p+3:2M-4p+2)} \end{bmatrix}.\end{aligned} \tag{15}$$

$\widetilde{\mathbf{Y}}_{11}$ and $\widetilde{\mathbf{Y}}_{21}$ are the submatrixes of $\widetilde{\mathbf{Y}}'$ and $\widetilde{\mathbf{Y}}''$, respectively, so the cross covariance matrix of $\widetilde{\mathbf{Y}}_{11}$ and $\widetilde{\mathbf{Y}}_{21}$ can be built with the proper entries of cross covariance matrix of $\widetilde{\mathbf{Y}}'$ and $\widetilde{\mathbf{Y}}''$:

$$\widetilde{\mathbf{R}}_1 = \widetilde{\mathbf{A}}_{11} \widetilde{\mathbf{R}}_{ss} {\widetilde{\mathbf{A}}_{21}}^H = \begin{bmatrix} \widetilde{\mathbf{R}}_{11} & \widetilde{\mathbf{R}}_{12} \\ \widetilde{\mathbf{R}}_{13} & \widetilde{\mathbf{R}}_{14} \end{bmatrix}, \tag{16}$$

where $\widetilde{\mathbf{A}}_{11}$ and $\widetilde{\mathbf{A}}_{21}$ are the ideal steering matrixes of arrays corresponding to $\widetilde{\mathbf{Y}}_{11}$ and $\widetilde{\mathbf{Y}}_{21}$, respectively,

$$\widetilde{\mathbf{R}} = E\left\{\widetilde{\mathbf{Y}}' \widetilde{\mathbf{Y}}''^H\right\}, \tag{17}$$

$$\widetilde{\mathbf{R}}_{11} = \widetilde{\mathbf{R}}_{(1:M-2p,1:M-2p),} \tag{18}$$

$$\widetilde{\mathbf{R}}_{12} = \widetilde{\mathbf{R}}_{(1:M-2p,M-2p+2:2M-4p+1)}, \tag{19}$$

$$\widetilde{\mathbf{R}}_{13} = \widetilde{\mathbf{R}}_{(M-2p+2:2M-4p+1,1:M-2p),} \tag{20}$$

$$\widetilde{\mathbf{R}}_{14} = \widetilde{\mathbf{R}}_{(M-2p+2:2M-4p+1,M-2p+2:2M-4p+1)}, \tag{21}$$

$$\widetilde{\mathbf{R}}_{ss} = \mathbf{T}_1 E\left\{\mathbf{S}\mathbf{S}^H\right\} {\mathbf{T}_2}^H. \tag{22}$$

Similarly, let $\widetilde{\mathbf{R}}_2$, $\widetilde{\mathbf{R}}_3$, and $\widetilde{\mathbf{R}}_4$, which can be constructed with the proper entries chosen from $\widetilde{\mathbf{R}}$ as $\widetilde{\mathbf{R}}_1$ in (16), be the cross covariance matrixes of $\widetilde{\mathbf{Y}}_{12}$ and $\widetilde{\mathbf{Y}}_{21}$, $\widetilde{\mathbf{Y}}_{11}$, and $\widetilde{\mathbf{Y}}_{22}$, and $\widetilde{\mathbf{Y}}_{12}$ and $\widetilde{\mathbf{Y}}_{22}$, respectively,

$$\widetilde{\mathbf{R}}_2 = \widetilde{\mathbf{A}}_{12} \widetilde{\mathbf{R}}_{ss} {\widetilde{\mathbf{A}}_{21}}^H = \widetilde{\mathbf{A}}_{11} \mathbf{\Phi}_1 \widetilde{\mathbf{R}}_{ss} {\widetilde{\mathbf{A}}_{21}}^H, \tag{23}$$

$$\widetilde{\mathbf{R}}_3 = \widetilde{\mathbf{A}}_{11} \widetilde{\mathbf{R}}_{ss} {\widetilde{\mathbf{A}}_{22}}^H = \widetilde{\mathbf{A}}_{11} \widetilde{\mathbf{R}}_{ss} \left(\widetilde{\mathbf{A}}_{21} \mathbf{\Phi}_2\right)^H = \widetilde{\mathbf{A}}_{11} {\mathbf{\Phi}_2}^H \widetilde{\mathbf{R}}_{ss} {\widetilde{\mathbf{A}}_{21}}^H, \tag{24}$$

$$\widetilde{\mathbf{R}}_4 = \widetilde{\mathbf{A}}_{12} \widetilde{\mathbf{R}}_{ss} {\widetilde{\mathbf{A}}_{22}}^H = \widetilde{\mathbf{A}}_{11} \mathbf{\Phi}_1 {\mathbf{\Phi}_2}^H \widetilde{\mathbf{R}}_{ss} {\widetilde{\mathbf{A}}_{21}}^H, \tag{25}$$

where $\widetilde{\mathbf{A}}_{12}$ and $\widetilde{\mathbf{A}}_{22}$ are the ideal steering matrixes of arrays corresponding to $\widetilde{\mathbf{Y}}_{12}$ and $\widetilde{\mathbf{Y}}_{22}$, respectively,

$$\begin{aligned}\mathbf{\Phi}_1 &= \mathrm{diag}\left\{{u_1}^{-1}, \ldots, {u_k}^{-1}, \ldots, {u_K}^{-1}\right\}, \\ \mathbf{\Phi}_2 &= \mathrm{diag}\left\{{v_1}^{-1}, \ldots, {v_k}^{-1}, \ldots, {v_K}^{-1}\right\}.\end{aligned} \tag{26}$$

The new matrix $\widetilde{\mathbf{R}}'$ consisting of the four cross covariance matrixes includes the rotational invariance factors,

$$\widetilde{\mathbf{R}}' = \begin{bmatrix} \widetilde{\mathbf{R}}_1 \\ \widetilde{\mathbf{R}}_2 \\ \widetilde{\mathbf{R}}_3 \\ \widetilde{\mathbf{R}}_4 \end{bmatrix} = \begin{bmatrix} \widetilde{\mathbf{A}}_{11} \\ \widetilde{\mathbf{A}}_{11}\boldsymbol{\Phi}_1 \\ \widetilde{\mathbf{A}}_{11}{\boldsymbol{\Phi}_2}^H \\ \widetilde{\mathbf{A}}_{11}\boldsymbol{\Phi}_1{\boldsymbol{\Phi}_2}^H \end{bmatrix} \widetilde{\mathbf{R}}_{ss}{\widetilde{\mathbf{A}}_{21}}^H. \tag{27}$$

Similar to the conventional propagator method, $\widetilde{\mathbf{R}}'$ can be partitioned as

$$\widetilde{\mathbf{R}}' = \left[\mathbf{G}^T \quad \mathbf{Q}^T\right]^T, \tag{28}$$

where $\mathbf{G}$ and $\mathbf{Q}$ are the first K and the last $8(M-2p)-K$ rows, respectively.

A matrix $\mathbf{P}$ (the propagator parameter) is defined to satisfy

$$\mathbf{P} = \min_{\mathbf{P}} \|\mathbf{Q} - \mathbf{P}\mathbf{G}\|^2. \tag{29}$$

The solution of (29) can be obtained as follows:

$$\mathbf{P} = \mathbf{Q}\mathbf{G}^+ = \mathbf{Q}\mathbf{G}^H\left(\mathbf{G}\mathbf{G}^H\right)^{-1}. \tag{30}$$

With the relationship between the propagator parameter and ideal steering matrix, we obtain an equation as

$$\mathbf{P}' = \begin{bmatrix} \mathbf{I} \\ \mathbf{P} \end{bmatrix} = \begin{bmatrix} \mathbf{P}_1 \\ \mathbf{P}_2 \\ \mathbf{P}_3 \\ \mathbf{P}_4 \end{bmatrix} = \begin{bmatrix} \widetilde{\mathbf{A}}_{11} \\ \widetilde{\mathbf{A}}_{11}\boldsymbol{\Phi}_1 \\ \widetilde{\mathbf{A}}_{11}{\boldsymbol{\Phi}_2}^H \\ \widetilde{\mathbf{A}}_{11}\boldsymbol{\Phi}_1{\boldsymbol{\Phi}_2}^H \end{bmatrix} \mathbf{T}_3, \tag{31}$$

where $\mathbf{P}_i$ $(i = 1, 2, 3, 4)$ is the $(2M - 4p) \times K$ matrix and $\mathbf{T}_3$ is the $K \times K$ matrix with rank K.

Similar to ESPRIT, from (31) we can have the equations correlated with azimuths and elevations as

$$\begin{aligned} {\mathbf{P}_1}^+\mathbf{P}_2 &= {\mathbf{T}_3}^{-1}\boldsymbol{\Phi}_1\mathbf{T}_3, \\ {\mathbf{P}_3}^+\mathbf{P}_4 &= {\mathbf{T}_3}^{-1}\boldsymbol{\Phi}_1\mathbf{T}_3, \\ {\mathbf{P}_1}^+\mathbf{P}_3 &= {\mathbf{T}_3}^{-1}{\boldsymbol{\Phi}_2}^H\mathbf{T}_3, \\ {\mathbf{P}_2}^+\mathbf{P}_4 &= {\mathbf{T}_3}^{-1}{\boldsymbol{\Phi}_2}^H\mathbf{T}_3. \end{aligned} \tag{32}$$

To solve the above equation sets and pair the azimuths and elevations, four times eigen-decomposing and $3[K(K + 1)/2 - 1]$ times calculating inner product of vectors are necessary in a general way. Now a method, which needs only once eigen-decomposing and some division operations to obtain and pair the azimuths and the elevations, is introduced with the relationship among the matrix, its eigenvalues, and corresponding eigenvectors.

First eigendecompose ${\mathbf{P}_1}^+\mathbf{P}_2$, and the eigenvalues and the eigenvectors are denoted by λ_{1k} and $\boldsymbol{\rho}_k$ $(k = 1, 2, \ldots, K)$, respectively Then substitute $\boldsymbol{\rho}_k$ into other equations, as the first one of the right equation sets in (32); the corresponding eigenvalue λ_{3k} can be obtained from

$${\mathbf{P}_1}^+\mathbf{P}_3\boldsymbol{\rho}_k = \lambda_{3k}\boldsymbol{\rho}_k. \tag{33}$$

Let ${\mathbf{P}_1}^+\mathbf{P}_3\boldsymbol{\rho}_k = \boldsymbol{\omega}_k$, and λ_{3k} can be expressed by

$$\lambda_{3k} = \frac{1}{K}\sum_{i=1}^{K}\frac{\boldsymbol{\omega}_{ki}}{\boldsymbol{\rho}_{ki}}, \tag{34}$$

where $\boldsymbol{\omega}_{ki}$ and $\boldsymbol{\rho}_{ki}$ are the ith element of $\boldsymbol{\omega}_k$ and $\boldsymbol{\rho}_k$, respectively.

Assume that λ_{2k} and λ_{4k} denote the corresponding eigenvalues of ${\mathbf{P}_3}^+\mathbf{P}_4$, and ${\mathbf{P}_2}^+\mathbf{P}_4$ respectively, and they can be calculated by (34).

Using the relationship among λ_{ik} $(i = 1, 2, 3, 4)$, u_k, v_k, α_k, and β_k, the elevation α_k and the azimuth β_k of the kth source can be represented as

$$\alpha_k = \frac{\{\arcsin\{\arg(\lambda_{3k})/\pi\} + \arcsin\{\arg(\lambda_{4k})/\pi\}\}}{2},$$

$$\beta_k = \frac{\{\arccos\{-\arg(\lambda_{1k})/\pi\cos\alpha_k\} + \arccos\{-\arg(\lambda_{2k})/\pi\cos\alpha_k\}\}}{2}. \tag{35}$$

Now give the computation load on the proposed method and PM algorithm with known mutual coupling. The computation load on PM algorithm with known mutual coupling is focused on the inverse of MCM, cross matrix of output of elements on x-axis and z-axis, eigen-decomposing a matrix with rank K, and pairing the parameters, so the computation load is $O((4M + 2)^3) + N(2M + 1)^2 + O(4K^3) + 3K^2[K(K + 1)/2 - 1]$ (N is the snapshots number); the computation load on the proposed method is focused on cross matrix of output of elements on x-axis and z-axis, once eigen-decomposing a matrix with rank K, and pairing the parameters, so the computation load is $N(2M - 4p + 2)^2 + O(K^3) + 3K(K^2 + K)$.

Finally, the necessary conditions for the proposed method are given as follows:

(1) for unique estimation, $2(M - 2p) > K$ is required;

(2) the sources can not be located at the blind angles which make the determinant of $\mathbf{T}_1$ or $\mathbf{T}_2$ zero.

4. Simulation Experiments

In this section, we carry out some representative simulation experiments to demonstrate the validity of the proposed calibration method. In all the experiments, we assume there are two uncorrelated equivalent-power sources at (20°, 10°) and (80°, 60°) that impinge on the cross array which consists of 53 elements ($M = 13$). The mutual coupling degree of freedom p is two and the coefficients of mutual coupling are denoted by $b_1 = 0.3065 + 0.3951j$, $b_2 = 0.1018 - 0.1721j$, and $d_{11} = 0.2154 - 0.2738j$.

In the first experiment, the 2-D spatial spectrums of the PM algorithm with unknown mutual coupling, the PM algorithm with known mutual coupling, and the proposed method (estimate the 2-D DOAs to get the coefficients of mutual coupling with the method in [7]) are shown in Figures 2 to 4 in the condition that the signal-to-noise ration (SNR) is 5 dB and the number of the snapshots is 300.

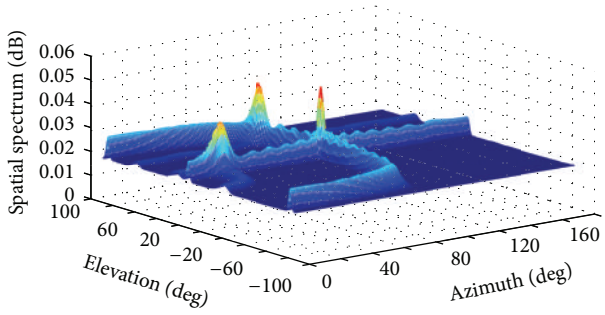

Figure 2: 2-D spatial spectrum of the PM algorithm in the presence of unknown mutual coupling.

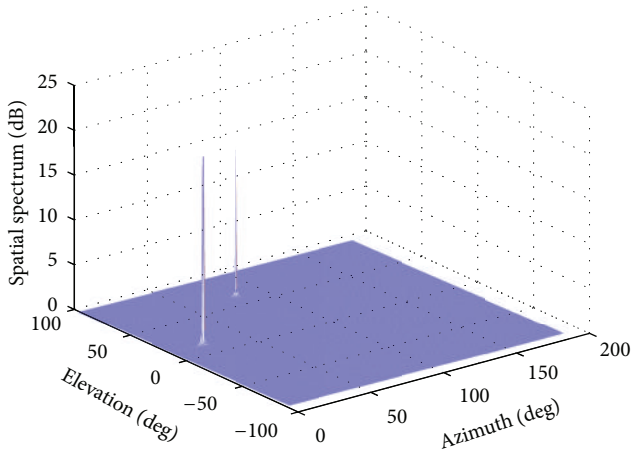

Figure 3: 2-D spatial spectrum of the PM algorithm in the presence of known mutual coupling.

From Figure 2 we can see that the PM algorithm without calibration has very poor resolution in the presence of mutual coupling. Though the peaks appear at the signal directions, there exist lots of pseudopeaks especially at $(80^\circ, 10^\circ)$ whose spatial spectrum is greater than the sources', which may result in the inaccurate estimation.

Comparing with Figure 4 and Figure 3, the spatial spectrum of proposed method has two sharp peaks at the signal directions, which is also shown in Figure 3. In other words, the proposed method can restrain the effects of mutual coupling and has a high resolution. Though the performance of proposed method is worse than that in Figure 3 for reasons of the array elements consumption, it eliminates pseudo peaks caused by mutual coupling, which can distinguish the two sources visibly.

In the second experiment, the effect of SNR on the performance of proposed method is explored. The number of snapshots is 300 and the SNR varies from −10 to 10 dB with the interval 1 dB. The root mean square error (RMSE) which is defined as (36) is shown in Figure 5 with 100 independent experiments:

$$\text{RMSE} = \frac{1}{2}\sum_{k=1}^{2} E\left\{\sqrt{\left(\widehat{\alpha}_k - \alpha_k\right)^2 + \left(\widehat{\beta}_k - \beta_k\right)^2}\right\}. \quad (36)$$

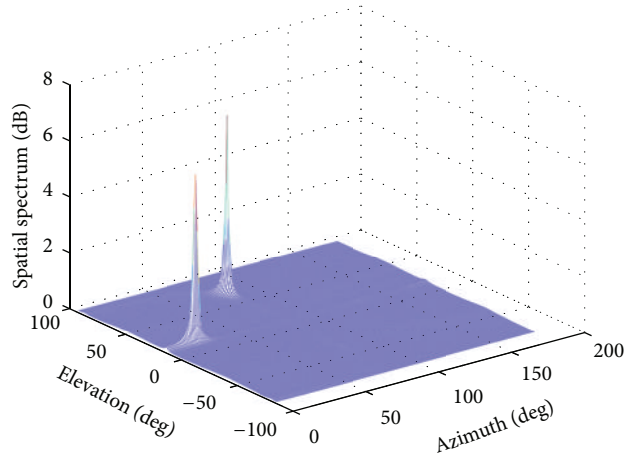

Figure 4: 2-D spatial spectrum of the proposed method.

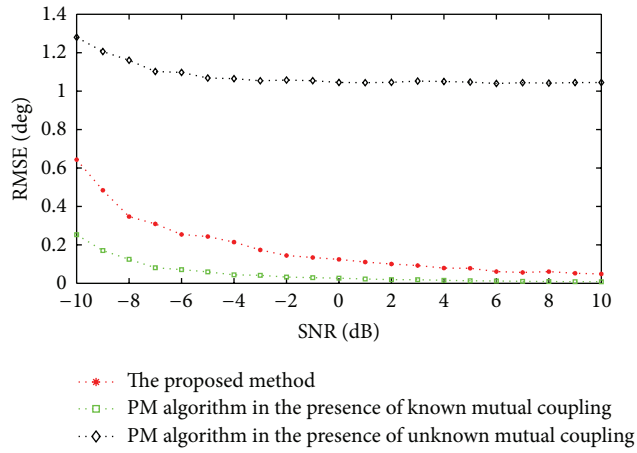

Figure 5: RMSE versus SNR.

The simulation results show the proposed method has an obvious performance improvement over the PM algorithm with unknown coupling, though it is a little inferior to the PM algorithm with known coupling as we think. As the SNR increases, the difference of the RMSE between the proposed method and the PM algorithm with known coupling gets closer; however, the accuracy of DOA estimates of the PM algorithm with unknown coupling stays at a low level as the main error is caused by the manifold error between the ideal and the actual one.

In the last experiment, the influence of the number of the snapshots on the performance of proposed method is investigated. SNR is 0 dB and the number of the snapshots varies from 100 to 800 with the interval 100. 100 independent experiments are carried out, and the RMSE curves are shown in Figure 6.

From Figure 6 we can see that the result is similar to that of the second experiment: the capability of proposed method is close to the one of the PM algorithm with known coupling, and the performance of the PM algorithm with unknown coupling is still poor when the number of the snapshots increases.

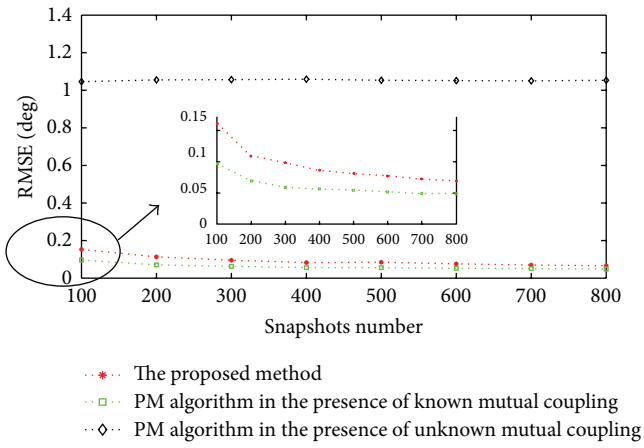

FIGURE 6: RMSE versus number of snapshots.

From the above three experiments, it is seen that the proposed method has compensated the effect caused by mutual coupling. It provides a significant improvement of DOA estimation accuracy and can achieve almost the same performance as that of PM algorithm with known mutual coupling.

5. Conclusion

A method compensating the effect of the mutual coupling is proposed for cross array to estimate the 2-D DOA. This method is based on PM algorithm and rotational invariance techniques for ULA. It can compensate the effect of the mutual coupling without any calibration sources, and it does not require any iterative procedure or spectral peak search. Simulations have shown that the proposed method can improve the DOA estimation accuracy well.

Conflict of Interests

The authors declare that there is no conflict of interests regarding the publication of this paper.

Acknowledgments

The authors would like to thank the editor and reviewers for their helpful comments and suggestions. In addition, this work is supported by the National High Technology Research and Development Program of China (863 Program) under Grant 2012AA0601101, the Key Laboratory of Intelligent Perception and Systems for High-Dimensional Information (Nanjing University of Science and Technology), Ministry of Education under Grant 3092013012205, and Research Fund for the Doctoral Program of Higher Education of China under Grant 20133219110027.

References

[1] C. Roller and W. Wasylkiwskyj, "Effects of mutual coupling on super resolution DF in linear arrays," in *Proceedings of the IEEE International Conference on Acoustics, Speech, and Signal Processing*, vol. 5, pp. 257–260, March 1992.

[2] A. J. Weiss and B. Friedlander, "Mutual coupling effects on phase-only direction finding," *IEEE Transactions on Antennas and Propagation*, vol. 40, no. 5, pp. 535–541, 1992.

[3] B. Friedlander and A. J. Weiss, "Direction finding in the presence of mutual coupling," *IEEE Transactions on Antennas and Propagation*, vol. 39, no. 3, pp. 273–284, 1991.

[4] F. Sellone and A. Serra, "A novel online mutual coupling compensation algorithm for uniform and linear arrays," *IEEE Transactions on Signal Processing*, vol. 55, no. 2, pp. 560–573, 2007.

[5] B.-H. Wang, Y.-L. Wang, and H. Chen, "A robust DOA estimation algorithm for uniform linear array in the presence of mutual coupling," in *Proceedings of the IEEE Antennas and Propagation Society International Symposium*, vol. 3, pp. 924–927, June 2003.

[6] M. Lin and L. Yang, "Blind calibration and DOA estimation with uniform circular arrays in the presence of mutual coupling," *IEEE Antennas and Wireless Propagation Letters*, vol. 5, no. 1, pp. 315–318, 2006.

[7] X. Hu, H. Chen, Y. Wang, and J. Chen, "A self-calibration algorithm for cross array in the presence of mutual coupling," *Science China Information Sciences*, vol. 54, no. 4, pp. 836–848, 2011.

[8] Z. Ye, J. Dai, X. Xu, and X. Wu, "DOA estimation for uniform linear array with mutual coupling," *IEEE Transactions on Aerospace and Electronic Systems*, vol. 45, no. 1, pp. 280–288, 2009.

[9] Z. Ye and C. Liu, "2-D DOA estimation in the presence of mutual coupling," *IEEE Transactions on Antennas and Propagation*, vol. 56, no. 10, pp. 3150–3158, 2008.

[10] C. Liu, Z. Ye, and Y. Zhang, "Autocalibration algorithm for mutual coupling of planar array," *Signal Processing*, vol. 90, no. 3, pp. 784–794, 2010.

Hindawi Publishing Corporation
International Journal of Antennas and Propagation
Volume 2014, Article ID 405487, 10 pages
http://dx.doi.org/10.1155/2014/405487

Research Article

Self-Interference Cancellation-Based Mutual-Coupling Model for Full-Duplex Single-Channel MIMO Systems

Pawinee Meerasri, Peerapong Uthansakul, and Monthippa Uthansakul

School of Telecommunication Engineering, Suranaree University of Technology, Muang, Nakhon Ratchasima 30000, Thailand

Correspondence should be addressed to Peerapong Uthansakul; uthansakul@sut.ac.th

Received 26 July 2013; Revised 1 December 2013; Accepted 2 December 2013; Published 16 January 2014

Academic Editor: Hon Tat Hui

The challenge of a full-duplex single-channel system is the method to transmit and receive signals simultaneously at the same time and on the same frequency. Consequently, a critical issue involved in such an operation is the resulting self-interference. Moreover, for MIMO system, the full-duplex single-channel system is subjected to the very strong self-interference signals due to multiple transmitting and receiving antennas. So far in the pieces of literature, there have not been any suitable techniques presented to reduce the self-interference for full-duplex single-channel MIMO systems. This paper initially proposes the method to cancel the self-interference by utilizing the mutual-coupling model for self-interference cancellation. The interference can be eliminated by using a preknown interference, that is, the mutual-coupling signals. The results indicate that the channel capacity performance of the proposed technique can significantly be improved due to the reduction of the self-interference power. The measurement results indicate that the proposed MIMO system can suppress the self-interference and mutual-interference signals with the reduction of 31 dB received power.

1. Introduction

Nowadays, multiple-input multiple-output (MIMO) system is the promising technology for the next generation of wireless communication systems as MIMO system can provide a wide coverage area, a high spectral efficiency, and an increased system capacity. The MIMO system employs the multiple antennas to transmit signals on the same frequency which cause the strong interference signals at the receiving antennas on the same side. These interferences are more pronounced when operating the full-duplex single-channel MIMO system.

The full-duplex single-channel system is one of the most interesting technologies for future wireless communications because it can offer double throughput from any conventional system without paying any expenses of spectrum. This is because the system is able to receive and transmit simultaneously within a single channel. In the literature, the problem of full-duplex interference has been addressed on the specific configuration of MIMO relay nodes. The self-interference cancellation is introduced to be used at only relaying node [1–3]. So far there have not been any techniques proposed for source or destination. In this light, the authors propose the new technique to suppress the self-interference for full-duplex single-channel MIMO systems. From the literature on RF interference cancellation, the work in [4–9] presents a full-duplex wireless system that can transmit and receive signals at the same time and on the same frequency band since it requires at least two antennas having one for transmitter (Tx) and one for receiver (Rx). The key challenge in realizing such a system lies in addressing the self-interference generated by the Tx antenna at the Rx antenna. For example, one can implement the above self-interference cancellation idea completely in analog domain using noise cancellation circuits reported by Radunovic et al. [5]. But the practical noise cancellation circuits can only handle a dynamic range of at most ~30 dB. Another technique in [6] employs the antenna cancellation by using three antennas to create a beam forming null. This method cancels the self-interference at the receiver antenna by using antenna placement as an additional cancellation technique or antenna cancellation. The antenna cancellation requires two asymmetrically placed transmitting

antennas and one receiving antenna. This three-antenna system can remove ~60 dB reduction of self-interference power for a802.15.4 system. Although it looks promising, the antenna cancellation-based designs have two major limitations. The first is that they require three antennas having two transmitting antennas and one receiving antenna, which are very sensitive to the relative location of antennas and any material around them. It is a fact that the full-duplex system can have double throughput, but with three antennas a MIMO system can have triple throughput. Hence, the use of multiple antennas for only full-duplex purpose is not worth. The second limitation is a bandwidth constraint, a theoretical limit which prevents supporting wideband signal such as WiFi.

The MIMO techniques for wireless communications have been studied extensively over the past decade as a means of achieving significant capacity gains needed for supporting high-rate wireless broadband applications [10]. A critical factor in the design and analysis of MIMO systems is the theoretical models which are used for representing the MIMO transceiver as well as the wireless fading channel. So far in the literature, the factor on realistic channel configuration has gained a lot of attention such as spatial correlation (see, e.g., [11, 12] and many others). One issue which has received less attention in comparison is that of mutual coupling [10, 13–15], which occurs due to electromagnetic interactions between the antennas in both transmitter and receiver. This effect, as well as spatial correlation, is particularly significant for applications with compact antennas, such as cellular mobile, in which the available space for placing the antennas is highly restrictive.

In this paper, we will investigate the effect of antenna mutual coupling (MC) on the full-duplex single-channel MIMO system with the aim of self-interference eliminations. Based on the mutual-coupling model, the signals with self-interference can be preknown. As a result, it is possible to eliminate all self-interference signals by subtracting from preknown signals. The concept of transmitting and receiving mutual impedances is employed to incorporate the antenna MC effect into the correlated channel model [16]. This model is applied to work out the suppression technique to reduce the self-interference performed by subtracting the interference signals from the transmitting signals that are suitably tuned according to the interaction between multiple antennas. This is because the self-interference signals do not depend on the environments. Then, the proposed technique can be done on the manufacturing process. The paper presents the comparison between the MC full-duplex single-channel systems with and without the proposed technique. The channel capacity performance is the key performance used to indicate the merit of proposed technique. The results show that the proposed technique is not only to suppress the interference but also to improve the system performance capacity.

2. Problem Formulation

This paper focuses on the full-duplex wireless communications operating on the same frequency and at the same time. The simultaneous transmitting and receiving signals can be achieved via the cancellation of the self-interference signal. However, the problem is that the self-interference is billions of times stronger (60–90 dB) than a received signal; for example, for WiFi the self-interference would be nearly up to 80 dB stronger. Hence, the main key success is to eliminate the self-interference as much as possible. In this section, the overview of full-duplex system is presented in order to be the basic knowledge before getting to the main problem of this work. Next, the survey of RF interference cancellation techniques is detailed.

2.1. Full-Duplex Wireless Communication. Currently, full-duplex wireless systems achieve the isolation required between the two directions of communication using independence in either time or frequency. Accordingly, these duplexings are called time division duplexing (TDD) and frequency division duplexing (FDD). The TDD system is the system that divides the access of each node in time. TDD is also commonly known as half-duplexing. Other full-duplex wireless systems separate the Tx and Rx functions in the frequency domain, the so-called FDD, and may operate using two different carrier frequencies for carrying transmissions. In this case, nodes 1 and 2 can send data to each other at the same time, although using two different frequencies. The use of different frequencies prevents the two signals from interfering with each other, even though the two transmissions occur at the same time. Time division duplexing exacerbates the inconsistency in the channel views across nodes. Since only one node among a pair of communicating nodes can transmit at a given time, the wireless channel around the transmitting node may look occupied, while the wireless channel around the receiving node may look unoccupied. Such inconsistencies are the root cause of many of the problems with time division duplexing wireless networks, such as packet losses due to hidden terminal effects. On the other hand, frequency division duplexing requires a wireless node to use twice the frequency bandwidth for sending and receiving signals of a given bandwidth. In some cases, this is expensive and infeasible. The key challenge in implementing a full-duplex wireless system, where a device can simultaneously transmit and receive signals over-the-air at the same time and in the same frequency band, is the large power differential between the self-interference from a node's own transmission and the signal of interest coming from a distant source.

2.2. Single-Channel Full-Duplex Wireless Communications. A basic perception of wireless communication is that a radio cannot transmit and receive on the same frequency and at the same time. As wireless signals attenuate quickly over distance, the signal from a local transmitting antenna is hundreds of thousands of times stronger than transmissions from other nodes. Figure 1 shows an example where nodes 1 and 2 are trying to send data to each other simultaneously using the same frequency. Node 1 own transmission is much stronger at its receiving antenna, compared to the signal it receives from node 2. With such strong self-interference, the receiver

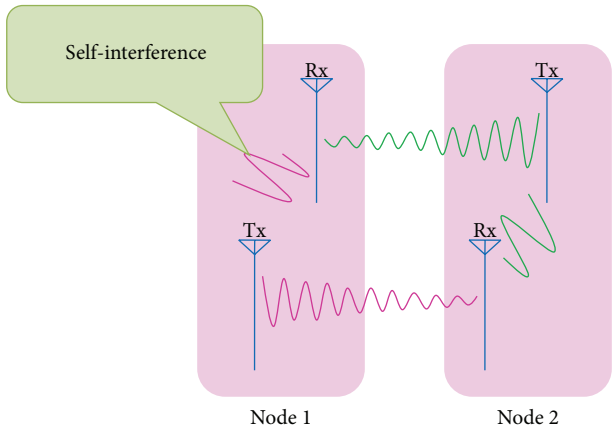

Figure 1: Self-interference in the single-channel full-duplex wireless communications using one transmitting antenna and one receiving antenna.

of node 1 is unable to decode any signals that node 2 is trying to send to node 1. This example shows that the biggest challenge in designing single-channel full-duplex wireless communications is to eliminate the self-interference signal from the receiver of the wireless node. In theory, this problem should be easy to solve. For a system with antennas each for transmitting and receiving, since the system knows the signal of transmitting antenna, it can subtract this from the signal of receiving antenna and decode the remainder.

2.3. Self-Interference Cancellation. The work in [17] proposed the design of full-duplex system that requires only one antenna using circulator to share the same antenna for transmitting and receiving paths as shown in Figure 2. The self-interference cancellation (SIC) uses the knowledge of transmission to cancel self-interference in the RF signal before it is digitized. In an ideal analog cancellation scenario, the amplitudes from the two paths would be perfectly matched at the receiver and phase of the two signals would differ by exact π. To cancel self-interference, the best performing prior design is obtained. The authors gain the inverse of the transmitted signal using a phase shifter with attenuator. The attenuator and phase shifter allow a modulator to control the angle and amplitude of a feed signal.

3. System Model

3.1. MIMO Model. In this section, the capacity formula of MIMO systems is briefly given. We assume an independent and identically distributed (i.i.d.) Rayleigh flat-fading channel in rich scattering environments, and the channel is unknown at the transmitter and perfectly known at the receiver. The basic MIMO structure is depicted in Figure 3. Let the number of transmitting and receiving antennas be N_T and M_R, respectively. We denote this MIMO communication link as (N_T, M_R). The $M_R \times 1$ received signal vector $\mathbf{y}$ can be written as

$$\mathbf{y} = \mathbf{H}\mathbf{x} + \mathbf{n}, \tag{1}$$

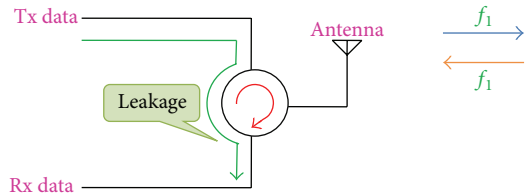

Figure 2: Self-interference in the single-channel full-duplex single-antenna wireless communications.

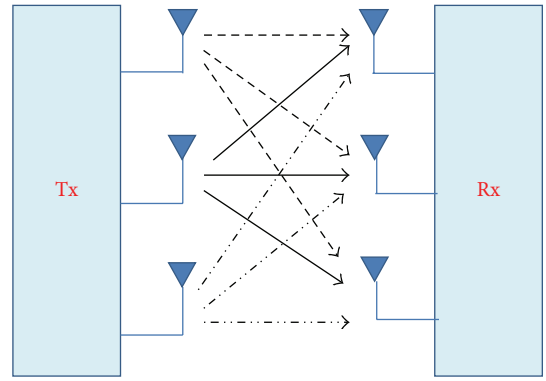

Figure 3: Basic structure of MIMO system.

with this notation channel output sequence that can be written in matrix form as

$$\begin{bmatrix} y_1 \\ y_2 \\ \vdots \\ y_{M_R} \end{bmatrix} = \begin{bmatrix} h_{11} & h_{12} & \cdots & h_{1N_T} \\ h_{21} & h_{22} & \cdots & h_{2N_T} \\ \vdots & \vdots & \ddots & \vdots \\ h_{M_{R^1}} & h_{M_{R^2}} & \cdots & h_{M_{R^{N_T}}} \end{bmatrix} \begin{bmatrix} x_1 \\ x_2 \\ \vdots \\ x_{N_T} \end{bmatrix} + \begin{bmatrix} n_1 \\ n_2 \\ \vdots \\ n_{M_R} \end{bmatrix}, \tag{2}$$

where $\mathbf{H}$ is $M_R \times N_T$ channel matrix with the entry $h_{i,j}$ describing the channel gain between the jth transmitting antenna and the ith receiving antenna, $\mathbf{x}$ is $N_T \times 1$ transmitted signal vector with independent symbols, and $\mathbf{n}$ is $M_R \times 1$ additive white Gaussian noise (AWGN) vector.

The AWGN vector $\mathbf{n}$ satisfies $E\{\mathbf{n}\mathbf{n}^H\} = \mathbf{I}_{M_R}$ in which $\mathbf{n}^H$ denotes the conjugate transpose of $\mathbf{n}$ and $\mathbf{I}_{M_R}$ denotes $M_R \times M_R$ identity matrix.

As the channel is unknown at the transmitter, equal power is allocated to each of the transmitting antennas. Then the MIMO capacity in bits per second per Hertz (bps/Hz) is derived as

$$C = \log_2 \det\left(\mathbf{I}_{M_R} + \frac{\rho}{N_T}\mathbf{H}\mathbf{H}^H\right), \tag{3}$$

where ρ is the average received signal to noise ratio (SNR). $\mathbf{H}$ is normalized channel matrix [18].

3.2. Mutual-Coupling Effects on MIMO. In this section, in order to support parallel signal transmission in a MIMO system, the antennas at transmitter and receiver have to be properly coupled to the modes offered by the wireless communication channel. Hence, in Figure 4, the array elements

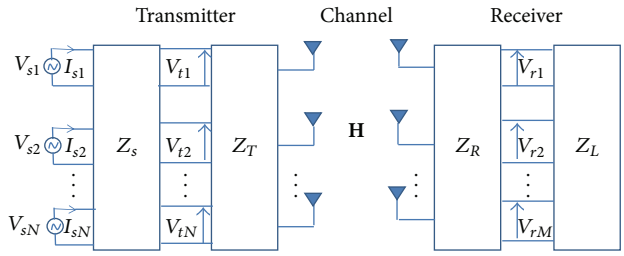

FIGURE 4: An $M_R \times N_T$ MIMO system based on mutual-coupling model.

location (including spacing and orientation) with respect to the scatterers is of paramount importance in the operation of the MIMO system. The interactions between the entire set of antennas and scatterers are initially described by the impedance matrix $\mathbf{Z}$. For dipoles, however, the mutual impedance can easily be calculated using classical induced electromagnetic force (EMF) method [19]. The value of the mutual impedance between the mth and nth dipoles Z_{mn} is given by [20]

$$Z_{mn} = \begin{cases} 30\left[0.5772 + \ln\left(\beta d_{\text{lam}}\right) - C_i\left(\beta d_{\text{lam}}\right)\right] \\ \quad + j\left[30 S_i\left(\beta d_{\text{lam}}\right)\right] & m = n, \\ 30\left[2C_i\left(u_0\right) - C_i\left(u_1\right) - C_i\left(u_2\right)\right] \\ \quad - j\left[30\left(2S_i\left(u_0\right) - S_i\left(u_1\right) - S_i\left(u_2\right)\right)\right] & m \neq n, \end{cases} \tag{4}$$

where $\beta = 2\pi/d_{\text{lam}}$ is the wave number, $d_{\text{lam}}/2$ is the dipole length, and the constants are given by [20]

$$\begin{aligned} u_0 &= \beta d_h, \\ u_1 &= \beta\left(\sqrt{d_h^2 + \left(d_{\text{lam}}/2\right)^2} + \left(d_{\text{lam}}/2\right)\right), \\ u_2 &= \beta\left(\sqrt{d_h^2 + \left(d_{\text{lam}}/2\right)^2} - \left(d_{\text{lam}}/2\right)\right), \end{aligned} \tag{5}$$

where d_h is the horizontal distance between the two dipole antennas and $C_i(u)$ and $S_i(u)$ are the cosine and sine integrals, respectively:

$$C_i\left(u\right) = \int_{\infty}^{u} \frac{\cos\left(x\right)}{x} dx, \qquad S_i\left(u\right) = \int_{0}^{u} \frac{\sin\left(x\right)}{x} dx. \tag{6}$$

It has to be noted that, while calculating Z_{mn}, we assume that the nth dipole is excited with current, while all the remaining dipoles are open circuited.

In general, mutual coupling can be characterized by numerical modelling techniques [19]. However, for dipoles, we can use analytical mutual coupling into the MIMO system model. The coupling matrix of transmitting antenna array $\mathbf{C}_T$ can be written using fundamental electromagnetic and circuit theory [19]. $\mathbf{C}_T$ has the meaning of transfer function matrix for the transmitting array and is given as

$$\mathbf{C}_T = \left(Z_A + Z_T\right)\left(\mathbf{Z} + Z_T \mathbf{I}_{N_T}\right)^{-1}, \tag{7}$$

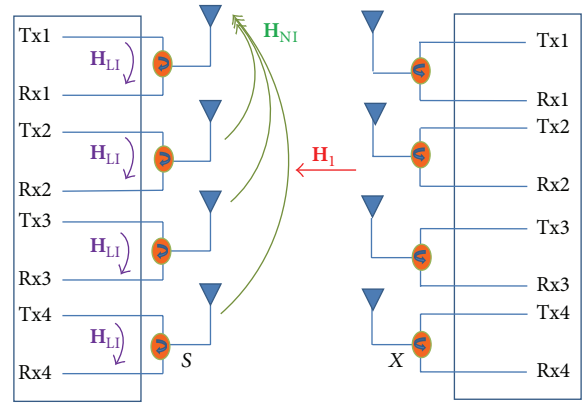

FIGURE 5: Model of full-duplex single-channel 4 × 4 MIMO system.

where Z_A is the element's impedance in isolation. The element Z_{mn} of matrix $\mathbf{Z}$ is defined by using the EMF method as described in (4). Also the coupling matrix of receiving antenna array $\mathbf{C}_R$ can be determined in a similar manner. $\mathbf{C}_R$ has the meaning of transfer function matrix for the receiving array and is given as

$$\mathbf{C}_R = \left(Z_A + Z_T\right)\left(\mathbf{Z} + Z_T \mathbf{I}_{M_R}\right)^{-1}. \tag{8}$$

4. Proposed Self-Interference Cancellation

In this section, we consider a generic MIMO radio unit equipped with M_R RF receivers antennas and N_T RF signal generators/transmitters. Among all generators, there are $N_s = N_T - M_R$ primary generators and M_R auxiliary generators. The primary generators are used to transmit up to N_S independent streams of data. The auxiliary generators are used to generate RF waveforms for SIC at the RF frontend of the receivers on the same frequency. See Figure 5.

Furthermore, we index the receiver by $k = 1, \ldots, M_R$ and the transmitter by $k = M_R + 1, \ldots, N_T$. Then, for each transmitted data packet subject to linear modulation, a RF signal stream transmitted from the kth generator ideally can be expressed by $\widetilde{x_k}(t) = \text{Re}\{x_k(t)\exp(j2\pi f_c t)\}$, where f_c is the carrier frequency and

$$x_k\left(t\right) = \sum_{i=1}^{I} g_k^{(i)}\left(t\right) * \sum_{n=-L}^{N-1} s_n^{(i)} p\left(t - nT\right), \tag{9}$$

where $x_k(t)$ is the complex baseband form (also called I/Q waveform) of $\widetilde{x_k}(t)$. Here, $g_k^{(i)}(t)$ is the complex impulse response of the kth transmission for data stream i (of total I streams), $s_n^{(i)}$ is the complex symbol sequence for data stream i, $N + L$ is the number of complex symbols per stream (including the L prefixed symbols as used in OFDM system), and $p(t)$ is the fundamental pulse waveform used for linear pulse modulation, which has the double-sided bandwidth W and the effective duration T. For high spectral efficiency, it is typical that T is equal to or only slightly larger than $1/W$. The operator $*$ denotes convolution.

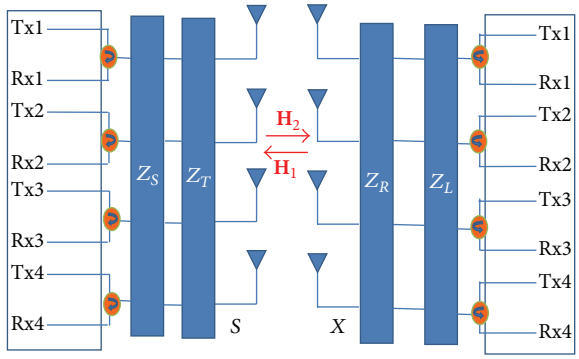

FIGURE 6: 4 × 4 MIMO system with mutual-coupling model.

The RF self-interference received by the by the lth receiver is $\widetilde{y}_l(t) = \mathrm{Re}\{y_l(t)\exp(j2\pi f_c t)\}$, where $l = 1,\ldots,M_R$, and $y_l(t) = \sum_{k=1}^{N_T} h_{\mathrm{mc}_{l,k}}(t) * x_k(t) = \sum_{i=1}^{I}([\sum_{k=1}^{N_T} h_{\mathrm{mc}_{l,k}}(t) * g_k^{(i)}(t)] * \sum_{n=0}^{N-1} s_n^{(i)} t(t-nT))$ is the I/Q waveform of $\widetilde{y}_l(t)$. In Figure 6, when the mutual coupling is presented, $h_{l,k}(t)$ is the complex baseband channel impulse response from the kth generator to the lth receiver on the same radio. Hence, the channel matrix $h_{l,k}(t)$ obtained from the case that this effect is absent has to be pre- and postmultiplied by coupling matrices $\mathbf{C}_R$ and $\mathbf{C}_T$. As a result, the new channel matrix is given by $\mathbf{H}_{\mathrm{mc}} = \mathbf{C}_R\mathbf{H}\mathbf{C}_T$. To cancel the RF self-interference $\widetilde{y}_l(t)$ for all l and t, it is necessary to find $g_k^{(i)}(t)$ for all k and i such that $y_l(t) = 0$ for all l or equivalently $\sum_{k=1}^{N_T} h_{\mathrm{mc}_{l,k}}(t) * g_k^{(i)}(t) = 0$ for all l and i. The matrix form of this condition is

$$\begin{bmatrix} h_{\mathrm{mc}_{1,1}}(t) & \cdots & h_{\mathrm{mc}_{1,N_T}}(t) \\ \cdots & \cdots & \cdots \\ h_{\mathrm{mc}_{M_R,1}}(t) & \cdots & h_{\mathrm{mc}_{M_R,N_T}}(t) \end{bmatrix} * \begin{bmatrix} g_1^{(i)}(t) \\ \cdots \\ g_{N_T}^{(i)}(t) \end{bmatrix} = 0 \quad (10)$$

or equivalently in more compact form:

$$\mathbf{H}_{\mathrm{mc}}(t) * \mathbf{g}^{(i)}(t) = 0. \quad (11)$$

Although given in baseband, (11) ensures SIC even at the RF frontend. Also note that when all elements in a row of $\mathbf{H}_{\mathrm{mc}}(t)$ are corrupted by a common scalar due to receiver phase noise, the solution $\mathbf{g}^{(i)}(t)$ to (11) is not affected.

To find the solution to (10), we need to apply a known notion of vector space in the field of functions of time. The rank $r_{\mathbf{H}(t)}$ of the matrix $\mathbf{H}_{\mathrm{mc}}(t)$ that are convolutely independent. It follows that $r_{\mathbf{H}(t)} \le \min\{M_R, N_T\} = M_R$. The dimension of the solution space of (10), which is also called the dimension of the (right) null space of $\mathbf{H}_{\mathrm{mc}}(t)$, is the number of convolutely independent solutions to (10), which is $d_{\mathrm{null}} = N_T - r_{\mathbf{H}(t)} \ge N_s$. If $d_{\mathrm{null}} = N_s$, we call it a typical case (very likely in practice), or otherwise, if $d_{\mathrm{null}} > N_s$, we call it atypical case (not very likely in practice). The number I of the data streams in (9) must be no larger than d_{null}.

In general, for $M_R \ge 1$ and $N_s \ge 1$, the ith in a set of N_s convolutely independent solutions to (12) can be written as

$$\mathbf{g}^{(i)}(t) = \begin{bmatrix} \overline{\mathbf{g}}^{(i)}(t) \\ \mathbf{0}_{i-1,1} \\ g_0^{(i)}(t) \\ \mathbf{0}_{I-1,1} \end{bmatrix}, \quad (12)$$

where $\mathbf{0}_{m,1}$ is the $m \times 1$ zero vector and $\overline{\mathbf{g}}^{(i)}(t)$ and $g_0^{(i)}(t)$ are a solution to $\mathbf{A}(t) * \overline{\mathbf{g}}^{(i)}(t) + \mathbf{b}_i(t) * g_0^{(i)}(t) = 0$, where $\mathbf{A}(t)$ is a square matrix equal to $\mathbf{H}_{\mathrm{mc}}(t)$ without its last N_s columns and $\mathbf{b}_i(t)$ is the $(M_R + i)$th column of $\mathbf{H}_{\mathrm{mc}}(t)$. Furthermore, we can choose the solution

$$\overline{\mathbf{g}}^{(i)}(t) = -\mathrm{adj}\{\mathbf{A}(t)\} * \mathbf{b}_i(t), \quad (13)$$

and $g_0^{(i)}(t) = \det\{\mathbf{A}(t)\}$. Both the adjoint adj{$\mathbf{A}(t)$}and the determinant det{$\mathbf{A}(t)$} can be obtained analytically in the same way as those of a matrix of numbers as shown in [21] except that all multiplications should be substituted by convolutions. It is important to note that expression (13) does not involve any division but only convolutions and sums.

The solutions shown in (12) are valid for arbitrary $\mathbf{H}_{\mathrm{mc}}(t)$ as long as $\det\{\mathbf{A}(t)\} \ne 0$. This condition can be met if $h_{k,k}(t)$ for $k = 1,\ldots,M_R$ have the largest norms among $h_{l,k}(t)$ for all l and k. To ensure that, we can either place the M_R auxiliary transmitting antennas close enough to the M_R receiving antennas or directly couple the M_R auxiliary generators to the M_R receivers at the RF frontend.

In this section, the proposed system is designed to formulate the self-interference based on mutual-coupling model. These self-interference signals are caused by multiple antennas. The proposed system for full-duplex single-channel MIMO system is illustrated in Figure 7. As shown in Figure 7, the self-interference based on mutual-coupling $\mathbf{H}_{\mathrm{mc}_I}$ can be written as

$$\mathbf{H}_{\mathrm{mc}_I}\mathbf{s} = \mathbf{H}_{\mathrm{LI}}\mathbf{s} + \mathbf{H}_{\mathrm{NI}}\mathbf{C}_R\mathbf{s}, \quad (14)$$

where $\mathbf{s} \in C^{s\times 1}$ is the transmitted signal, $\mathbf{H}_{\mathrm{LI}} \in C^{s\times s}$ is a diagonal matrix that represents the self-interference signals, and $\mathbf{H}_{\mathrm{NI}} \in C^{s\times s}$ is a symmetric matrix that represents the mutual-interference signals caused by the other antennas.

Next, the proposed method to suppress the interference signals is performed as shown in Figure 7. The transmitted signals are coupled to matrix W in order to perform the negative self-interference and mutual-interference signals as closely as possible. Inside matrix W, the attenuation and phase shifter are employed to adjust the preknown signals for compensating the self-interference signals and mutual-interference signals. The compensation matrix, $\mathbf{W}$, is given by

$$\mathbf{W}\mathbf{s} = \mathbf{T}_x\mathbf{C}_T\mathbf{s} + \mathbf{G}\mathbf{s}, \quad (15)$$

where $\mathbf{T}_x \in C^{s\times s}$ is a symmetric matrix that represents the mutual-interference signals caused by the other antennas,

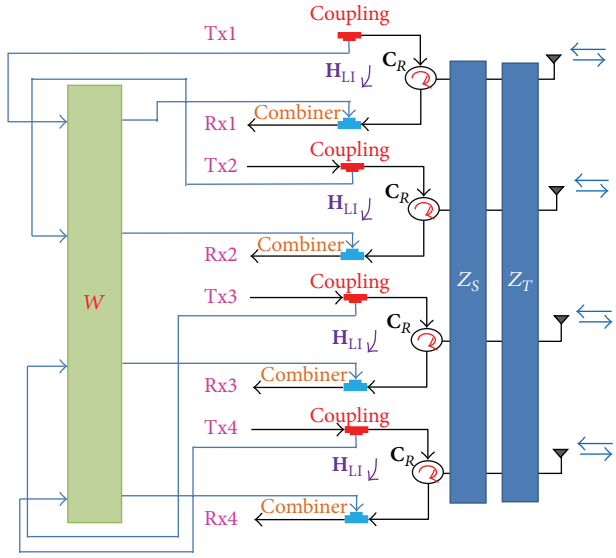

FIGURE 7: Proposed self-interference cancellation for full-duplex single-channel 4 × 4 MIMO system based on mutual-coupling model.

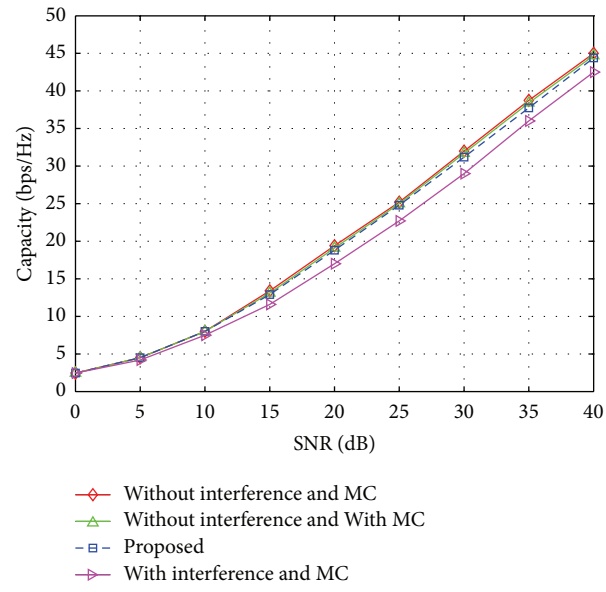

FIGURE 8: Channel capacity versus SNR for 80% interference reduction.

$\mathbf{G} \in C^{s\times s}$ is a diagonal matrix that represents the self-interference signals.

Then, the received signal at the destination with the proposed compensation matrix for the interference suppression can be rewritten as

$$\mathbf{y} = \mathbf{H}_{\text{mc}}\mathbf{x} + \mathbf{H}_{\text{mc}_I}\mathbf{s} - \mathbf{W}\mathbf{s} + \mathbf{N}, \tag{16}$$

where $\mathbf{N} \sim \text{CN}(0, \sigma_d^2\mathbf{I}_s)$ is the AWGN contribution at the destination.

5. Results and Discussion

5.1. Channel Capacity. In order to investigate the effect of mutual coupling on MIMO capacity, in this section the channel capacity for our 4 × 4 MIMO system can be given by (17) [2]. This capacity denotes the average of channel capacity in bps/Hz. Also, we assume the uniform transmitting power for each antenna ($E\{\mathbf{x}\mathbf{x}^H\} = (P_0/N_s)\mathbf{I}_x$). Consider

$$C = \log_2 \det\left[\mathbf{I}_s + \frac{P_0}{N_s}\mathbf{H}_{\text{mc}}\mathbf{H}_{\text{mc}}^H \times\left(\sigma_I^2\mathbf{H}'_{\text{mc}_I}\mathbf{H}'^H_{\text{mc}_I} + \sigma_d^2\mathbf{I}_s\right)^{-1}\right]. \tag{17}$$

We assume that P_0 is the maximum available power at the source and N_s is the power of the self-interference signals.

The performance of channel capacity is presented by considering four cases. The first case is that there is neither self-interference nor mutual-coupling effect (called without interference and MC) in the system. In the second case, there is no interference but including mutual-coupling effect (called without interference and with MC). The third case is the case that the system uses the self-interference cancellation and there is a mutual-coupling effect in the systems (called proposed). For the last case, the system experiences both interference and mutual-coupling effect but no any cancellation technique is applied (called with interference and MC).

The simulation produced by MATLAB programming can be described as follows. The source and the destination are equipped with four transmitting and four receiving antennas; that is, $s = x = 4$. We assume that the source-destination channels experience Rayleigh fading. Hence, the new channel matrix $\mathbf{H}_{\text{mc}}$ is an independent matrix containing independent identically distributed (i.i.d.) entries in which the random distribution is explained by CN(0, 1). For the self-interference channels, they also experience Rayleigh fading. Hence, the self-interference channel matrices $\mathbf{H}_{\text{LI}}$ and $\mathbf{H}_{\text{NI}}$ are independent matrices containing independent identically distributed (i.i.d.) entries distributed as CN(0, 1). For simplicity, we assume that the noise variances are equal in each antenna, σ^2.

Figure 8 shows the channel capacity versus SNR for 80% interference reduction when the MIMO system is affected by mutual coupling. It can be noticed that the proposed technique lies between with and without the interference suppression. The channel capacity of the proposed system is about 0.70 bps/Hz (at SNR = 20 dB) higher than the system with self-interference and the system with mutual coupling. In Figure 9, the relation between capacity and the percentage of interference reduction is presented. It can be noticed that the channel capacity of the proposed system requires only 90% interference reduction to achieve the capacity close to the system without any interference.

5.2. Self-Interference Reduction. The work in [6, 8, 17, 22–25] shows that a single-channel full-duplex system can be worked by using the method of self-interference cancellation. Two key techniques are RF interference cancellation (RFIC) and

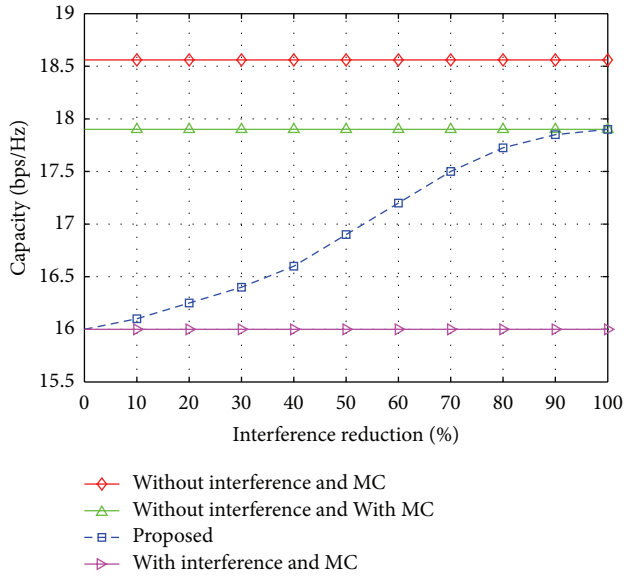

Figure 9: Relation between channel capacity and interference reduction for SNR = 20 dB.

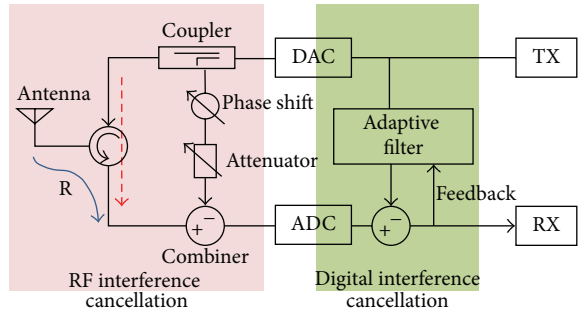

Figure 10: Block diagram of the proposed system in practice.

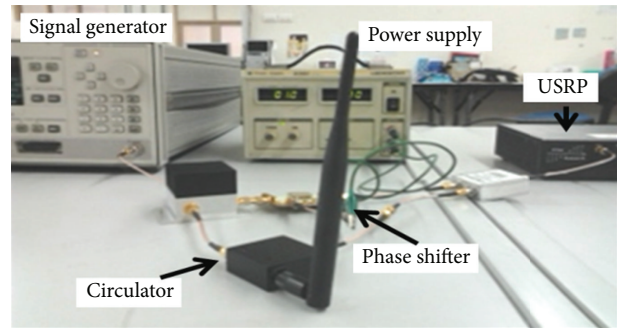

Figure 11: Photograph of experimental scenario.

digital interference cancellation (DIC) which utilize the signals from both the transmitting and receiving paths. Figure 10 presents the signal diagram of self-interference cancellation consisting of both RFIC and DIC. RFIC uses the knowledge of transmitting signals to cancel the self-interference in the RF signal before it is digitized. For analog cancellation, the amplitudes from two paths have to be perfectly matched at the receiver. Then, the phase of the two signals would be ideally differed by the exact π. To cancel self-interference, the best performing prior design is obtained. The authors gain the inverse of the transmitted signal using phase shifter and attenuator, dynamically adjusting the attenuation and phase of the inverse signal to match the self-interference leaking from circulator. After combining both inverse and leak signals, the received signal can be passed through the processing unit with the minimum effect of self-interference.

In measurement, the operating frequency band is on 2.45 GHz in order to match with a practical wireless channel as IEEE 802.11. The measurement has been performed to investigate the concept of a single-channel full-duplex wireless system. The results show that the system can reduce the self-interference about −75 dB. This reduction is good enough to investigate the concept of a single-channel full-duplex wireless system. The results show that the system can reduce the self-interference about −75 dB. This reduction is good enough to transmit and receive on the same frequency at the same time. However, we have proposed the self-interference suppression for MIMO system in which the self-interference signals are caused by mutual coupling. The proposed suppression technique can also be applied to the MIMO system by separating the multiple antennas into individual measurement. In this paper, the RFIC is performed according to the diagram shown in Figure 10. Then the DIC is performed inside USRP (Universal Software Radio Peripheral) processors.

The Universal Software Radio Peripheral (USRP) is a platform developed by Ettus Research LLC. Inside the USRP, there are two main components. The first component is a mother board containing an Altera Cyclone EP1C12 Field Programmable Gate Array (FPGA). It has 4 ADCs with 12 bits per sample and 4 DACs with 14 bits per sample. The second component is a daughter board that all working processes are in a field of RF-Front End. This paper employs XCVR2450 daughter board which responses to radio frequency in dual band, both 2.4 GHz and 5.9 GHz. All components are assembled in one USRP box using 3 A-6 V power supply. USRP is connected to the host PC via USB 2.0 (Universal Serial Bus 2.0).

The digital interference cancellation technique in our design employs a finite impulse response (FIR) filter to cancel the remainder of the self-interference signals after RF interference cancellation. The transmitted digital samples are passed through the FIR filter to create digital interference cancellation samples which are subtracted from the received samples to further clean interference from the received signal.

Figure 11 shows the photograph of the experimental scenario for measuring the self-interference signal. The block diagram of each antenna with both RFIC and DIC is shown in Figure 10.

Figure 12 shows the measured spectrum of self-interference signal. In Figure 12(a), the spectrum of the self-interference leakage without any cancellation is noticeably high. In Figure 12(b), the measured spectrum of self-interference signal with RF interference cancellation is reduced by 58 dB. In Figure 12(c), the measured spectrum of

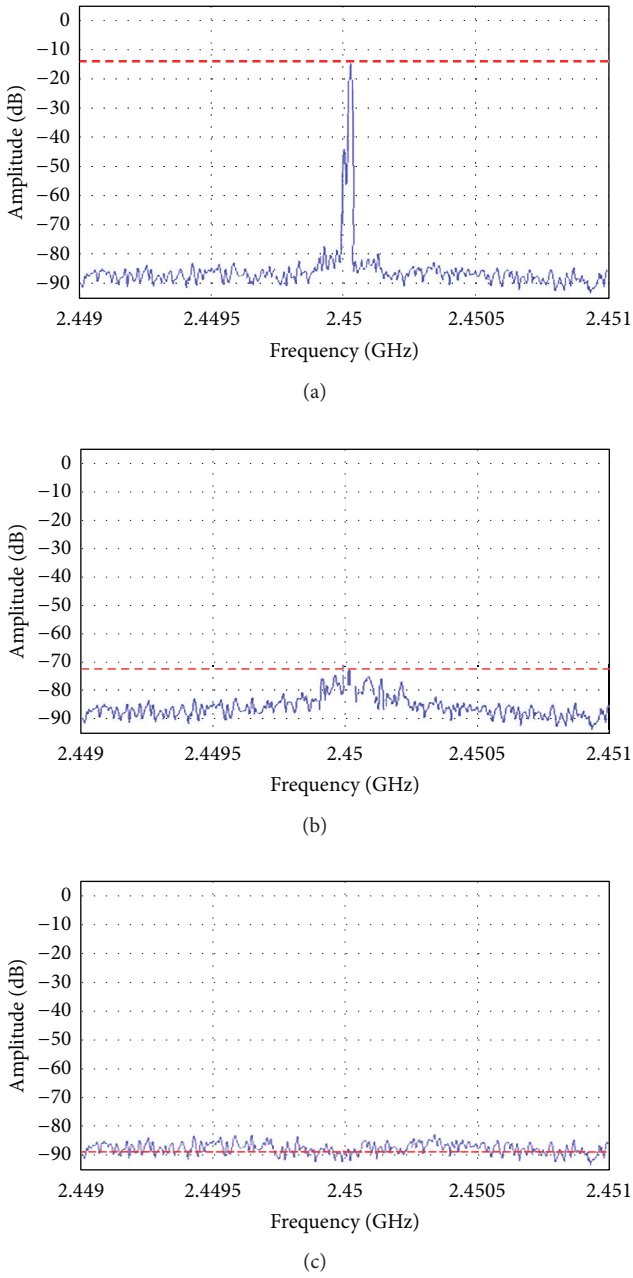

Figure 12: Measured spectrum of the self-interference signal (a) without any cancellations, (b) with RF interference cancellation but without digital interference cancellation, and (c) with both RF and digital interference cancellations.

self-interference signals with both RF and digital cancellations is very low and close to the noise floor level with the reduction of 75 dB. At this stage, the self-interference signal is low enough to provide a little impact on the desirably received signals. It means that the full-duplex system can be operated on the same channel at the same time because the self-interference is treated to be a noise for both forward and reserve links. Consequently, the throughput can be doubled by using our proposed method.

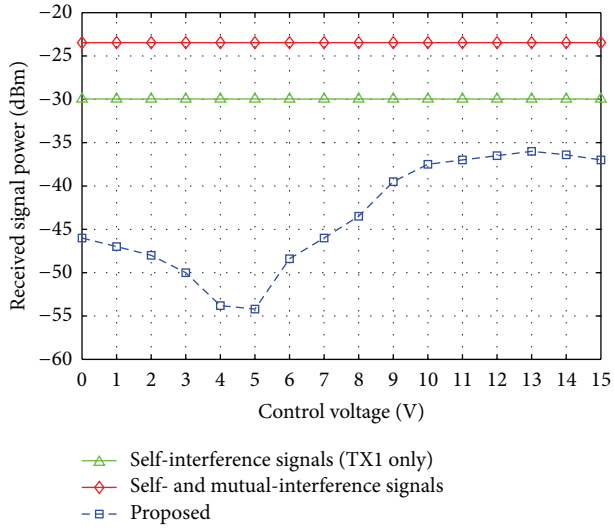

Figure 13: The received signal power of interference signals at Rx1.

5.3. Mutual-Interference Reduction. In the previous section, the reduction of self-interference power is observed. However, in MIMO system, there are other interference signals called mutual-interference signals. The proposed work also considers the reduction of mutual interference as well. By using the same measurement as previous section but increasing all sets for 4×4 MIMO operation, the mutual-interference power can be observed. The operating frequency band is on 2.45 GHz for all transmitting antennas. The attenuations and phase shifters are employed to perform the suitable matrix **W** which is illustrated in Figure 7. The power inputs of Tx1, Tx2, Tx3, and Tx4 are equal. Figure 13 shows the measured powers from Rx1 output. There are three curves presented in Figure 13. The first curve is named as self-interference signals because the signal is sent by only Tx1 while there is no input power for Tx2, Tx3, and Tx4. This is the same situation as in the previous section except that it might be the effect of mutual coupling from the neighbour antenna. For the second curve named as self- and mutual-interference signals, there are equal powers for Tx1, Tx2, Tx3, and Tx4, but there is no matrix **W** in the system. It can be observed that the total power of this curve is higher than the first curve. In the third curve named as proposed, the matrix **W** is performed to suppress both self-interference and mutual-interference signals. In this measurement, there is no signal coming from the other side. Hence, Rx1 should not receive any power if matrix W works very well. In our measurement, it can be noticed that the received power of the proposed method is the least. The self-interference and mutual-interference signals can be reduced by adjusting the suitable voltage control for phase shifter. Actually, there are four phase shifters related to this curve and all are needed to be properly adjusted at the same time. To explain the mechanism of phase adjustment, only one voltage control has been presented in Figure 13. It can be clearly seen that the right voltage offers the maximum reduction of interference signals. At control voltage 4-5 V,

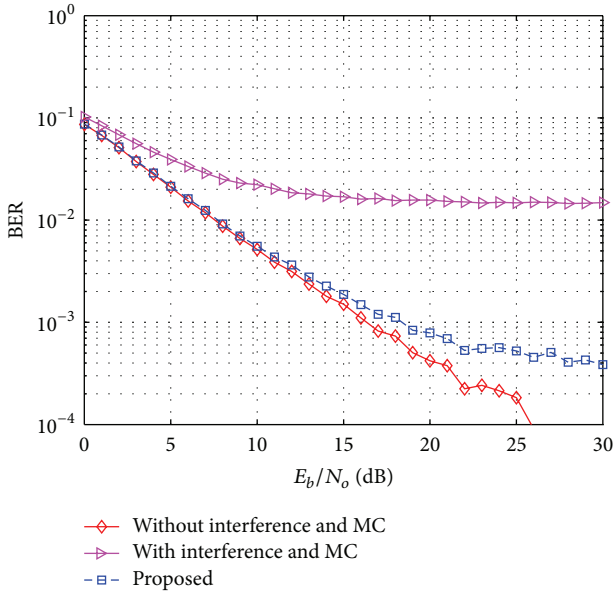

FIGURE 14: BER performance for 4 × 4 MIMO system.

the received power of self-interference and mutual-interference signals is reduced by 31 dB.

5.4. Performance of Proposed MIMO System. After getting the suitable matrix W, the other side of communication sends the data signal through the wireless 4 × 4 channel. It is a fact that the channel capacity is a theoretical quantity which cannot be directly measured. In practice, throughput and bit error rate (BER) are two indicators to judge the merit of system. In this paper, BER can be obtained by using the zero forcing technique to decode the data. All signals are sent with QPSK modulation. Figure 14 shows BER performance for 4 × 4 MIMO system. It is clearly seen that the proposed technique can provide a similar BER to the system without interference when Eb/No is less than 15 dB. Even though Eb/No is more than 15 dB, the proposed system still significantly improves the BER performance in comparison with the system with interference.

Note that even the BER of proposed system is nearly the same as that of the system without interference but the throughput of proposed system is a double of that of normal full-duplex system. This is because the proposed MIMO system can transmit and receive at the same time and on the same frequency.

6. Conclusions

In this paper, we proposed the method of self-interference cancellation for full-duplex single-channel MIMO system based on mutual-coupling model. The performance of proposed technique can suppress the self-interference signals by using the preknown interferences which are affected by mutual coupling between antennas. Simulation results illustrate that the proposed system outperforms the system with interference. This implies the success of using the proposed concept for full-duplex single-channel MIMO system. In addition, the measurement results indicate that the self-interference and mutual-interference reductions are good enough to successfully transmit and receive on the same frequency at the same time in practice. As a result, the proposed throughput can be actually twice the conventional system.

Conflict of Interests

The authors declare that there is no conflict of interests regarding the publication of this paper.

Acknowledgment

The authors got a financial support from Thailand Research Fund through the Royal Golden Jubilee Ph.D. Program (Grant no. PHD/0076/2554).

References

[1] T. Riihonen, S. Werner, and R. Wichman, "Spatial loop interference suppression in full-duplex MIMO relays," in *Proceedings of the 43rd Asilomar Conference on Signals, Systems and Computers (Asilomar '09)*, pp. 1508–1512, Pacific Grove, Calif, USA, November 2009.

[2] Y. Y. Kang and J. H. Cho, "Capacity of MIMO wireless channel with full-duplex amplify-and-forward relay," in *Proceedings of the IEEE 20th Personal, Indoor and Mobile Radio Communications Symposium (PIMRC '09)*, pp. 117–121, Tokyo, Japan, September 2009.

[3] P. Larsson and M. Prytz, "MIMO on-frequency repeater with self-interference cancellation and mitigation," in *Proceedings of the IEEE 69th Vehicular Technology Conference (VTC '09)*, pp. 1–5, Bercelona, Spain, April 2009.

[4] A. Goldsmith, *Wireless Communications*, Cambridge University Press, Cambridge, UK, 2005.

[5] B. Radunovic, D. Gunawardena, P. Key et al., "Rethinking indoor wireless mesh design: low power, low frequency, full-duplex," in *Proceedings of the 5th Annual IEEE Workshop on Wireless Mesh Networks (WiMesh '10)*, pp. 25–30, Boston, Mass, USA, June 2010.

[6] J. Choi II, M. Jain, K. Srinivasan, P. Levis, and S. Katti, "Achieving single channel, full duplex wireless communication," in *Proceedings of the 16th Annual Conference on Mobile Computing and Networking (MobiCom '10)*, pp. 1–12, Chicago, Ill, USA, September 2010.

[7] N. Singh, D. Gunawardena, A. Proutiere, B. Radunovic, H. V. Balan, and P. Key, "Efficient and fair MAC for wireless networks with self-interference cancellation," in *Proceedings of the International Symposium of on Modeling and Optimization in Mobile, Ad Hoc and Wireless Networks (WiOpt '11)*, pp. 94–101, Princeton, NJ, USA, May 2011.

[8] M. Jain, J. I. Choi, T. Kim et al., "Practical, real-time, full duplex wireless," in *Proceedings of the 17th Annual International Conference on Mobile Computing and Networking (MobiCom '11)*, pp. 301–312, Las Vegas, Nev, USA, September 2011.

[9] M. A. Khojastepour, K. Sundaresan, S. Rangarajan, X. Zhang, and S. Barghi, "The case for antenna cancellation for scalable full-duplex wireless communications," in *Proceedings of the*

10th ACM SIGCOMM Workshop on Hot Topics in Networks (HotNets-X '11), article 17, Cambridge, Mass, USA, November 2011.

[10] L. Sun, P. Li, M. R. McKay, and R. D. Murch, "Capacity of MIMO systems with mutual coupling: transmitter optimization with dual power constraints," *IEEE Transactions on Signal Processing*, vol. 60, no. 2, pp. 848–861, 2012.

[11] T. Nguyen, W. Meng, and H. Wang, "Channel capacity analysis on cooperative MIMO with antenna spatial correlation and multi-path," in *Proceedings of the 6th International ICST Conference on Communications and Networking in China (CHINACOM '11)*, pp. 181–185, Harbin, China, August 2011.

[12] R. M. Legnain, R. H. M. Hafez, I. D. Marsland, and A. M. Legnain, "A novel spatial modulation using MIMO spatial multiplexing," in *Proceedings of the 1st International Conference on Communications Signal Processing and their Applications (ICCSPA '13)*, pp. 1–4, Sharjah, United Arab Emirates, February 2013.

[13] P. Li, L. Sun, M. R. McKay, and R. D. Murch, "Transmitter optimization for MIMO systems with mutual coupling at high SNR," in *Proceedings of the 45th Asilomar Conference on Signal Systems and Computers (ASILOMAR '11)*, pp. 1058–1588, Pacific Grove, Calif, USA, November 2011.

[14] H.-B. Shi, S. Gong, and T.-C. Zheng, "The effect of mutual coupling on the channel performance of MIMO communication system," in *Proceedings of the 10th International Symposium on Antennas Propagation & EM Theory (ISAPE '12)*, pp. 335–339, Xian, China, October 2012.

[15] S. Lu, H. T. Hui, and M. Bialkowski, "Optimizing MIMO channel capacities under the influence of antenna mutual coupling," *IEEE Antennas and Wireless Propagation Letters*, vol. 7, pp. 287–290, 2008.

[16] P. Uthansakul, *Adaptive MIMO Systems: Explorations for Indoor Wireless Communications*, VDM, Berlin, Germany, 2009.

[17] N. Phungamngern, P. Uthansakul, and M. Uthansakul, "Digital and RF interference cancellation for single-channel full-duplex transceiver using a single antenna," in *Proceedings of the 10th International Conference on Electrical Engineering/Electronics, Computer, Telecommunications and Information Technology (ECTI-CON '13)*, pp. 1–5, Krabi, Thailand, May 2013.

[18] E. Telatar, "Capacity of multi-antenna Gaussian channels," *European Transactions on Telecommunications*, vol. 10, no. 6, pp. 585–595, 1999.

[19] C. A. Balanis, *Antena Theory*, John Wiley & Sons, Hoboken, NJ, USA, 3rd edition, 2005.

[20] S. Durrani and M. E. Bialkowski, "Effect of mutual coupling on the interference rejection capabilities of linear and circular arrays in CDMA systems," *IEEE Transactions on Antennas and Propagation*, vol. 52, no. 4, pp. 1130–1134, 2004.

[21] H. Lutkepohl, *Handbook of Matrices*, John Wiley & Sons, New York, NY, USA, 1996.

[22] M. Duarte and A. Sabharwal, "Full-duplex wireless communications using off-the-shelf radios: feasibility and first results," in *Proceedings of the 44th Asilomar Conference on Signals, Systems and Computers (ASILOMAR '10)*, pp. 1558–1562, Pacific Grove, Calif, USA, November 2010.

[23] M. A. Khojastepour and S. Rangarajan, "Wideband digital cancellation for full-duplex communications," in *Proceedings of the 46th Asilomar Conference on Signals, Systems and Computers (ASILOMAR '12)*, pp. 1300–1304, Pacific Grove, Calif, USA, November 2012.

[24] M. Duarte, C. Dick, and A. Sabharwal, "Experiment-driven characterization of full-duplex wireless systems," *IEEE Transactions on Wireless Communications*, vol. 11, no. 12, pp. 4296–4307, 2012.

[25] N. Li, W. Zhu, and H. Han, "Digital interference cancellation in single channel, full duplex wireless communication," in *Proceedings of the 8th International Conference on Wireless Communications, Networking and Mobile Computing (WiCOM '12)*, pp. 1–4, Shanghai, China, September 2012.

Hindawi Publishing Corporation
International Journal of Antennas and Propagation
Volume 2014, Article ID 918964, 8 pages
http://dx.doi.org/10.1155/2014/918964

Research Article

Root-MUSIC Based Angle Estimation for MIMO Radar with Unknown Mutual Coupling

Jianfeng Li, Xiaofei Zhang, and Weiyang Chen

Department of Electronic Engineering, Nanjing University of Aeronautics & Astronautics, Nanjing 210016, China

Correspondence should be addressed to Xiaofei Zhang; njxnd88@126.com

Received 5 August 2013; Revised 18 December 2013; Accepted 19 December 2013; Published 16 January 2014

Academic Editor: Hoi-Shun Lui

Direction of arrival (DOA) estimation problem for multiple-input multiple-output (MIMO) radar with unknown mutual coupling is studied, and an algorithm for the DOA estimation based on root multiple signal classification (MUSIC) is proposed. Firstly, according to the Toeplitz structure of the mutual coupling matrix, output data of some specified sensors are selected to eliminate the influence of the mutual coupling. Then the reduced-dimension transformation is applied to make the computation burden lower as well as obtain a Vandermonde structure of the direction matrix. Finally, Root-MUSIC can be adopted for the angle estimation. The angle estimation performance of the proposed algorithm is better than that of estimation of signal parameters via rotational invariance techniques (ESPRIT)-like algorithm and MUSIC-like algorithm. Furthermore, the proposed algorithm has lower complexity than them. The simulation results verify the effectiveness of the algorithm, and the theoretical estimation error of the algorithm is also derived.

1. Introduction

Multiple-input multiple-output (MIMO) radars have attracted a lot of attention recently for their potential advantages over conventional phased-array radars [1–4]. MIMO radar systems can overcome fading effect, enhance spatial resolution, strengthen parameter identifiability, and improve target detection performance for the additional degrees of freedom [5–7]. Angle estimation is a key issue in MIMO radar and has been studied by a lot of researchers. Estimation of signal parameters via rotational invariance techniques (ESPRIT) algorithms [8–10] can obtain the closed-form estimations via rotational invariance in the subspace. Capon algorithm [11] and multiple signal classification (MUSIC) algorithm [12] both estimate the angles via the peak searches. Polynomial root finding technique can transform the peak searches into root finding problem when the arrays are uniform linear arrays (ULA) [13]. Based on the uniqueness of trilinear decomposition, parallel factor analysis (PARAFAC) algorithms [14–16] can also be adopted for the angle estimation. For monostatic MIMO radar, low-complexity ESPRIT [17] and Capon [18] can achieve better angle estimation performance with lighter computation burden based on the reduced-dimension transformation. However, these methods strongly depend on the array manifold, which is often perturbed by the mutual coupling in practical situations. The mutual coupling will make the above methods have performance degradation or even fail to work, and various methods for mutual coupling compensation have been studied. The Receiving-Mutual-Impedance Methods (RMIM) [19, 20] can obtain the decoupled voltages via the known terminated impedance and the receiving mode antennas. The calibration methods [21–23], which will be studied in this paper, can utilize the special characteristics of the mutual coupling coefficients of uniform linear arrays (ULA). Reference [24] proposed a MUSIC-like algorithm for the angle estimation in the presence of mutual coupling. Through reconstructing the MUSIC function based on the Toeplitz structure of the mutual coupling matrix, the angles can be estimated via the peak searches. To avoid the high-computational peak search, an ESPRIT-like algorithm was proposed in [25] by removing the auxiliary sensors to eliminate the influence of mutual coupling. The rotational invariance can be extracted in the new data for the angle estimation.

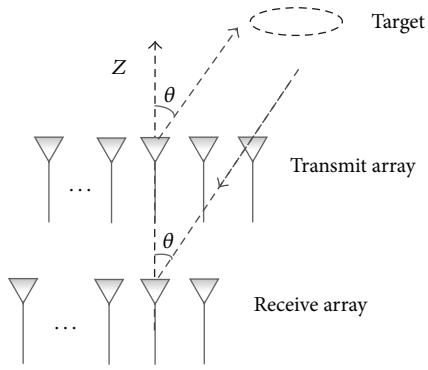

Figure 1: Array structure of monostatic MIMO radar.

Although MUSIC-like algorithm can achieve high resolution angle estimation with unknown mutual coupling, the high computational peak searches will make it ineffective. As a faster method, ESPRIT-like can obtain the close-form solution of the angle estimation, but it only exploits the relationship between the subarrays, which will lead to a performance loss.

Our goal is to develop an effective method for angle estimation in MIMO radar with unknown mutual coupling. So, in this paper, we propose a Root-MUSIC based method, which is fast and can deal with the mutual coupling problem, which often occurrs in practical situation. The nonauxiliary sensors are also used to eliminate the influence of mutual coupling. Then a transformation is utilized to reduce the dimension of the data, meanwhile a direction matrix with Vandermonde structure can be obtained. Finally, Root-MUSIC, which is a root-finding form of the MUSIC peak searching, can be adopted for the angle estimation. The angle estimation performance of the proposed algorithm is better than that of ESPRIT-like algorithm and MUSIC-like algorithm. Furthermore, it may also have lower complexity.

Notation. $(\cdot)^T$, $(\cdot)^H$, $(\cdot)^{-1}$, and $(\cdot)^+$ denote transpose, conjugate-transpose, inverse, and pseudo-inverse operations, respectively. diag $(\mathbf{v})$ stands for diagonal matrix whose diagonal element is a vector $\mathbf{v}$. $\mathbf{I}_K$ is a $K \times K$ identity matrix. $\otimes$ is the Kronecker product. Re $(\cdot)$ is to get real part of the complex, and angle $(\cdot)$ means taking phase operation.

2. Data Model

As shown in Figure 1, the monostatic MIMO radar system is equipped with both uniformlinear arrays (ULA) for the transmit and receive arrays, and the arrays are both located in the y-axis with half-wavelength spacing between adjacent antennas, respectively. Assume that there are K targets in the y-z plane, and the output of the matched filters at the receiver can be expressed as [5, 23, 24]

$$\mathbf{x}(t) = \left[\widetilde{\mathbf{a}}_r(\theta_1) \otimes \widetilde{\mathbf{a}}_t(\theta_1), \ldots, \widetilde{\mathbf{a}}_r(\theta_K) \otimes \widetilde{\mathbf{a}}_t(\theta_K)\right] \mathbf{s}(t) + \mathbf{n}(t), \tag{1}$$

where θ_K is the direction of arrival (DOA) of the kth target with respect to the transmit array normal or the receive array normal, $\mathbf{s}(t) = [s_1(t), s_2(t), \ldots, s_K(t)]^T \in \mathbb{C}^{K\times 1}$, $s_k(t) = \beta_k e^{j2\pi f_k t}$ with f_k and β_k being the Doppler frequency and the reflect coefficient, respectively, $\mathbf{n}(t)$ is an $MN \times 1$ Gaussian white noise vector of zero mean and covariance matrix $\sigma^2\mathbf{I}_{MN}$, and $\widetilde{\mathbf{a}}_r(\theta_k)$ and $\widetilde{\mathbf{a}}_t(\theta_k)$ are the receive and transmit steering vectors for the kth target under the influence of mutual coupling, respectively. They satisfy

$$\widetilde{\mathbf{a}}_r(\theta_k) = \mathbf{C}_r \mathbf{a}_r(\theta_k), \tag{2a}$$

$$\widetilde{\mathbf{a}}_t(\theta_k) = \mathbf{C}_t \mathbf{a}_t(\theta_k), \tag{2b}$$

where $\mathbf{C}_r \in \mathbb{C}^{N\times N}$ and $\mathbf{C}_t \in \mathbb{C}^{M\times M}$ represent the matrices containing the mutual coupling coefficients. With the assumption of ULA, they are Toeplitz matrices [24]

$$\mathbf{C}_r = \text{toeplitz}\left(c_0^r, \ldots, c_n^r, 0, \ldots, 0\right), \tag{3a}$$

$$\mathbf{C}_t = \text{toeplitz}\left(c_0^t, \ldots, c_m^t, 0, \ldots, 0\right), \tag{3b}$$

where c_p^r $(p = 0 \ldots n)$ and c_q^t $(q = 0 \ldots m)$ stand for the mutual coupling coefficients. If the first sensors are the reference points, then $c_0^r = c_0^t = 1$. $\mathbf{a}_r(\theta_k)$ and $\mathbf{a}_t(\theta_k)$ in (2a) and (2b) are expressed as Vandermonde structures

$$\mathbf{a}_r(\theta_k) = \left[1, z_k, \ldots, z_k^{N-1}\right]^T, \tag{4a}$$

$$\mathbf{a}_t(\theta_k) = \left[1, z_k, \ldots, z_k^{M-1}\right]^T, \tag{4b}$$

where $z_k = e^{-j\pi \sin\theta_k}$.

By collecting J samples, and representing the received data as $\mathbf{X} = [\mathbf{x}(1), \mathbf{x}(2), \ldots, \mathbf{x}(J)]$, the received data can be expressed as

$$\mathbf{X} = \widetilde{\mathbf{A}}\mathbf{S} + \mathbf{N}, \tag{5}$$

where $\widetilde{\mathbf{A}} = [\widetilde{\mathbf{a}}_r(\theta_1) \otimes \widetilde{\mathbf{a}}_t(\theta_1), \ldots, \widetilde{\mathbf{a}}_r(\theta_K) \otimes \widetilde{\mathbf{a}}_t(\theta_K)] \in \mathbb{C}^{MN\times K}$ is the direction matrix, $\mathbf{S} = [\mathbf{s}(1), \mathbf{s}(2), \ldots, \mathbf{s}(J)] \in \mathbb{C}^{K\times J}$, and $\mathbf{N} \in \mathbb{C}^{MN\times J}$ stands for the noise matrix.

3. Root-MUSIC Based Angle Estimation for MIMO Radar with Unknown Mutual Coupling

3.1. Mutual Coupling Elimination. According to [25], define the selecting matrices as

$$\mathbf{J}_1 = \left[\mathbf{0}_{(N-2n)\times n}, \mathbf{I}_{(N-2n)\times(N-2n)}, \mathbf{0}_{(N-2n)\times n-1}\right], \tag{6a}$$

$$\mathbf{J}_2 = \left[\mathbf{0}_{(M-2m)\times m}, \mathbf{I}_{(M-2m)\times(M-2m)}, \mathbf{0}_{(M-2m)\times m}\right]. \tag{6b}$$

Then,

$$\mathbf{J}_1\widetilde{\mathbf{a}}_r(\theta_k) = \mathbf{J}_1\mathbf{C}_r\mathbf{a}_r(\theta_k) = \alpha_{rk}\mathbf{a}_{r1}(\theta_k), \tag{7a}$$

$$\mathbf{J}_2\widetilde{\mathbf{a}}_t(\theta_k) = \mathbf{J}_2\mathbf{C}_t\mathbf{a}_t(\theta_k) = \alpha_{tk}\mathbf{a}_{t1}(\theta_k), \tag{7b}$$

where $\alpha_{rk} = \sum_{p=-n}^{n} c_{|p|}^r z_k^{p+n}$, $\alpha_{tk} = \sum_{q=-m}^{m} c_{|q|}^t z_k^{q+m}$, and $\mathbf{a}_{r1}(\theta_k)$ and $\mathbf{a}_{t1}(\theta_k)$ are the first $(N-2n)$ and $(M-2m)$ elements of

$\mathbf{a}_r(\theta_k)$ and $\mathbf{a}_t(\theta_k)$, respectively. Define $\overline{M} = M - 2m$ and $\overline{N} = N - 2n$, then

$$\mathbf{a}_{r1}(\theta_k) = \left[1, z_k, \ldots, z_k^{\overline{N}-1}\right]^T, \tag{8a}$$

$$\mathbf{a}_{t1}(\theta_k) = \left[1, z_k, \ldots, z_k^{\overline{M}-1}\right]^T. \tag{8b}$$

The new steering vector of the output can be now characterized as

$$\begin{aligned}\mathbf{a}_c(\theta_k) &= (\mathbf{J}_1 \otimes \mathbf{J}_2)\left(\widetilde{\mathbf{a}}_r(\theta_k) \otimes \widetilde{\mathbf{a}}_t(\theta_k)\right) \\ &= \alpha_{rk}\alpha_{tk}\mathbf{a}_{r1}(\theta_k) \otimes \mathbf{a}_{t1}(\theta_k).\end{aligned} \tag{9}$$

According to (9), the steering vector can be expressed as a kronecker product of two Vandermonde vectors without considering the scalar coefficients α_{rk} and α_{tk}. Thus, the mutual coupling can be considered to be eliminated through this procedure.

3.2. Reduced-Dimension Transformation. The length of the new steering vector $\mathbf{a}_c(\theta_k)$ is $\overline{MN}$, which is too long and will add high computation burden. Furthermore, it will make the later root finding hard to implement for the high-order polynomials. So the reduced-dimension transformation is necessary. According to [17], steering vectors with Vandermonde structures will satisfy

$$\mathbf{a}_{r1}(\theta_k) \otimes \mathbf{a}_{t1}(\theta_k) = \mathbf{G}\mathbf{b}(\theta_k), \tag{10}$$

where

$$\mathbf{G} = \begin{bmatrix} \left.\begin{matrix} 1 & 0 & \cdots & 0 & 0 & \cdots & 0 \\ 0 & 1 & \cdots & 0 & 0 & \cdots & 0 \\ \vdots & \vdots & \ddots & \vdots & \vdots & \ddots & 0 \\ 0 & 0 & \cdots & 1 & 0 & \cdots & 0 \end{matrix}\right\}\overline{M} \\ \left.\begin{matrix} 0 & 1 & \cdots & 0 & 0 & \cdots & 0 \\ 0 & 0 & 1 & 0 & 0 & \cdots & 0 \\ \vdots & \vdots & \vdots & \ddots & \vdots & \ddots & 0 \\ 0 & 0 & \cdots & 0 & 1 & 0 & 0 \end{matrix}\right\}\overline{M} \\ \begin{matrix} \vdots & \vdots & \vdots & \vdots & \vdots & \vdots & \vdots \end{matrix} \\ \left.\begin{matrix} 0 & \cdots & 0 & 1 & 0 & \cdots & 0 \\ 0 & \cdots & 0 & 0 & 1 & \cdots & 0 \\ \vdots & \ddots & \vdots & \vdots & \vdots & \ddots & \vdots \\ 0 & \cdots & 0 & 0 & 0 & \cdots & 1 \end{matrix}\right\}\overline{M} \end{bmatrix} \in \mathbb{R}^{\overline{MN}\times(\overline{M}+\overline{N}-1)} \tag{11}$$

$\mathbf{b}(\theta_k) = [1, z_k, \ldots, z_k^{\overline{M}+\overline{N}-2}]^T \in \mathbb{C}^{(\overline{M}+\overline{N}-1)\times 1}$. Then define $\mathbf{W} \triangleq \mathbf{G}^H\mathbf{G}$,

$$\mathbf{W} = \operatorname{diag}\left(1, 2, \ldots, \underbrace{\min\left(\overline{M}, \overline{N}\right), \ldots, \min\left(\overline{M}, \overline{N}\right)}_{|\overline{M}-\overline{N}|+1}, \ldots, 2, 1\right). \tag{12}$$

Using the reduced-dimension transformation $\mathbf{W}^{-1/2}\mathbf{G}^H$ for the receive signal after the mutual coupling elimination, and combining (9) and (10), then

$$\begin{aligned}\mathbf{y}(t) &= \mathbf{W}^{-1/2}\mathbf{G}^H(\mathbf{J}_1 \otimes \mathbf{J}_2)\mathbf{x}(t) \\ &= \mathbf{W}^{-1/2}\mathbf{G}^H\left[\mathbf{a}_c(\theta_1), \mathbf{a}_c(\theta_2), \ldots, \mathbf{a}_c(\theta_K)\right]\mathbf{s}(t) \\ &\quad + \mathbf{W}^{-1/2}\mathbf{G}^H(\mathbf{J}_1 \otimes \mathbf{J}_2)\mathbf{n}(t) \\ &= \mathbf{W}^{-1/2}\mathbf{W}\left[\mathbf{b}(\theta_1), \mathbf{b}(\theta_2), \ldots, \mathbf{b}(\theta_K)\right]\boldsymbol{\Phi}\mathbf{s}(t) + \mathbf{n}_y(t) \\ &= \mathbf{W}^{1/2}\mathbf{B}\boldsymbol{\Phi}\mathbf{s}(t) + \mathbf{n}_y(t),\end{aligned} \tag{13}$$

where $\mathbf{B} = [\mathbf{b}(\theta_1), \mathbf{b}(\theta_2), \ldots, \mathbf{b}(\theta_K)]$, $\boldsymbol{\Phi} = \operatorname{diag}(\alpha_{r1}\alpha_{t1}, \ldots, \alpha_{rK}\alpha_{tK})$ and $\mathbf{n}_y(t) = \mathbf{W}^{-1/2}\mathbf{G}^H(\mathbf{J}_1 \otimes \mathbf{J}_2)\mathbf{n}(t)$. The covariance matrix of $\mathbf{y}(t)$ is

$$\begin{aligned}\mathbf{R} &= E\left[\mathbf{y}(t)\mathbf{y}^H(t)\right] \\ &= \mathbf{W}^{1/2}\mathbf{B}\boldsymbol{\Phi}\left(E\left[\mathbf{s}(t)\mathbf{s}^H(t)\right]\right)\boldsymbol{\Phi}^H\mathbf{B}^H\mathbf{W}^{1/2} \\ &\quad + E\left[\mathbf{n}_y(t)\mathbf{n}_y^H(t)\right] \\ &= \mathbf{W}^{1/2}\mathbf{B}\mathbf{R}_s\mathbf{B}^H\mathbf{W}^{1/2} + \sigma^2\mathbf{I}_L,\end{aligned} \tag{14}$$

where $\mathbf{R}_s = \boldsymbol{\Phi}(E[\mathbf{s}(t)\mathbf{s}^H(t)])\boldsymbol{\Phi}^H$ and $L = \overline{M} + \overline{N} - 1$. $\mathbf{W}^{1/2}\mathbf{B}$ can be regarded as the new direction matrix.

3.3. Root-MUSIC Based Angle Estimation. The covariance matrix in (14) can be decomposed as

$$\mathbf{R} = \mathbf{E}_s\mathbf{D}_s\mathbf{E}_s^H + \mathbf{E}_n\mathbf{D}_n\mathbf{E}_n^H, \tag{15}$$

where $\mathbf{D}_s$ denotes a $K\times K$ diagonal matrix formed by K largest eigenvalues $\lambda_1, \ldots, \lambda_K$ and $\mathbf{D}_n$ denotes a diagonal matrix formed by the rest $L-K$ smaller eigen-values ($\lambda_{K+1} = \lambda_{K+2} = \cdots = \lambda_L = \sigma^2$). $\mathbf{E}_s$ and $\mathbf{E}_n$ represent the signal subspace and noise subspace, respectively, of which $\mathbf{E}_s$ stands for the eigenvectors corresponding to the K largest eigen-values, and $\mathbf{E}_n$ consists of the rest eigenvectors.

According to the MUSIC peak search function [12], the space spanned by the direction matrix is orthogonal to the noise subspace, and the angle can be estimated by searching the following function:

$$F(\theta) = \frac{1}{\mathbf{b}^H(\theta)\mathbf{W}^{1/2}\mathbf{E}_n\mathbf{E}_n^H\mathbf{W}^{1/2}\mathbf{b}(\theta)}, \tag{16}$$

where $\mathbf{b}(\theta) = [1, e^{-j\pi\sin\theta}, \ldots, e^{-j(L-1)\pi\sin\theta}]^T$. To avoid the peak searching, let $z = e^{-j\pi\sin\theta}$; then $\mathbf{b}(\theta)$ can be expressed as $\mathbf{b}(z) = [1, z, \ldots, z^{L-1}]^T$. Equation (16) can be transformed into the root finding problem

$$\mathbf{b}^T\left(\frac{1}{z}\right)\mathbf{U}_n\mathbf{b}(z) = 0, \tag{17}$$

where $\mathbf{U}_n = \mathbf{W}^{1/2}\mathbf{E}_n\mathbf{E}_n^H\mathbf{W}^{1/2}$. According to [26], the polynomial in (17) can be expressed as

$$\left[z^{-L+1}, \ldots, z^{-1}, 1, z, \ldots, z^{L-1}\right]\mathbf{c} = 0, \tag{18}$$

where $\mathbf{c} \in \mathbb{C}^{2L-1}$ is a column vector which contains the coefficients of the polynomial and the lth coefficient ($\mathbf{c}(l)$, $l = 1, \ldots, 2L-1$) is given by the sum of the $(l-L)$th diagonal elements of $\mathbf{U}_n$.

The K roots which are most close to the unit circle will be the solutions, and they are denoted as $\widehat{z}_1, \ldots, \widehat{z}_K$. The angle θ_k can be estimated via

$$\theta_k = -\frac{\text{angle}\left(\widehat{z}_k\right)}{\pi}, \quad k = 1, \ldots, K. \tag{19}$$

With respect to (14), the covariance matrix can be estimated via

$$\widehat{\mathbf{R}} = \frac{1}{J}\sum_{t=1}^{J}\mathbf{y}\left(t\right)\mathbf{y}^H\left(t\right). \tag{20}$$

The major steps of the proposed algorithm for DOA estimation in MIMO-radar are shown as follows.

(1) Construct the new output via (13) to eliminate the mutual coupling and reduce the data dimension.

(2) Estimate the covariance matrix of the data through $\widehat{\mathbf{R}} = (1/J)\sum_{t=1}^{J}\mathbf{y}(t)\mathbf{y}^H(t)$.

(3) Perform eigen-value decomposition of $\widehat{\mathbf{R}}$ to get the noise subspace $\widehat{\mathbf{E}}_n$.

(4) Construct the MUSIC function and use root finding technique to obtain the angle estimation $\widehat{\theta}_k$ via (18)-(19).

3.4. Complexity Analysis. The proposed algorithm has lower complexity than ESPRIT-like algorithm and MUSIC-like algorithm for it requires no peak searches and has lower dimension. Figure 2 shows the run time of the three algorithms in computer versus the number of antennas, and here we choose $M = N$ for simplify. From Figure 2, we find that our algorithm has lower complexity, and the change trend versus the number of antennas of the proposed algorithm is smaller than those of the other two algorithms.

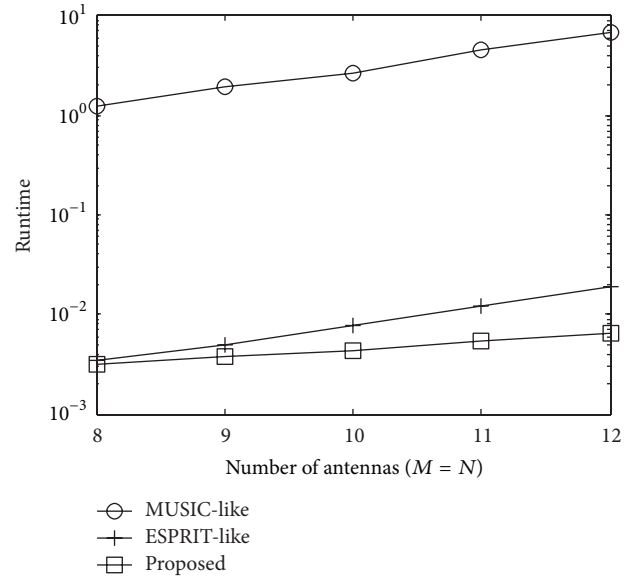

Figure 2: Complexity comparison against the number of antennas ($J = 100$, $K = 3$).

4. Theoretical Analysis and Cramer-Rao Bound (CRB)

4.1. Theoretical Analysis of the Proposed Algorithm. The decomposition of $\widehat{\mathbf{R}}$ in (20) can be expressed as

$$\widehat{\mathbf{R}} = \widehat{\mathbf{E}}_s\widehat{\mathbf{D}}_s\widehat{\mathbf{E}}_s^H + \widehat{\mathbf{E}}_n\widehat{\mathbf{D}}_n\widehat{\mathbf{E}}_n^H, \tag{21}$$

where $\widehat{\mathbf{E}}_s$ and $\widehat{\mathbf{E}}_n$ denote the estimated signal and noise subspaces, respectively.

According to [27], Root-MUSIC and MUSIC peak search method have the same angle estimation error as they both seek for the extreme points of $f(\theta) = \mathbf{b}^H(\theta)\widehat{\mathbf{U}}_n\mathbf{b}(\theta)$, where $\widehat{\mathbf{U}}_n = \mathbf{W}^{1/2}\widehat{\mathbf{E}}_n\widehat{\mathbf{E}}_n^H\mathbf{W}^{1/2}$. The first-order derivative of $f(\theta)$ on $\widehat{\theta}_k$ will be equal to zero; that is,

$$\begin{aligned} f'\left(\widehat{\theta}_k\right) &= \mathbf{d}^H\left(\widehat{\theta}_k\right)\widehat{\mathbf{U}}_n\mathbf{b}\left(\widehat{\theta}_k\right) + \mathbf{b}^H\left(\widehat{\theta}_k\right)\widehat{\mathbf{U}}_n\mathbf{d}\left(\widehat{\theta}_k\right) \\ &= 2\,\text{Re}\left[\mathbf{b}^H\left(\widehat{\theta}_k\right)\widehat{\mathbf{U}}_n\mathbf{d}\left(\widehat{\theta}_k\right)\right] \\ &= 0, \end{aligned} \tag{22}$$

where $\mathbf{d}(\widehat{\theta}_k) = \partial\mathbf{b}(\widehat{\theta}_k)/\partial\widehat{\theta}_K$. Taking the first-order Taylor series expansion, then

$$\begin{aligned} f'\left(\widehat{\theta}_k\right) &\cong f'\left(\theta_k\right) + f''\left(\theta_k\right)\left(\widehat{\theta}_k - \theta_k\right) \\ &= 2\,\text{Re}\left[\mathbf{b}^H\left(\theta_k\right)\widehat{\mathbf{U}}_n\mathbf{d}\left(\theta_k\right)\right] \\ &\quad + 2\,\text{Re}\left[\mathbf{d}^H\left(\theta_k\right)\widehat{\mathbf{U}}_n\mathbf{d}\left(\theta_k\right)\right. \\ &\qquad \left. + \mathbf{b}^H\left(\theta_k\right)\widehat{\mathbf{U}}_n\mathbf{d}'\left(\theta_k\right)\right]\left(\widehat{\theta}_k - \theta_k\right) \\ &\cong 2\,\text{Re}\left[\mathbf{b}^H\left(\theta_k\right)\widehat{\mathbf{U}}_n\mathbf{d}\left(\theta_k\right)\right] \\ &\quad + 2\left[\mathbf{d}^H\left(\theta_k\right)\mathbf{U}_n\mathbf{d}\left(\theta_k\right)\right]\left(\widehat{\theta}_k - \theta_k\right) \\ &= 0, \end{aligned} \tag{23}$$

where some small items are neglected. The mean square error of the angle estimation can be shown as

$$E\left[\left(\widehat{\theta}_k - \theta_k\right)^2\right] = \frac{\left(\text{Re}\left[\mathbf{b}^H\left(\theta_k\right)\widehat{\mathbf{U}}_n\mathbf{d}\left(\theta_k\right)\right]\right)^2}{\left(\mathbf{d}^H\left(\theta_k\right)\mathbf{U}_n\mathbf{d}\left(\theta_k\right)\right)^2}. \tag{24}$$

According to [28],

$$\left(\mathrm{Re}\left[\mathbf{b}^H(\theta_k)\,\widehat{\mathbf{U}}_n\mathbf{d}(\theta_k)\right]\right)^2 = \frac{1}{2J}\mathbf{d}^H(\theta_k)\,\mathbf{U}_n\mathbf{d}(\theta_k)\cdot\mathbf{b}^H(\theta_k)\,\mathbf{W}^{1/2}\mathbf{U}\mathbf{W}^{1/2}\mathbf{b}(\theta_k), \tag{25}$$

where $\mathbf{U} = \mathbf{E}_s\mathbf{W}_s\mathbf{E}_s^H$ with $\mathbf{W}_s = \mathrm{diag}\{\lambda_1\sigma^2/(\lambda_1-\sigma^2)^2, \ldots, \lambda_K\sigma^2/(\lambda_K-\sigma^2)^2\}$. Thus the theoretical mean error of the angle estimation of the proposed algorithm can be derived as

$$E\left[\left(\widehat{\theta}_k-\theta_k\right)^2\right] = \frac{1}{2J}\frac{\mathbf{b}^H(\theta_k)\,\mathbf{W}^{1/2}\mathbf{U}\mathbf{W}^{1/2}\mathbf{b}(\theta_k)}{\mathbf{d}^H(\theta_k)\,\mathbf{U}_n\mathbf{d}(\theta_k)}. \tag{26}$$

The theoretical result and the simulation result of the proposed algorithm will be compared in Section 5, where it can be shown that they are almost the same, which demonstrate the correctness of the derivation above.

4.2. Advantages of the Proposed Algorithm. The advantages of the proposed algorithm can be summarized as follows.

(1) It works well with unknown mutual coupling. According to (9), (13), and (14), it can be shown the mutual coupling can be eliminated regardless of the specific distribution of the mutual coupling (the number of the antennas that are influenced by the mutual coupling should be known, i.e., m and n [21, 22]).

(2) It requires no peak search and has lower complexity, which has been shown in Figure 2.

(3) It has better angle estimation performance than MUSIC-like algorithm and ESPRIT-like algorithm. Part of the reason of this advantage can be refered to "Remark 1", and another reason may be the reduced-dimension transformation. According to (13)-(14), the signal to noise ratios (SNRs) of the data before the reduced-dimension transformation and the data after the reduced-dimension transformation are

$$\begin{aligned}\mathrm{SNR}_{xc} &= \frac{\mathrm{tr}\left(\mathbf{A}_1\mathbf{R}_s\mathbf{A}_1^H\right)}{\mathrm{tr}\left(\mathbf{J}_1\otimes\mathbf{J}_2E\left[\mathbf{n}(t)\,\mathbf{n}^H(t)\right]\mathbf{J}_1^H\otimes\mathbf{J}_2^H\right)} = \frac{\mathrm{tr}\left(\mathbf{A}_1\mathbf{R}_s\mathbf{A}_1^H\right)}{\overline{MN}\sigma^2},\\ \mathrm{SNR}_y &= \frac{\mathrm{tr}\left(\mathbf{W}^{1/2}\mathbf{B}\mathbf{R}_s\mathbf{B}^H\mathbf{W}^{1/2}\right)}{\mathrm{tr}\left(\sigma^2\mathbf{I}_L\right)} = \frac{\mathrm{tr}\left(\mathbf{G}^H\mathbf{A}_1\mathbf{R}_s\mathbf{B}^H\right)}{L\sigma^2}\\ &= \frac{\mathrm{tr}\left(\mathbf{A}_1\mathbf{R}_s\mathbf{A}_1^H\right)}{\left(\overline{M}+\overline{N}-1\right)\sigma^2},\end{aligned} \tag{27}$$

where $\mathbf{A}_1 = [\mathbf{a}_{r1}(\theta_1)\otimes\mathbf{a}_{t1}(\theta_1), \ldots, \mathbf{a}_{r1}(\theta_K)\otimes\mathbf{a}_{t1}(\theta_K)]$. It can be shown that $(\mathrm{SNR}_y/\mathrm{SNR}_{xc}) = \overline{MN}/(\overline{M}+\overline{N}-1)$, so the reduced-dimension transformation can obtain SNR gain. Advantage 3 can also be verified in Section 5, where the three algorithms are compared.

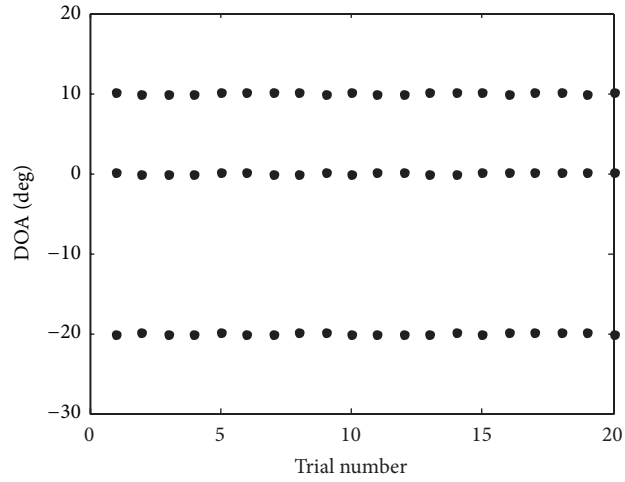

Figure 3: Angle estimation result of the proposed algorithm (SNR = 5 dB).

Remark 1. Although MUSIC-like algorithm [24] can achieve high resolution angle estimation with unknown mutual coupling, the peak searches with high complexity will make it ineffective. ESPRIT-like algorithm [25] can obtain the close-form solution of the angle estimation with lower complexity, but it only exploits the relationship between the subarrays, which will lead to the performance loss.

4.3. Cramer-Rao Bound (CRB). According to [29], the CRB for DOA estimation in monostatic MIMO radar with unknown mutual coupling can be derived as

$$\mathrm{CRB} = \frac{\sigma^2}{2}\left\{\mathrm{Re}\left[\mathbf{D}^H\mathbf{\Pi}_{\mathbf{G}}^{\perp}\mathbf{D}\right]\right\}^{-1}, \tag{28}$$

where $\mathbf{D} = [\partial\mathbf{u}/\partial\theta_1, \ldots, \partial\mathbf{u}/\partial\theta_K, \partial\mathbf{u}/\partial c_1^t, \ldots, \partial\mathbf{u}/\partial c_m^t, \partial\mathbf{u}/\partial c_1^r, \ldots, \partial\mathbf{u}/\partial c_n^r]$ with $\mathbf{u} = \begin{bmatrix}\widetilde{\mathbf{A}}\mathbf{s}(1)\\ \vdots\\ \widetilde{\mathbf{A}}\mathbf{s}(J)\end{bmatrix}$; $\mathbf{\Pi}_{\mathbf{G}}^{\perp} = I_J\otimes\mathbf{\Pi}_{\widetilde{\mathbf{A}}}^{\perp}$ with $\mathbf{\Pi}_{\widetilde{\mathbf{A}}}^{\perp} = \mathbf{I}_{MN} - \widetilde{\mathbf{A}}(\widetilde{\mathbf{A}}^H\widetilde{\mathbf{A}})^{-1}\widetilde{\mathbf{A}}^H$.

5. Simulation Results

Define root mean square error (RMSE) as $(1/K)\sum_{k=1}^{K}\sqrt{((1/1000)\sum_{l=1}^{1000}[(\widehat{\theta}_{k,l}-\theta_k)^2])}$, where $\widehat{\theta}_{k,l}$ is the estimate of DOA θ_k of the lth Monte Carlo trial. We assume that there are $K = 3$ targets with the angles being $(\theta_1,\theta_2,\theta_3) = (-20^\circ, 0^\circ, 10^\circ)$. The reflect coefficients are $(\beta_1, \beta_2, \beta_3) = [1, e^{j\pi/5}, 0.8e^{j\pi/4}]$ and the Doppler frequencies are $(f_1, f_2, f_3) = [1000\,\mathrm{Hz}, 2550\,\mathrm{Hz}, 5000\,\mathrm{Hz}]/10^5$. The mutual coupling coefficients are $[1, 0.1174 + 0.0577j]$ and $[1, -0.0121 - 0.1029j]$ for the transmit and receive arrays, respectively.

Figure 3 depicts angle estimation result of the proposed algorithm with $M = 10$, $N = 8$, $J = 100$, and SNR = 5 dB. It is shown that the DOAs can be clearly observed.

The angle estimation performance comparison between the proposed algorithm, ESPRIT-like algorithm, and

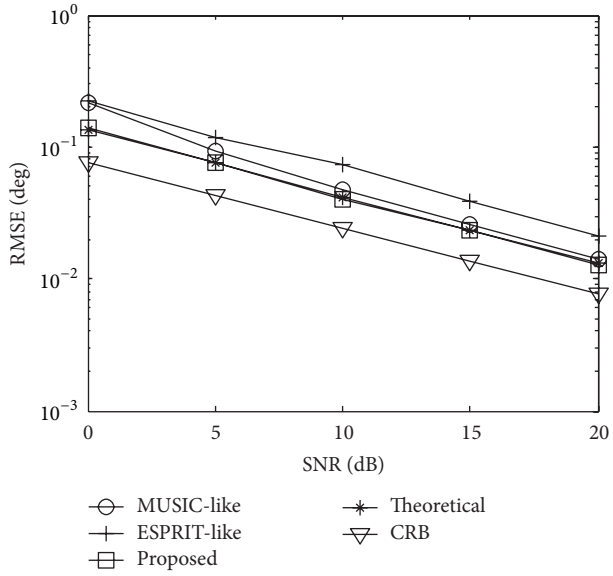

Figure 4: Angle estimation performance comparison ($M = 10, N = 8, J = 100$).

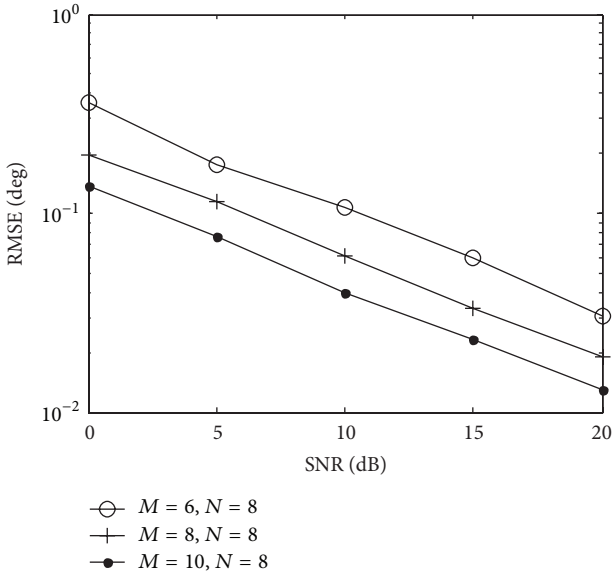

Figure 5: Angle estimation performance with different M.

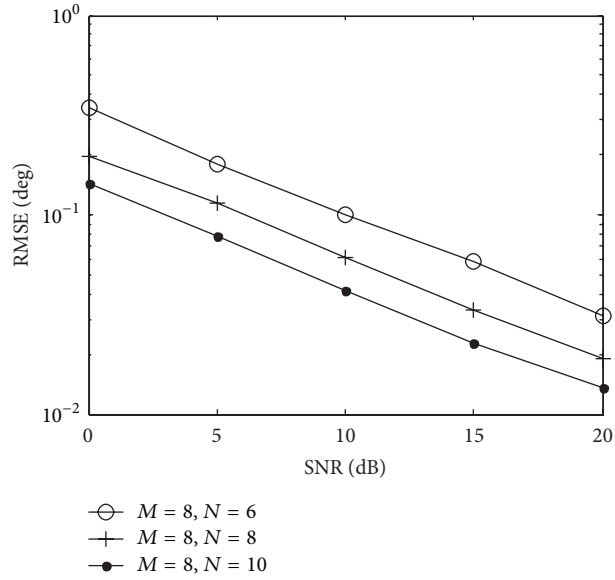

Figure 6: Angle estimation performance with different N.

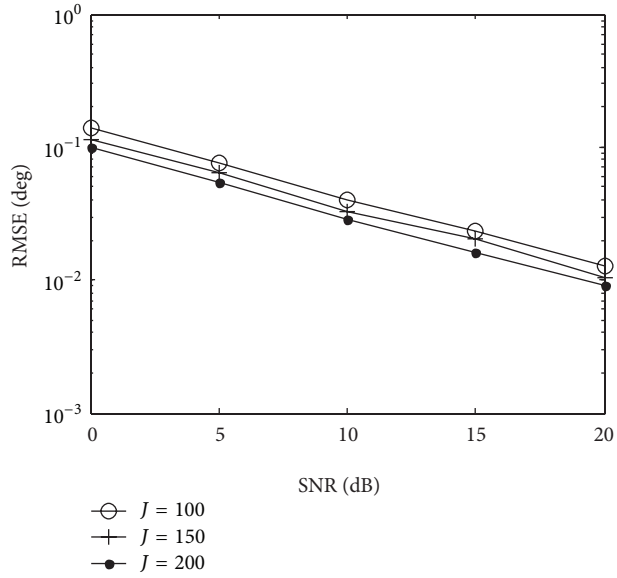

Figure 7: Angle estimation performance with different J.

MUSIC-like algorithm is shown in Figure 4, from which we can find that the angle estimation performance of the proposed algorithm is better than that of ESPRIT-like and MUSIC-like. It can also be indicated that the theoretical estimation error and the simulation error of the proposed algorithm are almost the same, which demonstrate the correctness of the derivation in (26).

Figures 5 and 6 present the estimation performance of the proposed algorithm with $J = 100$ and variable values of M or N. It can be indicated that the angle estimation performance of the proposed algorithm is improved with the increase of receive or transmit antenna numbers because of the diversity gain.

Figure 7 presents the angle estimation performance of our scheme with $M = 10$, $N = 8$, and different values of J. It has been shown in (26) that the angle estimation error will be reduced when J increases.

To further demonstrate the advantages of the proposed algorithm, another set of parameters is chosen to test the algorithms. Assume that the angles are $(\theta_1, \theta_2, \theta_3) = (-30^\circ, -20^\circ, 10^\circ)$. The reflect coefficients are $(\beta_1, \beta_2, \beta_3) = [1, 0.7e^{j\pi/6}, e^{j\pi/4}]$ and the Doppler frequencies are $(f_1, f_2, f_3) = [2000\,\text{Hz}, 3550\,\text{Hz}, 6000\,\text{Hz}]/10^5$. The mutual coupling coefficients are $[1, 0.2134 + 0.1537j]$ and $[1, -0.1121 - 0.1425j]$ for the transmit and receive arrays, respectively. The RMSE comparison of the algorithms is shown in Figure 8, from

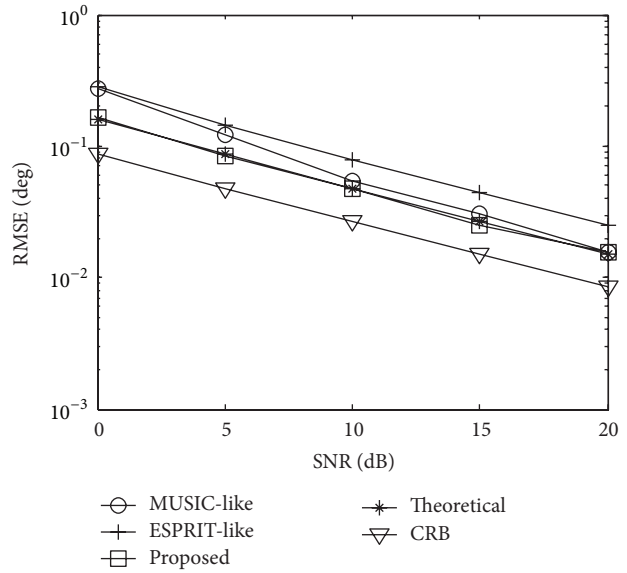

Figure 8: Angle estimation performance comparison (different configuration).

which we can still find that the angle estimation performance of the proposed algorithm is better than the other two algorithms. It can also be indicated that the theoretical estimation error and the simulation error of the proposed algorithm are still the same.

6. Conclusion

In this paper, a DOA estimation algorithm based on Root-MUSIC has been proposed for monostatic MIMO radar with unknown mutual coupling. The proposed algorithm has low complexity and works fast, requires neither peak searches nor iterations, and can work well with practical unknown mutual coupling. So it can support practical online processing. Furthermore, the proposed algorithm has better angle estimation performance then the ESPRIT-like algorithm and MUSIC-like algorithm, which have higher complexity. Many thanks are due to the reviewer's comments; our future work is to test the algorithms with real world data, and try to convert the theories into practical applications.

Conflict of Interests

The authors declare that there is no conflict of interests regarding the publication of this paper.

Acknowledgments

This work is supported by the China NSF Grants (61371169, 61071164), the Jiangsu Planned Projects for Postdoctoral Research Funds (1201039C), the China Postdoctoral Science Foundation (2012M521099, 2013M541661), the Open project of key laboratory of underwater acoustic communication and marine information technology (Xiamen University), the Hubei Key Laboratory of Intelligent Wireless Communications (IWC2012002), the Open project of Key Laboratory of modern acoustic of Ministry of Education (Nanjing University), the Aeronautical Science Foundation of China (20120152001), Funding of Jiangsu Innovation Program for Graduate Education (CXZZ13_0165), Funding for Outstanding Doctoral Dissertation in NUAA (BCXJ13-09), the Qing Lan Project, priority academic program development of Jiangsu high education institutions, and the Fundamental Research Funds for the Central Universities (NS2013024, kfjj130114).

References

[1] E. Fishler, A. Haimovich, R. Blum, D. Chizhik, L. Cimini, and R. Valenzuela, "MIMO radar: an idea whose time has come," in *Proceedings of the IEEE Radar Conference*, pp. 71–78, April 2004.

[2] J. Li and P. Stoica, "MIMO radar-diversity means superiority," in *Proceedings of the Adaptive Sensor Array Processing Workshop (ASAP '06)*, pp. 1–6, Lincoln Lab, December 2006.

[3] X.-R. Li, Z. Zhang, W.-X. Mao, X.-M. Wang, J. Lu, and W.-S. Wang, "A study of frequency diversity MIMO radar beamforming," in *Proceedings of the IEEE 10th International Conference on Signal Processing (ICSP '10)*, pp. 352–356, October 2010.

[4] R. Sharma, "Analysis of MIMO radar ambiguity functions and implications on clear region," in *Proceedings of the IEEE International Radar Conference (RADAR '10)*, pp. 544–548, June 2010.

[5] J. Li, G. Liao, and H. Griffiths, "Bistatic MIMO radar space-time adaptive processing," in *Proceedings of the IEEE Radar Conference: In the Eye of the Storm (RadarCon '11)*, pp. 498–501, Westin Crown Center in Kansas City, May 2011.

[6] X. H. Wu, A. A. Kishk, and A. W. Glisson, "MIMO-OFDM radar for direction estimation," *IET Radar, Sonar & Navigation*, vol. 4, no. 1, pp. 28–36, 2010.

[7] J. Li, G. Liao, K. Ma, and C. Zeng, "Waveform decorrelation for multitarget localization in bistatic MIMO radar systems," in *Proceedings of the IEEE International Radar Conference (RADAR '10)*, pp. 21–24, May 2010.

[8] C. Duofang, C. Baixiao, and Q. Guodong, "Angle estimation using ESPRIT in MIMO radar," *Electronics Letters*, vol. 44, no. 12, pp. 770–771, 2008.

[9] C. Jinli, G. Hong, and S. Weimin, "Angle estimation using ESPRIT without pairing in MIMO radar," *Electronics Letters*, vol. 44, no. 24, pp. 1422–1423, 2008.

[10] G. Zheng, B. Chen, and M. Yang, "Unitary ESPRIT algorithm for bistatic MIMO radar," *Electronics Letters*, vol. 48, no. 3, pp. 179–181, 2012.

[11] J. Li, H. Yan, and G. Liao, "Multitarget identification and localization using bistatic MIMO radar systems (EURASIP Journal on Advances in Signal Processing)," *Eurasip Journal on Advances in Signal Processing*, vol. 2008, Article ID 973932, 2008.

[12] X. Zhang, L. Xu, L. Xu, and D. Xu, "Direction of departure (DOD) and direction of arrival (DOA) estimation in MIMO radar with reduced-dimension MUSIC," *IEEE Communications Letters*, vol. 14, no. 12, pp. 1161–1163, 2010.

[13] M. L. Bencheikh, Y. Wang, and H. He, "Polynomial root finding technique for joint DOA DOD estimation in bistatic MIMO radar," *Signal Processing*, vol. 90, no. 9, pp. 2723–2730, 2010.

[14] D. Nion and N. D. Sidiropoulos, "A PARAFAC-based technique for detection and localization of multiple targets in a MIMO

radar system," in *Proceedings of the IEEE International Conference on Acoustics, Speech, and Signal Processing (ICASSP '09)*, pp. 2077–2080, April 2009.

[15] X. Zhang, Z. Xu, L. Xu, and D. Xu, "Trilinear decomposition-based transmit angle and receive angle estimation for multiple-input multiple-output radar," *IET Radar, Sonar and Navigation*, vol. 5, no. 6, pp. 626–631, 2011.

[16] D. Nion and N. D. Sidiropoulos, "Adaptive algorithms to track the PARAFAC decomposition of a third-order tensor," *IEEE Transactions on Signal Processing*, vol. 57, no. 6, pp. 2299–2310, 2009.

[17] X. Zhang and D. Xu, "Low-complexity ESPRIT-based DOA estimation for colocated MIMO radar using reduced-dimension transformation," *Electronics Letters*, vol. 47, no. 4, pp. 283–284, 2011.

[18] X. Zhang, Y. Huang, C. Chen et al., "Reduced-complexity Capon for direction of arrival estimation in a monostatic multiple-input multiple-output radar," *IET Radar, Sonar & Navigation*, vol. 6, no. 8, pp. 796–801, 2012.

[19] H.-S. Lui, H. T. Hui, and M. S. Leong, "A note on the mutual-coupling problems in transmitting and receiving antenna arrays," *IEEE Antennas and Propagation Magazine*, vol. 51, no. 5, pp. 171–176, 2009.

[20] H. S. Lui and H. T. Hui, "Mutual coupling compensation for direction-of-arrival estimations using the receiving-mutual-impedance method," *International Journal of Antennas and Propagation*, vol. 2010, Article ID 373061, 7 pages, 2010.

[21] J. Dai, D. Zhao, and X. Ji, "A sparse representation method for DOA estimation with unknown mutual coupling," *IEEE Antennas and Wireless Propagation Letters*, vol. 11, pp. 1210–1213, 2012.

[22] Z. Ye, J. Dai, X. Xu, and X. Wu, "DOA estimation for uniform linear array with mutual coupling," *IEEE Transactions on Aerospace and Electronic Systems*, vol. 45, no. 1, pp. 280–288, 2009.

[23] J. Li and X. Zhang, "Joint angles and mutual coupling estimation algorithm for bistatic MIMO radar," *International Journal of Antennas and Propagation*, vol. 2012, Article ID 921878, 8 pages, 2012.

[24] X. Liu and G. Liao, "Direction finding and mutual coupling estimation for bistatic MIMO radar," *Signal Processing*, vol. 92, no. 2, pp. 517–522, 2012.

[25] Z. D. Zheng, J. Zhang, and J. Y. Zhang, "Joint DOD and DOA estimation of bistatic MIMO radar in the presence of unknown mutual coupling," *Signal Processing*, vol. 92, no. 12, pp. 3039–3048, 2012.

[26] P. Chargé, Y. Wang, and J. Saillard, "A non-circular sources direction finding method using polynomial rooting," *Signal Processing*, vol. 81, no. 8, pp. 1765–1770, 2001.

[27] B. D. Rao and K. V. S. Hari, "Performance analysis of Root-Music," *IEEE Transactions on Acoustics, Speech, and Signal Processing*, vol. 37, no. 12, pp. 1939–1949, 1989.

[28] P. Stoica and A. Nehorai, "MUSIC, maximum likelihood, and Cramer-Rao bound," *IEEE Transactions on Acoustics, Speech, and Signal Processing*, vol. 37, no. 5, pp. 720–741, 1989.

[29] P. Stoica and A. Nehorai, "Performance study of conditional and unconditional direction-of-arrival estimation," *IEEE Transactions on Acoustics, Speech, and Signal Processing*, vol. 38, no. 10, pp. 1783–1795, 1990.

Hindawi Publishing Corporation
International Journal of Antennas and Propagation
Volume 2013, Article ID 919545, 8 pages
http://dx.doi.org/10.1155/2013/919545

Research Article

Accurate DOA Estimations Using Microstrip Adaptive Arrays in the Presence of Mutual Coupling Effect

Qiulin Huang, Hongxing Zhou, Jianhui Bao, and Xiaowei Shi

Science and Technology on Antenna and Microwave Laboratory, Xidian University, Xi'an 710071, China

Correspondence should be addressed to Qiulin Huang; qiulhuang@mail.xidian.edu.cn

Received 30 August 2013; Accepted 24 October 2013

Academic Editor: Hon Tat Hui

A new mutual coupling calibration method is proposed for adaptive antenna arrays and is employed in the DOA estimations to calibrate the received signals. The new method is developed via the transformation between the embedded element patterns and the isolated element patterns. The new method is characterized by the wide adaptability of element structures such as dipole arrays and microstrip arrays. Additionally, the new method is suitable not only for the linear polarization but also for the circular polarization. It is shown that accurate calibration of the mutual coupling can be obtained for the incident signals in the 3 dB beam width and the wider angle range, and, consequently, accurate [1D] and [2D] DOA estimations can be obtained. Effectiveness of the new calibration method is verified by a linearly polarized microstrip ULA, a circularly polarized microstrip ULA, and a circularly polarized microstrip UCA.

1. Introduction

In the last several decades, many direction-of-arrival (DOA) estimation algorithms with superresolution have been proposed, such as the multiple signal classification (MUSIC), the estimations of signal parameters via rotational invariance techniques (ESPRIT), the maximum likelihood (ML), and the subspace fitting (SF) [1–4]. Employing the ideal array manifold, these algorithms can provide excellent DOA estimation performances. For the actual antenna array, however, the array manifold cannot be regarded as that of the ideal point source array. The magnitude and phase of the received array signals are disturbed by the mutual coupling effect of the actual array, which would degrade the performances of the DOA estimation algorithms [5].

Many interests have been focused on the DOA estimations in the presence of mutual coupling effect over the past years. In order to obtain accurate DOA estimations, DOA estimation methods employing the actual array manifold were proposed [6–8]. Essentially, the actual manifold is equivalent to the array pattern. However, great effort is required to calculate and measure the actual manifold. Additionally, mass storage is needed for the manifold data in these methods. The transformation relationship between the actual array manifold and the array manifold of the ideal point source was proposed to decrease the storage of the manifold data [9, 10]. In this method, a distortion matrix was employed to carry out the transformation with assuming that the distortion matrix is angular independent. The validity of this method was verified in the 1D DOA estimations using the antenna array composed of the collinear dipoles. However, for the antenna array that is composed of microstrip elements, this method is valid only in a very limited angle range. In the literature, the universal steering vector was used in DOA estimations employing the antenna array with arbitrary geometry [11]. In this method, the received signal can be used directly to carry out the DOA estimations without calibration. However, the universal steering vector is dependent on the incident angles and the polarization of the incoming signals.

In addition to the DOA estimation methods in the presence of the mutual coupling effect, the mutual coupling calibration methods are also employed in the DOA estimations. In these methods, the calibration matrix was obtained through various approaches, such as the open-circuit voltage method, the receiving mutual impedance method, and the

minimum-norm method [5, 12, 13]. The research in [14] investigated the effects of ground parameters on the mutual impedance for DOA estimations, and some suggestions were put forward to improve the DOA estimations. In the open-circuit voltage method, the open-circuit voltages of the array were treated as the decoupled voltages [5]. For the antenna array composed of wire elements, accurate DOA estimations can be obtained by adopting the open circuit voltage method. For the antenna array composed of planar elements such as the microstrip antenna, however, the open-circuit voltage method would not take the positive role in the mutual coupling calibration owing to the strong open scattering effect. By contrast, the receiving mutual impedance method and the minimum-norm method can provide better calibration of the mutual coupling effect owing to consideration of the secondary scattering effect of the array. However, these methods are more suitable for the antenna array composed of wire elements, such as dipoles and monopoles.

In the research of the mutual coupling calibration, joint estimation methods of the DOAs and calibration matrix were also proposed [15–18]. This kind of methods utilized the array processing to obtain the DOAs and the calibration matrix simultaneously and can be employed in the arrays composed of various element geometries. These methods were usually used in the array with regular array structures, such as the uniform linear arrays (ULAs) and the uniform circular arrays (UCAs). For regular arrays, the number of mutual coupling parameters can be decreased owing to the regular array structure, which would benefit the joint estimations of the DOAs and calibration matrix. Presently, the time consumption to find the DOAs and calibration matrix is not acceptable for many actual applications, and many efforts have been made to decrease the complexity of the joint estimation algorithms.

In this paper, the element pattern reconstruction method is proposed to calibrate the mutual coupling effect. In this method, the calibration matrix is developed through the transformation relationship between the embedded element patterns and the isolated element patterns. The new method is based on the fact that when all of the embedded element patterns are transformed to coincide with the corresponding isolated element patterns in a certain direction, the received signals owing to this direction would be decoupled after being transformed with the same means. This method is characterized by the wide adaptability of element structures. It can be used in microstrip antenna arrays to obtain highly accurate calibration of the mutual coupling effect. In general, it can be done to reconstruct the element patterns of an array to coincide with those in the isolated state in the 3 dB beam width or a little wider angle range. This means that the calibration method can calibrate the incident signals coming from the angle range and provide necessary conditions for accurate DOA estimations. In order to testify the performance of the new calibration method, two microstrip arrays including a linearly polarized microstrip array and a circularly polarized microstrip array are designed to carry out the DOA estimations. In the numerical examples, the classical MUSIC algorithm is employed to find the directions of the incident signals.

2. Theory

Consider an antenna array composed of N elements; each element is terminated with the load Z_L. In the development of the new calibration method, the main polarization component of the electric field of the array element is used since the main polarization component takes the dominant part in the total electric field of the array. For the linearly polarized array, the main polarization component is the θ component or the φ component. For the circularly polarized array, it is the left-hand circular polarization (LHCP) component or the right-hand circular polarization (RHCP) component. According to the basis of the new method, (1) is used to realize the transformation of the element patterns. Consider

$$\begin{bmatrix} E_1^i(\theta,\varphi) \\ E_2^i(\theta,\varphi) \\ \vdots \\ E_N^i(\theta,\varphi) \end{bmatrix} = \mathbf{C} \begin{bmatrix} E_1(\theta,\varphi) \\ E_2(\theta,\varphi) \\ \vdots \\ E_N(\theta,\varphi) \end{bmatrix}, \tag{1}$$

where $E_n^i(\theta,\varphi)$ and $E_n(\theta,\varphi)$ for element n represent the electric field of the isolated element and that of the embedded element, respectively. It is to be noted that the embedded element pattern for each element should be calculated with each element terminated with a load Z_L. The calibration matrix $\mathbf{C}$ has the dimension of $N \times N$. In order to solve the matrix $\mathbf{C}$, some directions should be sampled from all element patterns in (1). And then (1) is transformed into a solvable matrix function as follows:

$$\begin{bmatrix} E_1^i(\theta_1,\varphi_1)\cdots E_1^i(\theta_M,\varphi_M) \\ E_2^i(\theta_1,\varphi_1)\cdots E_2^i(\theta_M,\varphi_M) \\ \vdots \\ E_N^i(\theta_1,\varphi_1)\cdots E_N^i(\theta_M,\varphi_M) \end{bmatrix} = \mathbf{C} \begin{bmatrix} E_1(\theta_1,\varphi_1)\cdots E_1(\theta_M,\varphi_M) \\ E_2(\theta_1,\varphi_1)\cdots E_2(\theta_M,\varphi_M) \\ \vdots \\ E_N(\theta_1,\varphi_1)\cdots E_N(\theta_M,\varphi_M) \end{bmatrix}. \tag{2}$$

Consequently, the least square solution that satisfies $\min_{||\mathbf{CE}-\mathbf{E}^i||}||\mathbf{C}||$ can be obtained; that is,

$$\mathbf{C} = \mathbf{E}^i\mathbf{E}^H\left(\mathbf{E}\mathbf{E}^H\right)^{-1}, \tag{3}$$

where $\mathbf{E}$ and $\mathbf{E}^i$ represent the pattern matrix for all of the embedded elements and isolated elements, respectively. The operator $||\cdot||$ denotes the F-norm of a matrix. For the matrix $\mathbf{C}$ with the dimension of $N \times N$, the F-norm is written as

$$||\mathbf{C}|| = \left\{\sum_{n=1}^{N}\sum_{m=1}^{N}|c_{nm}|^2\right\}^{1/2}, \tag{4}$$

where c_{nm} is an entry of the matrix $\mathbf{C}$.

The electric fields in the previous equations can be calculated by various methods, such as the method of moments (MOM), the finite-element method (FEM), and the finite-difference time domain (FDTD) method.

The matrix **C** calculated from (3) can be used to reconstruct the element patterns and to calibrate the mutual coupling effect of the array. Assume that the sample matrix of the received signals is $\mathbf{X}'$ and can be written by

$$\mathbf{X}' = \mathbf{AS} + \mathbf{N_0}, \tag{5}$$

where **A** represents the direction matrix, **S** represents the sampled stochastic data matrix, and $\mathbf{N}_0$ represents the add white Gaussian noise matrix. The calibrated sample matrix can be calculated by the following formula:

$$\mathbf{X} = \mathbf{CX}'. \tag{6}$$

For the actual antenna array, the received signals influenced by the mutual coupling effect can be generated via the embedded element pattern matrix **E** which acts as the actual direction matrix. Another method to obtain the actual direction matrix is calculating the induced terminal voltage vectors when a plane wave impinges on the array in the same direction of the incident signal.

When the received signals are calibrated by the calibration matrix, they can be imported to the MUSIC algorithm to find the directions of the incident signals. The covariance matrix of the calibrated received signals **X** is written as

$$\mathbf{R}_{XX} = E\left\{\mathbf{XX}^H\right\}, \tag{7}$$

where $E\{\cdot\}$ represents the statistical expectation and the superscript H represents the complex conjugate transpose. Both the signal eigenvectors and the noise eigenvectors can be calculated by the previous covariance matrix. And then the orthogonal property between the signal eigenvectors and noise eigenvectors is employed to estimate the DOAs of the incident signals by searching the peaks of the MUSIC spectrum given by

$$P_{\mathrm{MUSIC}}(\theta,\varphi) = \frac{\mathbf{a}^H(\theta,\varphi)\,\mathbf{a}(\theta,\varphi)}{\left[\mathbf{a}^H(\theta,\varphi)\,\mathbf{U}_N\mathbf{U}_N^H\mathbf{a}^H(\theta,\varphi)\right]}, \tag{8}$$

where $\mathbf{U}_N$ is the matrix whose columns are the noise eigenvectors of the covariance matrix $\mathbf{R}_{XX}$ and $\mathbf{a}(\theta,\varphi)$ denotes the ideal steering vector of the antenna array.

In general, the new calibration method utilizes the relationship between the embedded element patterns and isolated element patterns. As is known, the received signal owing to the isolated element is not influenced by the mutual coupling effect. Consequently, accurate mutual coupling calibration can be provided by the new method. In Su's method that is proposed in [9], the relationship between the embedded element patterns and the patterns of ideal point source was employed. However, Su's method catered for the ideal point source model in the array processing, which would introduce extra mutual coupling effect. Of course, Su's method can provide good mutual coupling calibration for dipole or monopole arrays since the H-plane pattern of the element is isotropic. By contrast, the new method can provide more accurate mutual coupling calibration, especially for arrays composed of planar elements. It can be seen from the following examples that the new method is suitable for the dipole array and the microstrip array and is effective for the linearly polarized array and the circularly polarized array.

Table 1: Parameters of the incident signals.

Incident signals	φ	θ	SNR (dB)
Signal 1	−50°	90°	20
Signal 2	−20°	90°	20
Signal 3	0°	90°	20

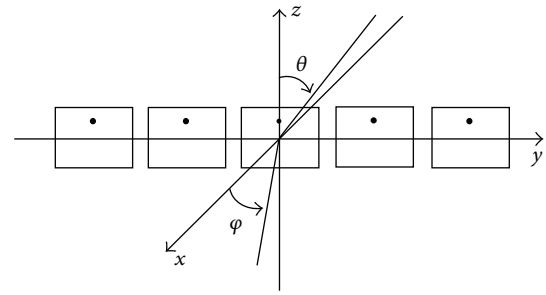

Figure 1: Structure of the linearly polarized microstrip array and the coordinate system.

3. Numerical Examples

In this section, a linearly polarized microstrip ULA, a circularly polarized microstrip ULA, and a circularly polarized microstrip UCA are employed to carry out the DOA estimations in the presence of mutual coupling effect. The two previous ULAs are used for one-dimensional DOA estimations, and the UCA is used for two-dimensional (2D) DOA estimations. The calibrated received signals are input to the MUSIC algorithm to find the directions of the incident signals, and the data sample is 1000 in the DOA estimations. Both arrays are composed of five elements, and they operate at the frequency of 3 GHz. Each element is terminated with the same load $Z_L = 50\ \Omega$. The microstrip arrays are fabricated on the substrate FR4 ($\varepsilon_r = 4.4$) with the thickness of 1.6 mm. The EM simulation tool HFSS 13 is used to calculate the element patterns.

Three incident signals are involved in the following DOA estimations of (A) and (B). Parameters of all the incident signals are listed in Table 1.

(A) Linearly Polarized Microstrip ULA. The structure of the linearly polarized microstrip array with five elements is shown in Figure 1. The element spacing is $d = 0.4\lambda$. The length and width of the patch is 30.2 mm and 22.8 mm, respectively. The feed point is set with the distance of 6.2 mm from the upper edge. The 3 dB beam width of the element is about 90° in the *xoy* plane. The incident angle of Signal 1 is in

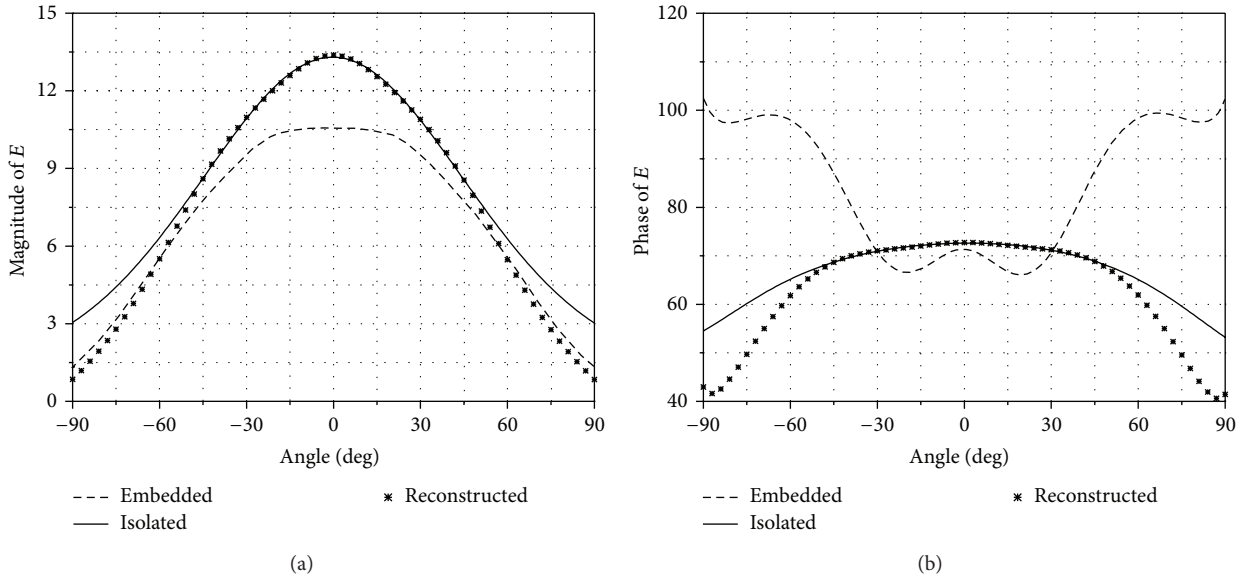

Figure 2: Magnitude and phase of θ component of the electric field in three cases for the linearly polarized microstrip array.

the outside of the 3 dB beam width, and the incident angles of the other two signals are in the 3 dB beam width. Assume that all incident signals are of the z-polarization. In the xoy plane, the main polarization component is the θ component or the z component of the electric field. In order to calculate the calibration matrix via (3), 101 directions of the θ component of electric field are sampled from the angle range of $[-50^\circ, 50^\circ]$ in the xoy plane.

The calibration matrix is first used to reconstruct the element patterns of the array. The magnitude and phase of the central element in three states are shown in Figure 2. It can be seen that both the magnitude and the phase of the reconstructed element pattern of the element are coincident with those of the isolated element pattern in the angle range that is slightly larger than the 3 dB beam width. This means that the incident signals in this angle range can be calibrated with high accuracy, and, consequently, the accurate DOA estimations can be obtained, which can be seen from Figure 3. The performance of the DOA estimations is seriously degraded by the mutual coupling effect of the array, and none of the DOAs of the incident signals can be found from the MUSIC spectrum without calibration. Large errors of the DOA estimations can be seen for all of the incident signals when the open-circuit voltage method is employed. For Su's method, the DOA estimation bias exists when the incident signals get far from the norm direction. However, the performance of the DOA estimations is significantly improved when the proposed method is used. More accurate DOA estimations are provided by the proposed method in the 3 dB beam width and the vicinity. The DOA estimation bias for the linearly polarized array can be found in Table 2.

(B) Circularly Polarized Microstrip ULA. The circularly polarized microstrip element and array are shown in Figures 4 and 5, respectively. The element spacing is also $d = 0.4\lambda$. The 3 dB beam width of the element is about 100°

Table 2: DOA estimation bias for the linearly polarized array.

φ	DOA estimation bias		
	Open circuit	Su's method	Proposed method
−50°	0.5°	3.4°	0.2°
−20°	3.5°	1.4°	0°
0°	2.8°	0.6°	0.2°

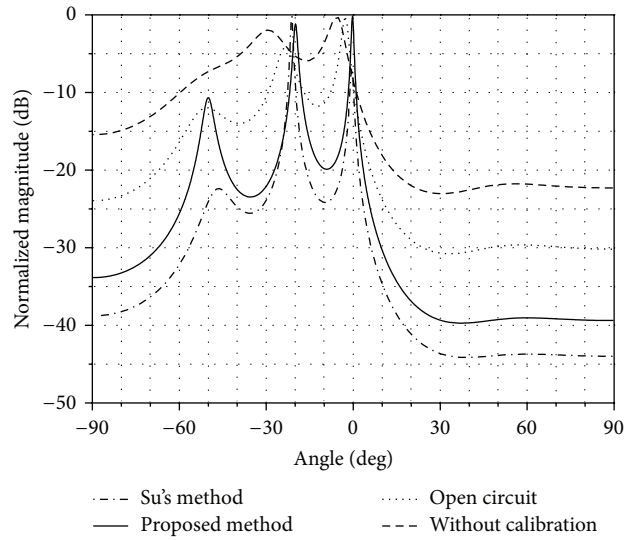

Figure 3: Spatial spectrum of DOA estimations for three incident signals employing the linearly polarized microstrip array.

in the xoy plane. It can be seen from Figure 6 that the RHCP component of the element pattern takes the dominant part in the total electric field. Therefore, the RHCP component of the electric field is employed to calculate the calibration matrix. Similar the example to previous, 101 directions of

Table 3: DOA estimation bias for the circularly polarized array.

φ	DOA estimation bias		
	Open circuit	Su's method	Proposed method
−50°	4.6°	1.8°	0°
−20°	3°	1.5°	0.2°
0°	1.5°	0.6°	0.3°

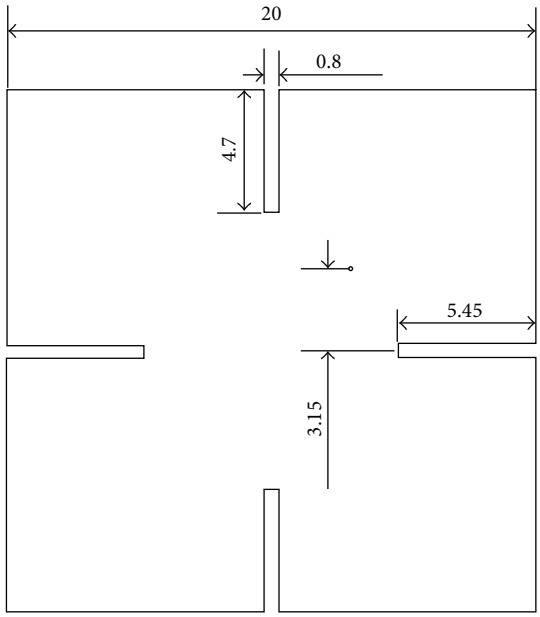

Figure 4: Profile of the circularly polarized microstrip element with the unit mm.

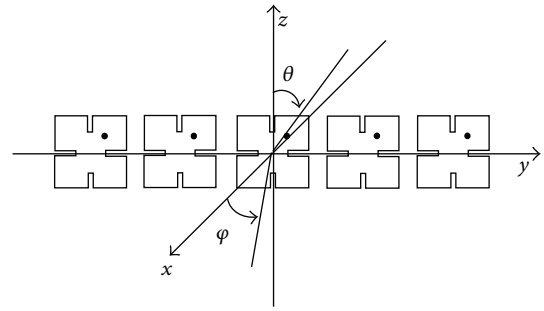

Figure 5: Structure of the circularly polarized microstrip array and the coordinate system.

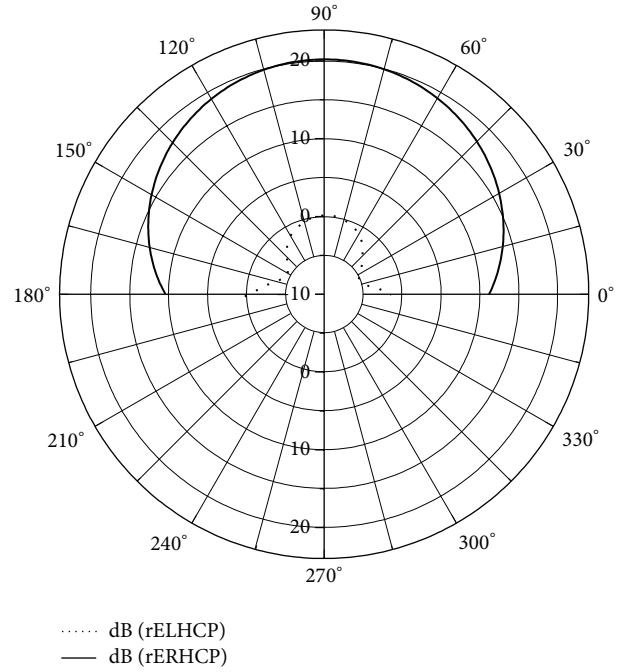

Figure 6: Isolated element pattern of the circularly polarized microstrip element.

the RHCP component of the electric field are chosen from the angle range of [−50°, 50°] in the *xoy* plane to calculate the calibration matrix.

The reconstruction results of the embedded element pattern for the central element are shown in Figure 7. It can be seen that the coincidence between the reconstructed element pattern and the isolated element pattern is obtained in the angle range that is larger than 120°, which would bring about accurate DOA estimations in a wide angle range. The DOA estimations of three RHCP incident signals are given in Figure 8. It is shown that limited improvement of the performance of DOA estimations is provided by the open-circuit voltage method, and apparent DOA estimation errors exist for all of the three incident signals. The DOA estimation errors are decreased when Su's method is used. In contrast, more accurate DOA estimations for all incident signals could be obtained due to the element pattern reconstruction method. The DOA estimation bias for the circularly polarized array can be seen in Table 3.

As seen from the pervious two numerical examples, proper calibration matrices can be obtained to carry out the mutual coupling calibration in the 3 dB beam width that is the main operating angle range of the array. And the generally, the coincidence between the reconstructed pattern and the isolated pattern is valid in the range beyond the 3 dB beam width. Therefore, the microstrip element with larger 3 dB beam width would be more favorable to the mutual coupling calibrations. As for the polarization of elements, the less cross-polarization is more beneficial to the mutual coupling calibrations. It is quite understandable that the larger the main polarization component is, the less the difference between the theoretical calibration matrix and the calibration matrix actually required is.

(C) Circularly Polarized Microstrip UCA. The circularly polarized microstrip UCA is composed of six elements as given in Figure 4. The structure of the UCA with a radius of 0.5λ is shown in Figure 9. It is designed for the 2D DOA estimations. Two incident signals are considered and the correlated parameters are listed in Table 4. In order to obtain a valid calibration matrix for 2D DOA estimations, enough direction samples are chosen in the main operating angular

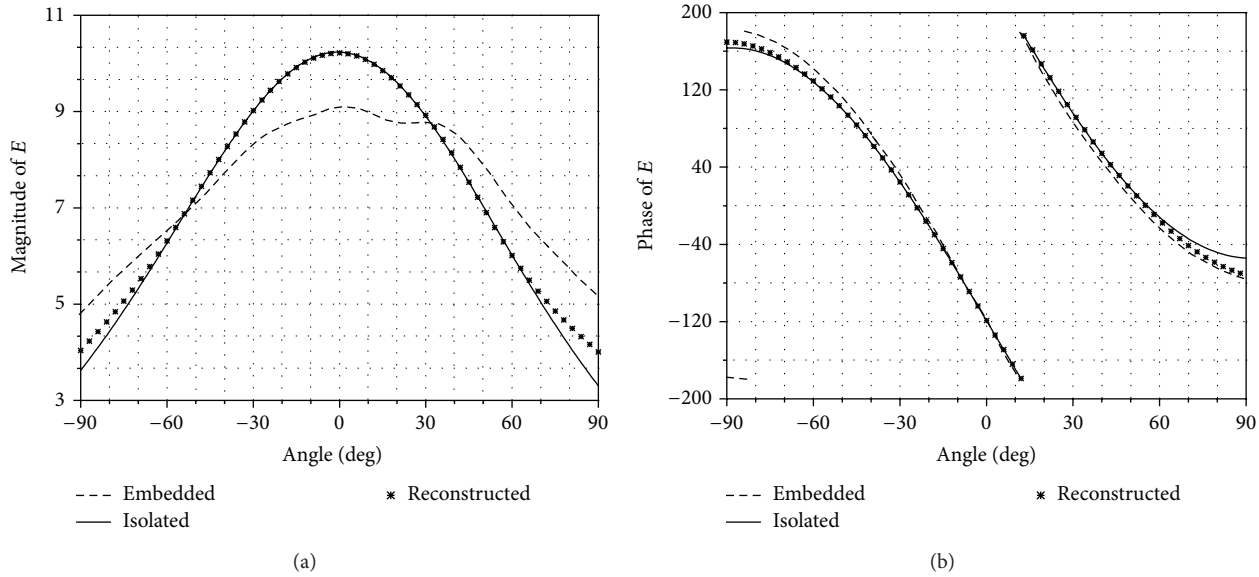

Figure 7: Magnitude and phase of θ component of the electric field in three cases for the circularly polarized microstrip array.

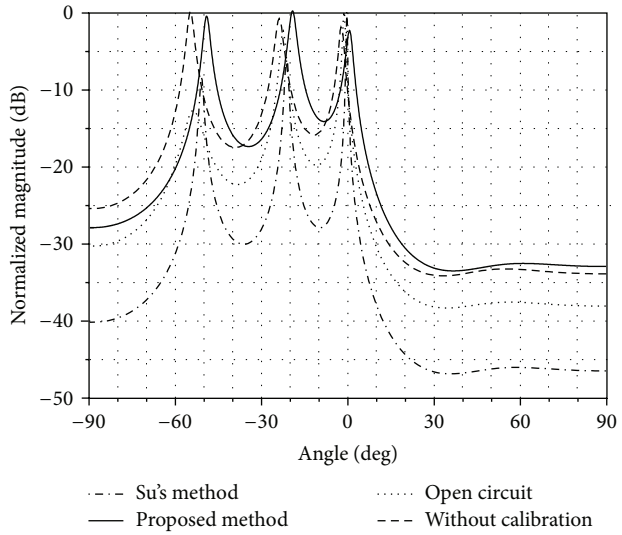

Figure 8: Spatial spectrum of DOA estimations for three incident signals employing the circularly polarized microstrip array.

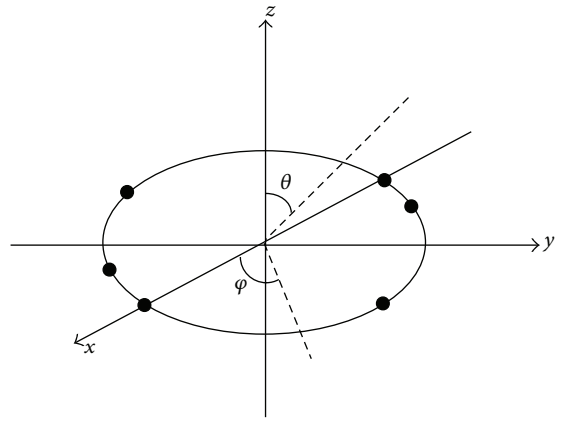

Figure 9: Structure of the UCA and the coordinate system.

Table 4: Parameters of the incident signals for 2D DOA estimations.

Incident signals	φ	θ	SNR (dB)
Signal 1	20°	10°	20
Signal 2	80°	60°	20

region of the array. Here, the direction sample is represented as $(\theta, \varphi) = (10\alpha^\circ, 5\beta^\circ)$, where $\alpha = 1, 2, \ldots, 6$ and $\beta = 1, 2, \ldots, 71$; that is, the directions with the total of 360 are employed to calculate the calibration matrix.

Performance comparisons of the three calibration methods can be made through the following contour charts of the 2D DOA estimations. As shown in Figure 10, two incident directions can be found due to the proposed method and the open-circuit method, and the proposed method can provide higher DOA estimation accuracy. Additionally, it can be seen that Su's method fails to find the incident directions, which is mainly caused by the extra mutual coupling effect introduced by the transformation between the embedded element patterns and the ideal point source patterns. DOA estimation bias corresponding to Figure 10 is listed in Table 5 which shows the advantages of the proposed method over other two methods.

Table 5: Two-dimensional DOA estimation bias for the UCA.

(θ, φ)	DOA estimation bias		
	Open circuit	Su's method	Proposed method
(10°, 20°)	(0°, 2.2°)	Failure	(0.4°, 0.6°)
(60°, 80°)	(7.2°, 0.8°)	Failure	(0.8°, 0°)

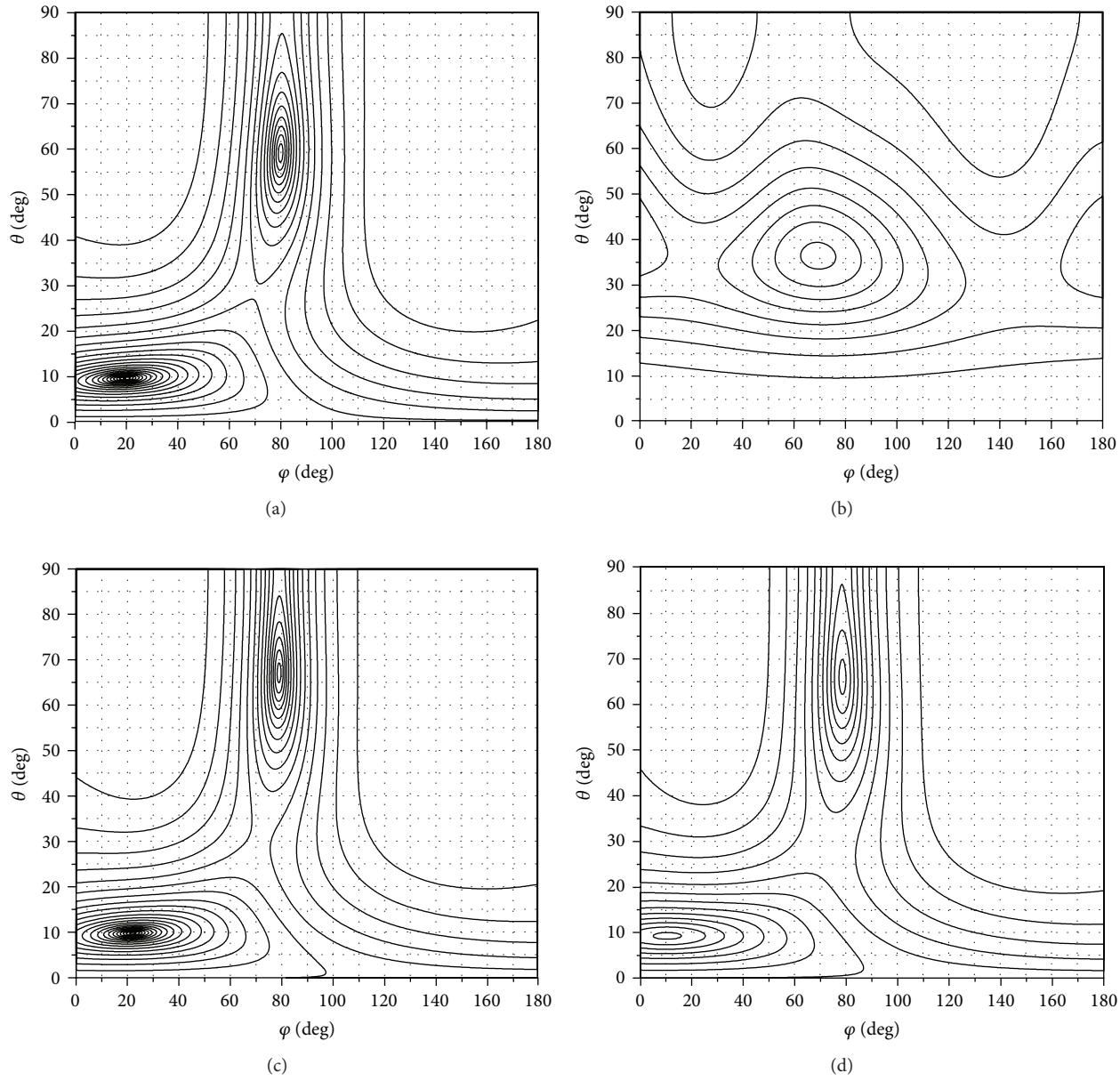

Figure 10: Contour charts of the 2D DOA estimations for (a) the proposed method, (b) Su's method, (c) the open-circuit voltage method, and (d) without calibration.

4. Conclusion

In this paper, the element pattern reconstruction method is proposed to calibrate the mutual coupling effect of adaptive antenna arrays. This method is based on the transformation between the embedded element patterns and the isolated element patterns. It is shown that the new method can be employed in microstrip arrays and can provide accurate mutual coupling calibration. Meanwhile, the new method can be used in the linearly polarized microstrip arrays and the circularly polarized microstrip arrays. Owing to the calibration effect of the new method, accurate 1D and 2D DOA estimations can be obtained by employing the MUSIC algorithm in the presence of mutual coupling effect.

Acknowledgments

This work was supported in part by the "Fundamental Research Funds for the Central Universities" (K5051202012) and the "National Natural Science Foundation of China" (61201019).

References

[1] R. O. Schmidt, "Multiple emitter location and signal parameter estimation," *IEEE Transactions on Antennas and Propagation*, vol. 34, no. 3, pp. 276–280, 1986.

[2] R. Roy and T. Kailath, "ESPRIT—estimation of signal parameters via rotational invariance techniques," *IEEE Transactions on*

Acoustics, Speech, and Signal Processing, vol. 37, no. 7, pp. 984–995, 1989.

[3] A. G. Jaffer, "Maximum likelihood direction finding of stochastic sources: a separable solution," in *Proceedings of the 1988 International Conference on Acoustics, Speech, and Signal Processing*, vol. 5, pp. 2893–2896, New York, NY, USA, 1988.

[4] J. A. Cadzow, "A high resolution direction-of-arrival algorithm for narrow-band coherent and incoherent sources," *IEEE Transactions on Acoustics, Speech, and Signal Processing*, vol. 36, no. 7, pp. 965–979, 1988.

[5] I. J. Gupta and A. A. Ksienski, "Effect of mutual coupling on the performance of adaptive arrays," *IEEE Transactions on Antennas and Propagation*, vol. 31, no. 5, pp. 785–791, 1983.

[6] R. O. Schmidt, "Multilinear array manifold interpolation," *IEEE Transactions on Signal Processing*, vol. 40, no. 4, pp. 857–866, 1992.

[7] A. J. Weiss and B. Friedlander, "Manifold interpolation for diversely polarized arrays," *IEE Proceedings*, vol. 141, no. 1, pp. 19–24, 1994.

[8] A. Manikas, H. R. Karimi, and I. Dacos, "Study of the detection and resolution capabilities of a one-dimensional array of sensors by using differential geometry," *IEE Proceedings*, vol. 141, no. 2, pp. 83–92, 1994.

[9] T. Su, K. Dandekar, and H. Ling, "Simulation of mutual coupling effect in circular arrays for direction-finding application," *Microwave and Optical Technology Letters*, vol. 26, no. 5, pp. 331–336, 2000.

[10] K. R. Dandekar, H. Ling, and G. Xu, "Experimental study of mutual coupling compensation in smart antenna applications," *IEEE Transactions on Wireless Communications*, vol. 1, no. 3, pp. 480–487, 2002.

[11] Q. Yuan, Q. Chen, and K. Sawaya, "Accurate DOA estimation using array antenna with arbitrary geometry," *IEEE Transactions on Antennas and Propagation*, vol. 53, no. 4, pp. 1352–1357, 2005.

[12] H. T. Hui, "Reducing the mutual coupling effect in adaptive nulling using a re-defined mutual impedance," *IEEE Microwave and Wireless Components Letters*, vol. 12, no. 5, pp. 178–180, 2002.

[13] C. K. E. Lau, R. S. Adve, and T. K. Sarkar, "Minimum norm mutual coupling compensation with applications in direction of arrival estimation," *IEEE Transactions on Antennas and Propagation*, vol. 52, no. 8, pp. 2034–2041, 2004.

[14] I. Ahmed, W. F. Perger, and S. A. Zekavat, "Effects of ground constituent parameters on array mutual coupling for DOA estimation," *International Journal of Antennas and Propagation*, vol. 2011, Article ID 425913, 5 pages, 2011.

[15] B. Friedlander and A. J. Weiss, "Direction finding in the presence of mutual coupling," *IEEE Transactions on Antennas and Propagation*, pp. 273–284, 1991.

[16] M. Lin and L. Yang, "Blind calibration and DOA estimation with uniform circular arrays in the presence of mutual coupling," *IEEE Antennas and Wireless Propagation Letters*, vol. 5, no. 1, pp. 315–318, 2006.

[17] F. Sellone and A. Serra, "An iterative algorithm for the compensation of toeplitz mutual coupling in UNIFORM and linear arrays," in *Proceedings of the IEEE 12th Digital Signal Processing Workshop*, pp. 438–443, September 2006.

[18] B. Liao, Z. Zhang, and S. Chan, "DOA estimation and tracking of ULAs with mutual coupling," *IEEE Transactions on Aerospace and Electronic Systems*, vol. 48, no. 1, pp. 891–905, 2012.

Hindawi Publishing Corporation
International Journal of Antennas and Propagation
Volume 2013, Article ID 386367, 6 pages
http://dx.doi.org/10.1155/2013/386367

Research Article

AR Model-Based Direction-of-Arrival Estimation of Coherent Signals in the Presence of Unknown Mutual Coupling

Zhi-Chao Sha, Zhang-Meng Liu, Zhi-Tao Huang, and Yi-Yu Zhou

College of Electronic Science and Engineering, National University of Defense Technology, Changsha, Hunan 410073, China

Correspondence should be addressed to Zhi-Chao Sha; shazhichao_163@163.com

Received 23 June 2013; Revised 17 September 2013; Accepted 1 October 2013

Academic Editor: Hao Ling

This paper addresses the problem of direction-of-arrival (DOA) estimation of coherent signals in the presence of unknown mutual coupling, and an autoregression (AR) model-based method is proposed. The effects of mutual coupling can be eliminated by the inherent mechanism of the proposed algorithm, so the DOAs can be accurately estimated without any calibration sources. After the mixing matrix is estimated by independent component analysis (ICA), several parameter equations are established upon the mixing matrix. Finally, all DOAs of coherent signals are estimated by solving these equations. Compared with traditional methods, the proposed method has higher angle resolution and estimation accuracy. Simulation results demonstrate the effectiveness of the algorithm.

1. Introduction

Direction-of-arrival (DOA) estimation is very important in a variety of wireless communication applications, such as mobile communication, radar, and distributed sensor networks. In particular, many effective high-resolution DOA estimation algorithms have been developed and deeply investigated in the last decades [1]. Since then, the attention of the signal processing community has focused on the factors that block the practical application of those algorithms. The first factor is the unknown mutual coupling, which will affect the array manifold of the array and result in poor accuracy of DOA estimation [2]. The other factor is that there may be highly correlated or coherent signals because of multipath propagation [3, 4]. When the incident signals are highly correlated or coherent in the presence of unknown mutual coupling, the performance of conventional high-resolution DOA estimation methods will deteriorate significantly.

In the last years, many array calibration algorithms have been proposed with respect to the mutual coupling effect [5–13]. Hung [5] uses an iterative least mean-square approach to estimate the calibration matrix, but it requires a preliminary calibration. The above algorithms may not be easily carried out in practice, because of the additional calibration sources or sensors. An iterative algorithm is given to compensate the mutual coupling and perturbation of gain and phase in [6]. However, the convergence rate is slow, and computational cost is very expensive. In [7], a novel online mutual coupling compensation algorithm is presented to estimate coupling parameters through an alternating minimization technique, but the convergence is not well guaranteed. In [8], an algorithm that applies a group of auxiliary sensors in uniform linear arrays (ULAs) has been proposed to estimate the DOAs, but the algorithm requires a large number of sensors, and it is difficult to be satisfied in practice. References [9, 10] present a unified framework and sparse Bayesian perspective for array calibration and DOA estimation. Moreover, Dai et al. proposed a sparse representation method to eliminate the effect of mutual coupling by its inherent mechanism [11]. However, the computational cost is expensive. Many studies have been made to reduce the computational complexity of the calculations by using a certain unitary transformation that converts complex-valued manifold matrices of uniform linear arrays (ULAs) into real ones [12, 13].

On the other hand, many techniques have been proposed to deal with the correlated or coherent situation. A forward/backward spatial smoothing (FBSS) method that can solve the coherent problem is presented in [3]. Malioutov

et al. propose the method of L1-SVD to address the general DOA estimation problem [14]. L1-SVD first decomposes the array output and extracts the signal energy into K (the signal number) singular vectors and then represents them under sparsity constraint to estimate the signal directions. The method in [15] estimates the uncorrelated and coherent signals separately but encounters the differencing matrix power loss and needs extra processing to recover the rank. Recently, independent component analysis (ICA) has been utilized to solve the DOA estimation problem [16, 17]. These methods can estimate the real steering vectors with unknown mutual coupling. However, owing to the complex structure of the MCM, all the methods taking care of the correlated or coherent situation cannot be utilised to estimate the DOAs in the presence of unknown mutual coupling.

However, it is more difficult to estimate DOAs of coherent signals in the presence of unknown mutual coupling. Dai and Ye [18] propose an improved spatial smoothing algorithm for DOA estimation of coherent signals in the presence of unknown mutual coupling, but it significantly deteriorates while angle interval is not large enough or several groups of coherent signals coexist. Inspired by [19] and based on the estimation of the real steering vectors by ICA, we develop a spatial AR model-based algorithm for coherent DOA estimation of ULA in the presence of mutual coupling. Simulations illustrate that the DOA estimation accuracy of our approach is higher than the improved spatial smoothing algorithm in [18].

The paper is organized as follows. The data model of the ULA is given in Section 2. The spatial AR model algorithm is described in detail in Section 3. Computer simulations and conclusions follow in Sections 4 and 5.

2. Data Model

Consider K narrowband non-Gaussian signals impinging on a uniform linear array (ULA) with M array elements, where the distance d between adjacent sensors is equal to half of the wavelength. Assume that there exist P groups of coherent signals because of multipath propagation, and the signals within the same group are coherent and independent in different groups. In the ith group, suppose the coherent signal coming from the direction θ_{il} is corresponding to the lth multipath propagation of the source $s_i(t)$, and $l = 1, \ldots, K_i$. The total number of coherent signals can be denoted as $K = \sum_{i=1}^{P} K_i$. The array output vector is expressed as

$$\mathbf{x}(t) = \mathbf{A}\mathbf{s}(t) + \mathbf{n}(t) = \sum_{i=1}^{P}\sum_{l}^{K_i} \mathbf{a}\left(\theta_{il}\right)\gamma_{il}\phi_{il}s_i(t) + \mathbf{n}(t), \quad (1)$$

where $\mathbf{a}(\theta_{il}) = [1, e^{-j2\pi d\sin(\theta_{il})/\lambda}, \ldots, e^{-j(M-1)2\pi d\sin(\theta_{il})/\lambda}]^T$ is the steering vector of the direction θ_{il}, λ is the wavelength of the signal, T is the transpose operator, γ_{il} and ϕ_{il} are corresponding to the amplitude and phase fading coefficients of the lth signal in the ith group, $\boldsymbol{\rho}_i = [\gamma_{i1}\phi_{i1}, \ldots, \gamma_{iK_i}\phi_{iK_i}]^T$, $\mathbf{A}_i = [\mathbf{a}(\theta_{i1}), \ldots, \mathbf{a}(\theta_{iK_i})]$, $\mathbf{s}(t) = [s_1(t), \ldots, s_P(t)]^T$, and $\mathbf{n}(t)$ is zero mean additive white Gaussian noise vector. The real steering vector of the ith group coherent signals is given by $\boldsymbol{\tau}_i = \mathbf{A}_i\boldsymbol{\rho}_i$.

In the presence of mutual coupling, the true steering vector should be modified as

$$\mathbf{x}(t) = \mathbf{C}\mathbf{A}\mathbf{s}(t) + \mathbf{n}(t), \quad (2)$$

where $\mathbf{C}$ is the mutual coupling matrix (MCM) and can be expressed as a banded symmetric Toeplitz matrix with just a few nonzero coefficients

$$\mathbf{C} = \text{Toeplitz}\left\{1, c_1, \ldots, c_{P-1}, \mathbf{0}_{1\times(M-P)}\right\}. \quad (3)$$

The covariance matrix of the received signals is defined by

$$\mathbf{R}_x = E\left\{\mathbf{x}(t)\,\mathbf{x}(t)^H\right\} = \mathbf{C}\mathbf{A}\mathbf{R}_s\mathbf{A}^H\mathbf{C}^H + \sigma^2\mathbf{I}_M, \quad (4)$$

where $E\{\cdot\}$ is the expectation operator, the superscript H denotes transpose complex conjugate operation, $\mathbf{R}_s = E\{\mathbf{s}(t)\mathbf{s}(t)^H\}$ is the sources covariance matrix, σ^2 is the variance of the additive noise, and $\mathbf{I}_M$ is an identity matrix.

3. Novel AR Model-Based DOA Estimation Algorithm

We assume L denotes the number of coherent signals in one group. Referring to [19], the mappings $e^{j\omega_k}(k = 1, \ldots, L)$ of the signal directions on the unit circle are distinct roots of an Lth order equation if no ambiguity occurs. The relationship between ω_k and the direction of the kth signal θ_k is $\omega_k = 2\pi d\sin(\theta_k)/\lambda$. Assuming that the coefficients of the unified equation are $\kappa_0, \ldots, \kappa_{L-1}$ and the unknown parameter is β, the equation is then given by

$$f(\beta) = \prod_{k=1}^{L}\left(\beta - e^{j\omega_k}\right) = \beta^L + \kappa_{L-1}\beta^{L-1} + \cdots + \kappa_1\beta + \kappa_0 = 0. \quad (5)$$

Equation (5) presents the relationship of the coherent signals directions. For one group of coherent signals without mutual coupling, the real steering vector is a linear mixture of L ideal steering vectors. The special relationship is then given by

$$\boldsymbol{\tau} = \left[\tau_0, \ldots, \tau_{M-1}\right]^T = \varepsilon\left[\sum_{k=1}^{L}\rho_k e^{j0\omega_k}, \ldots, \sum_{k=1}^{L}\rho_k e^{j(M-1)\omega_k}\right]^T, \quad (6)$$

where ρ_k is the corresponding fading coefficient in the kth multipath propagation and ε is the corresponding scaling ambiguity coefficient caused by ICA processing.

According to (6), the Jth element of $\boldsymbol{\tau}$ is

$$\tau_J = \sum_{k=1}^{L}\varepsilon\rho_k e^{jJ\omega_k}, \quad J = 0, 1, \ldots, M-1. \quad (7)$$

Because $e^{j\omega_k}(k = 1, \ldots, L)$ are the roots of (5), the following L equations hold:

$$e^{jL\omega_k} + \kappa_{L-1}e^{j(L-1)\omega_k} + \cdots + \kappa_1 e^{j\omega_k} + \kappa_0 = 0, \quad k = 1, \ldots, L. \quad (8)$$

According to the idea of [19], multiplying both sides of (8) with $\varepsilon\rho_k e^{jL\omega_k}$ ($k = 1,\ldots,L$) and then summing up the L equations yield

$$\sum_{k=1}^{L}\varepsilon\rho_k e^{j(L+\xi)\omega_k} + \kappa_{L-1}\sum_{k=1}^{L}\varepsilon\rho_k e^{j(L+\xi-1)\omega_k} + \cdots + \kappa_1\sum_{k=1}^{L}\varepsilon\rho_k e^{j(1+\xi)\omega_k} + \kappa_0\sum_{k=1}^{L}\varepsilon\rho_k e^{j\xi\omega_k} = 0; \quad \xi = 0,1,\ldots,M-L-1. \tag{9}$$

Substituting (7) into (9), we obtain the relationship between the equation coefficients and vector $\boldsymbol{\tau}$

$$\tau_{L+\xi} + \kappa_{L-1}\tau_{L+\xi-1} + \cdots + \kappa_1\tau_{1+\xi} + \kappa_0\tau_\xi = 0, \quad \xi = 0,1,\ldots,M-L-1. \tag{10}$$

The real steering vectors in the presence of unknown mutual coupling can be given by

$$\mathbf{G} = \mathbf{CA} = \begin{bmatrix} 1 & c_1 & \cdots & c_{N_c} & \cdots & 0 \\ c_1 & 1 & c_1 & \cdots & \ddots & 0 \\ \vdots & c_1 & 1 & \ddots & \cdots & c_{N_c} \\ c_{N_c} & \cdots & \ddots & \ddots & c_1 & \vdots \\ 0 & \ddots & \cdots & c_1 & 1 & c_1 \\ 0 & \cdots & c_{N_c} & \cdots & c_1 & 1 \end{bmatrix}_{M\times M} \times \left[\boldsymbol{\tau}_1,\ldots,\boldsymbol{\tau}_P\right]_{M\times P}. \tag{11}$$

Each of $\mathbf{g}_i$ contains all the spatial information of one group of coherent signals. The real steering vectors $\mathbf{G}$ can be estimated by ICA [16, 17].

Then we will introduce the proposed method to solve the problem of DOA estimation of coherent signals in the presence of unknown mutual coupling.

3.1. The Case of $N_c = 1$. For any given column vector $\mathbf{g}$, we get

$$\begin{aligned} g_0 &= \tau_0 + c_1\tau_1 \\ g_1 &= c_1\tau_0 + \tau_1 + c_1\tau_2 \\ g_2 &= c_1\tau_1 + \tau_2 + c_1\tau_3 \\ &\vdots \\ g_{M-2} &= c_1\tau_{M-3} + \tau_{M-2} + c_1\tau_{M-1} \\ g_{i,M-1} &= c_1 t_{M-2} + t_{M-1}. \end{aligned} \tag{12}$$

For the second equation to the $(L+2)$th equation, multiplying both sides of (8) with $\{\kappa_0,\ldots,\kappa_{L-1},1\}$ and then summing up the L equations yield

$$g_{L+1} + \kappa_{L-1}g_L + \cdots + \kappa_1 g_2 + \kappa_0 g_1 = 0. \tag{13}$$

Using the same principle to process all the adjacent $L+1$ equations, we get

$$\begin{bmatrix} g_1 & g_2 & \cdots & g_L \\ g_2 & g_3 & \cdots & g_{L+1} \\ \vdots & \vdots & \ddots & \vdots \\ g_{M-L-2} & g_{M-L-1} & \cdots & g_{M-3} \end{bmatrix}\begin{bmatrix} \kappa_0 \\ \kappa_1 \\ \vdots \\ \kappa_{L-1} \end{bmatrix} = -\begin{bmatrix} g_{L+1} \\ g_{L+2} \\ \vdots \\ g_{M-2} \end{bmatrix}. \tag{14}$$

In addition, as the signals are of complex value, we utilize their conjugate information to improve the precision of the proposed method as [19]. Similarly, the following equations hold:

$$g_\xi^* + \kappa_{L-1}g_{\xi+1}^* + \cdots + g_1\tau_{\xi+L-1}^* + \kappa_0 g_{\xi+L}^* = 0, \quad \xi = 1,\ldots,M-L-2. \tag{15}$$

Combining (10) and (15), we establish the following equation set:

$$\begin{bmatrix} g_1 & g_2 & \cdots & g_L \\ g_2 & g_3 & \cdots & g_{L+1} \\ \vdots & \vdots & \ddots & \vdots \\ g_{M-L-2} & g_{M-L-1} & \cdots & g_{M-3} \\ g_{L+1}^* & g_L^* & \cdots & g_2^* \\ g_{L+2}^* & g_{L+1}^* & \cdots & g_3^* \\ \vdots & \vdots & \ddots & \vdots \\ g_{M-2}^* & g_{M-3}^* & \cdots & g_{M-L-1}^* \end{bmatrix}\begin{bmatrix} \kappa_0 \\ \kappa_1 \\ \vdots \\ \kappa_{L-1} \end{bmatrix} = -\begin{bmatrix} g_{L+1} \\ g_{L+2} \\ \vdots \\ g_{M-2} \\ g_1^* \\ g_2^* \\ \vdots \\ g_{M-L-2}^* \end{bmatrix} \tag{16}$$

in which the superscript $*$ denotes the conjugate operation.

3.2. The Case of $N_c > 1$. From the case of $N_c = 1$, we note that the elements of real steering vectors can be utilized adequately due to the mutual coupling. If $N_c > 1$, the elements $\{g_0,\ldots g_{N_c-1}\}$ and $\{g_{M-N_c},\ldots g_{M-1}\}$ are useless to estimate the DOAs. The number of useful elements is

$$N_g = M - 2 * N_c. \tag{17}$$

According to (16), the new formulation is given by

$$\begin{bmatrix} g_{N_c} & g_{N_c+1} & \cdots & g_{N_c+L-1} \\ g_{N_c+1} & g_{N_c+2} & \cdots & g_{N_c+L} \\ \vdots & \vdots & \ddots & \vdots \\ g_{M-L-N_c-1} & g_{M-L-N_c} & \cdots & g_{M-N_c-2} \\ g^*_{N_c+L} & g^*_{N_c+L-1} & \cdots & g^*_{N_c+1} \\ g^*_{N_c+L+1} & g^*_{N_c+L} & \cdots & g^*_{N_c+2} \\ \vdots & \vdots & \ddots & \vdots \\ g^*_{M-N_c-1} & g^*_{M-N_c-2} & \cdots & g^*_{M-L-N_c} \end{bmatrix} \begin{bmatrix} \kappa_0 \\ \kappa_1 \\ \vdots \\ \kappa_{L-1} \end{bmatrix} = - \begin{bmatrix} g_{N_c+L} \\ g_{N_c+L+1} \\ \vdots \\ g_{M-N_c-1} \\ g^*_{N_c} \\ g^*_{N_c+1} \\ \vdots \\ g^*_{M-L-N_c-1} \end{bmatrix}. \tag{18}$$

By comparing (16) with (18), we know that (16) is a special case of (18). The right vectors $\mathbf{g}$ of (18) can be estimated by ICA. So, the coefficient vector $\boldsymbol{\kappa}$ can be estimated under the least mean-square error criterion. The least square solution is then given by

$$\boldsymbol{\kappa} = - \begin{bmatrix} g_{N_c} & g_{N_c+1} & \cdots & g_{N_c+L-1} \\ g_{N_c+1} & g_{N_c+2} & \cdots & g_{N_c+L} \\ \vdots & \vdots & \ddots & \vdots \\ g_{M-L-N_c-1} & g_{M-L-N_c} & \cdots & g_{M-N_c-2} \\ g^*_{N_c+L} & g^*_{N_c+L-1} & \cdots & g^*_{N_c+1} \\ g^*_{N_c+L+1} & g^*_{N_c+L} & \cdots & g^*_{N_c+2} \\ \vdots & \vdots & \ddots & \vdots \\ g^*_{M-N_c-1} & g^*_{M-N_c-2} & \cdots & g^*_{M-L-N_c} \end{bmatrix}^{\dagger} \times \begin{bmatrix} g_{N_c+L} \\ g_{N_c+L+1} \\ \vdots \\ g_{M-N_c-1} \\ g^*_{N_c} \\ g^*_{N_c+1} \\ \vdots \\ g^*_{M-L-N_c-1} \end{bmatrix}, \tag{19}$$

where $[\cdot]^{\dagger}$ denotes Moore-Penrose inverse.

All roots of (8) can be estimated with the known equation coefficients $\kappa_0, \ldots, \kappa_{L-1}$. The DOAs of coherent signals in one group are given by

$$\theta_k = \sin^{-1}\left(\operatorname{Arg}\left(\beta_k\right)\lambda/\left(2\pi d\right)\right), \quad k = 1, \ldots, L, \tag{20}$$

where $\beta_1, \ldots, \beta_L$ are the roots of (8) and $\operatorname{Arg}(\cdot)$ denotes the phase angle of complex value. Thus, the DOAs of coherent signals in one group are estimated according to (20).

3.3. Discussion. Due to (18), in order to make sure the equation has a unique solution, the left matrix of (18) must be of full rank. Therefore, the following inequality must be satisfied:

$$2\left(M - L - 2N_c\right) \geq L. \tag{21}$$

It is not difficult to see that the number of coherent signals in one group $L \leq \lfloor (2/3)(M - 2N_c) \rfloor$. As we know, the maximum number of independent sources resolved by ICA is equal to the number of sensors [17]. So, the maximum detectable number of source signals by the proposed method is

$$K_{\max} = \left\lfloor \frac{2}{3}\left(M - 2N_c\right) \right\rfloor \cdot M. \tag{22}$$

For the improved FBSS, the detectable number of source K and the length of subarrays M_0 must satisfy

$$\begin{aligned} K &< M_0, \\ K - P &< M - M_0 - 2N_c + 1. \end{aligned} \tag{23}$$

When $M_0 = K + 1$, (23) can be rewrite as

$$K < \frac{\left(M + P - 2N_c\right)}{2}. \tag{24}$$

4. Simulation Experiment

In this section, some computer simulations are reported to illustrate the performance of our proposed method. In the following simulations, we will compare the proposed method to FBSS [3] and the improved FBSS algorithm in [18] for DOA estimation.

In the first simulation, we consider one group of two coherent signals impinging on an 8-element ULA from the directions $[-10^\circ, 20^\circ]$, and the number of the mutual coupling coefficients is $N_c = 1$ with $c_1 = 0.3844 - 0.3476i$ [18]. The amplitude fading factor is $[1, 0.8]$. Figure 1 shows the root mean square error (RMSE) of each DOA estimate against input SNR computed via 200 Monte Carlo runs for each SNR and 500 snapshots of data for each run. As shown in Figure 1, the proposed method outperforms the improved FBSS method, and achieves similar performance as the original FBSS method with known mutual coupling.

In the second simulation, we consider the more complicated situation: two groups of two coherent signals impinge on an 8-element ULA from the directions $[-32^\circ, -8^\circ]$ and $[15^\circ, 42^\circ]$, and the number of the mutual coupling coefficients is $N_c = 2$ with $c_1 = 0.3844 - 0.3476i$ and $c_2 = 0.24 + 0.1i$. The amplitude fading factors are $[1, 0.9]$ and $[1, 0.8]$. Figure 2 shows the RMSE of each DOA estimate against input SNR computed via 200 Monte Carlo runs for each SNR and 500 snapshots of data for each run. The results illustrate that our method can get high-resolution in the complex structure of the MCM when the level of SNR is large enough. However, the improved FBSS maintains a coarse accuracy no matter what the levels of SNR are.

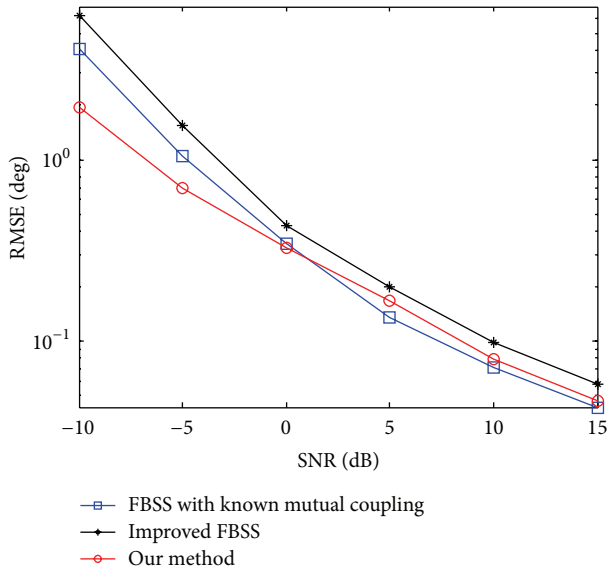

Figure 1: RMSE of DOA estimates against SNR ($N_c = P = 1$).

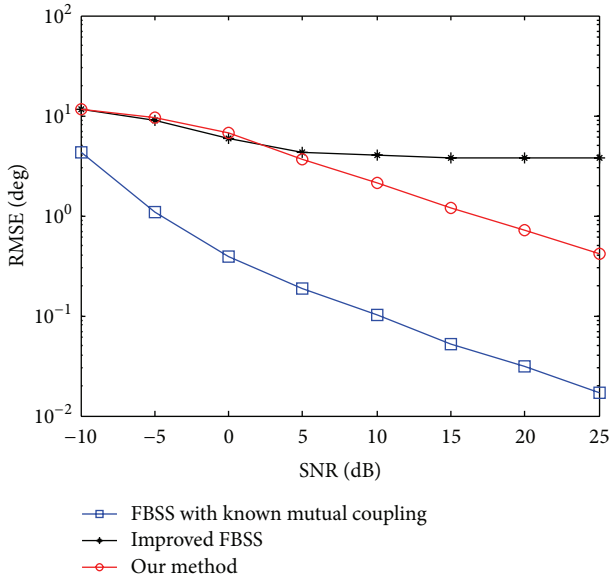

Figure 2: RMSE of DOA estimates against SNR ($N_c = P = 2$).

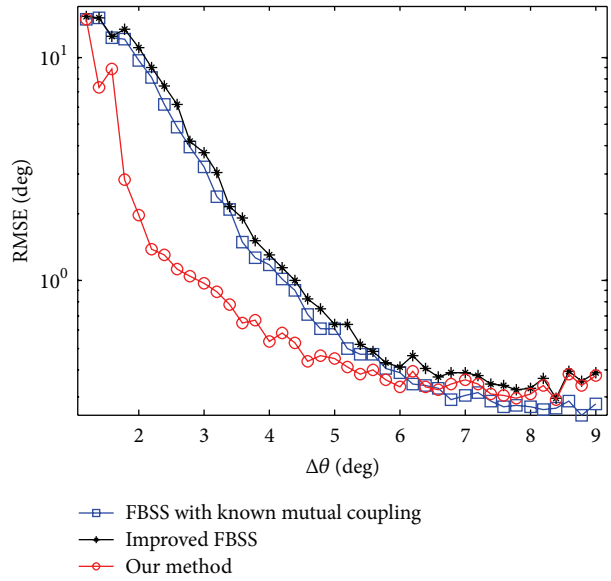

Figure 3: The RMSE of DOA estimation versus the angle interval.

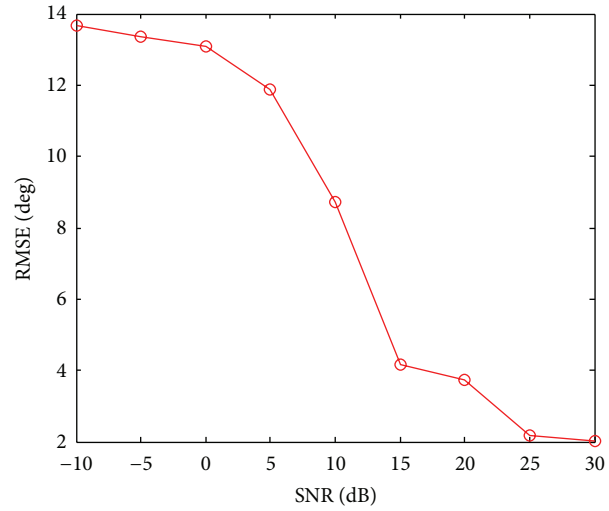

Figure 4: The RMSE of DOA estimation against SNR ($N_c = 1$, $P = 5$, $K = 10$).

In the third simulation, we will validate the high spatial resolution of the proposed method. Consider one group of two coherent signals with SNR of 10 dB impinging on an 8-element ULA, where the amplitude factors are the same as simulation 1. Assume that the directions of two coherent signals are -10° and $-9^\circ + \Delta\theta$, where $1 + \Delta\theta$ denotes the angle interval between the two source signals. We have 200 Monte Carlo trials with 500 snapshots to demonstrate the performance of the proposed method. Figure 3 shows the RMSE of DOA estimation using different algorithms versus the angle interval $\Delta\theta$. It can be seen from Figure 3 that the proposed method outperforms the other two methods when the angle interval is not large enough.

To verify the maximum detectable number of source signals by the proposed method, in the forth simulation, we consider five groups of two coherent signals impinging on a 5-element ULA from the directions $[-40^\circ, 10^\circ]$, $[-30^\circ, 20^\circ]$, $[-20^\circ, 30^\circ]$, $[-10^\circ, 40^\circ]$, and $[0^\circ, 50^\circ]$, and the number of the mutual coupling coefficients is $N_c = 1$ with $c_1 = 0.3844 - 0.3476i$. According to (22), the number of source signals is the maximum detectable number of our method $\lfloor (2/3)(M - 2N_c) \rfloor \cdot M = 10$. However, the improved FBSS and other sparse representation methods are incapable of processing the 10 sources with 5-element ULA due to their conditions. Figure 4 shows the RMSE of each DOA estimate against input SNR computed via 500 Monte Carlo runs for each SNR and 500 snapshots of data for each run. The result illustrates that

the maximum detectable number of sources by the proposed method is consistent with (24).

5. Conclusion

In this paper, an AR model-based DOA estimation algorithm is proposed for coherent signals in the presence of unknown mutual coupling. The effects of mutual coupling can be eliminated by solving a mathematical equation. Simulation results demonstrate that the proposed method has high spatial resolution and DOA estimation accuracy compared to the improved FBSS algorithm. Furthermore, the number of signals resolved by our method is larger than that of others.

Acknowledgments

The authors would like to thank the anonymous reviewers for their valuable comments and suggestions which vastly improved the content and presentation of this paper. This research was supported by the National Natural Science Foundation of China (no. 61072120) and the Program for New Century Excellent Talents in University of China (NCET).

References

[1] H. Krim and M. Viberg, "Two decades of array signal processing research: the parametric approach," *IEEE Signal Processing Magazine*, vol. 13, no. 4, pp. 67–94, 1996.

[2] A. J. Weiss and B. Friedlander, "Mutual coupling effects on phase-only direction finding," *IEEE Transactions on Antennas and Propagation*, vol. 40, no. 5, pp. 535–541, 1992.

[3] S. U. Pillai and B. H. Kwon, "Forward/backward spatial smoothing techniques for coherent signal identification," *IEEE Transactions on Acoustics, Speech, and Signal Processing*, vol. 37, no. 1, pp. 8–15, 1989.

[4] F. Han and X. Zhang, "An ESPRIT-like algorithm for coherent DOA estimation," *IEEE Antennas and Wireless Propagation Letters*, vol. 4, no. 1, pp. 443–446, 2005.

[5] E. K. L. Hung, "Matrix-construction calibration method for antenna arrays," *IEEE Transactions on Aerospace and Electronic Systems*, vol. 36, no. 3, pp. 819–828, 2000.

[6] B. Friedlander and A. J. Weiss, "Direction finding in the presence of mutual coupling," *IEEE Transactions on Antennas and Propagation*, pp. 273–284, 1991.

[7] F. Sellone and A. Serra, "A novel online mutual coupling compensation algorithm for uniform and linear arrays," *IEEE Transactions on Signal Processing*, vol. 55, no. 2, pp. 560–573, 2007.

[8] Z. Ye and C. Liu, "On the resiliency of MUSIC direction finding against antenna sensor coupling," *IEEE Transactions on Antennas and Propagation*, vol. 56, no. 2, pp. 371–380, 2008.

[9] Z. Liu, Z. Huang, F. Wang, and Y. Zhou, "DOA estimation with uniform linear arrays in the presence of mutual coupling via blind calibration," *Signal Processing*, vol. 89, no. 7, pp. 1446–1456, 2009.

[10] Z. Liu and Y. Zhou, "A unified framework and sparse Bayesian perspective for direction-of-arrival estimation in the presence of array imperfections," *IEEE Transactions on Signal Processing*, vol. 61, no. 15, pp. 3786–3798, 2013.

[11] J. Dai, D. Zhao, and X. Ji, "A sparse representation method for DOA estimation with unknown mutual coupling," *IEEE Antennas and Wireless Propagation Letters*, vol. 11, pp. 1210–1213, 2012.

[12] J. Dai, W. Xu, and D. Zhao, "Real-valued DOA estimation for uniform linear array with unknown mutual coupling," *Signal Processing*, vol. 92, no. 9, pp. 2056–2065, 2012.

[13] J. Dai, X. Xu, and D. Zhao, "Direction-of-arrival estimation via real-valued sparse representation," *IEEE Antennas and Wireless Propagation Letters*, vol. 12, pp. 376–379, 2013.

[14] D. Malioutov, M. Çetin, and A. S. Willsky, "A sparse signal reconstruction perspective for source localization with sensor arrays," *IEEE Transactions on Signal Processing*, vol. 53, no. 8, pp. 3010–3022, 2005.

[15] Z. Ye and X. Xu, "DOA estimation by exploiting the symmetric configuration of uniform linear array," *IEEE Transactions on Antennas and Propagation*, vol. 55, no. 12, pp. 3716–3720, 2007.

[16] Y. Shimada, H. Yamada, and Y. Yamaguchi, "Blind array calibration technique for uniform linear array using ICA," in *Proceedings of the IEEE Region 10 Conference (TENCON '07)*, Taipei, Taiwan, November 2007.

[17] J. Kim, H. J. Yang, B. W. Jung, and J. Chun, "Blind calibration for a linear array with gain and phase error using independent component analysis," *IEEE Antennas and Wireless Propagation Letters*, vol. 9, pp. 1259–1262, 2010.

[18] J. Dai and Z. Ye, "Spatial smoothing for direction of arrival estimation of coherent signals in the presence of unknown mutual coupling," *IET Signal Processing*, vol. 5, no. 4, pp. 418–425, 2011.

[19] Z. Liu, Z. Huang, and Y. Zhou, "Computationally efficient direction finding using uniform linear arrays," *IET Radar, Sonar and Navigation*, vol. 6, no. 1, pp. 39–48, 2012.